

**Investigation of protein-protein interactions involving  
Retinoblastoma Binding Protein 6 using immunoprecipitation and  
Nuclear Magnetic Resonance Spectroscopy**



A thesis submitted in fulfillment of the requirements for the degree of Master of Science in  
Biotechnology

Department of Biotechnology, Faculty of Natural Sciences,  
University of the Western Cape

December 2019

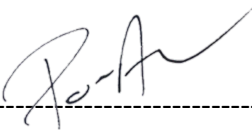
<http://etd.uwc.ac.za/>

## PLAGIARISM DECLARATION

Name: Po-An Chen

Student number: 3240694

1. I hereby declare that I know what plagiarism entails, namely to use another's work and to present it as my own without attributing the sources in the correct way. (Refer to University Calendar part 1 for definition)
2. I know that plagiarism is a punishable offence because it constitutes theft.
3. I understand the plagiarism policy of the Faculty of Natural Science of the University of the Western Cape.
4. I know what the consequences will be if I plagiarize in any of the assignments for my course.
5. I declare therefore that all work presented by me for every aspect of my course, will be my own, and where I have made use of another's work, I will attribute the source in the correct way.



-----

Signature

19 December 2019

Date

## Acknowledgements

I would like to thank my supervisor, Prof David Pugh, for allowing me the opportunity to take on this research project. I am extremely grateful for his support during this project, and I have learnt many valuable things through him. His wisdom has definitely inspired me to grow and improve myself as a scientist, and I hope to one day reach that level of wisdom.

I like to extend my gratitude to Dr Brandon Weber of the Electron Microscopy Unit at UCT for assisting and allowing me to use the Size Exclusion Chromatography machine. I wish to also extend my gratitude to Dr Andrew Atkinson at King's College London for sharing his expertise in NMR with me.

I would also like to thank Dr Andrew Faro for always providing assistance when I needed it the most, as well as much needed advice, constructive criticism and moral support throughout this project. I would like to thank Dr Penelope Rodriguez-Zamora for providing her NMR expertise at the early stages of this project as well as providing not just advice on NMR but life advice as well; and has become like a big sister figure to me despite her short time in our laboratory.

A special mention must be made to my laboratory mate Taskeen Simons, whom I have known since undergrad and become very good friends during our time in Honours and Masters. She out of everyone, understands the struggles we go through during our Masters, and has always been there for moral support. I am extremely grateful for her friendship and presence in the laboratory. I would also like to thank Mihlali Mlaza and Zaida Parsons for their constant moral support as well as the friendships we have developed over the years and making the laboratory environment an enjoyable one.

Lastly, I would like to thank the National Research Foundation for funding this research project.

## Abstract

Retinoblastoma Binding Protein 6 (RBBP6) is a 200 KDa multi-domain protein that has been shown to play a role in mRNA processing, cell cycle arrest and apoptosis. RBBP6 interacts with tumour suppressor proteins such as p53 and pRb and has been shown cooperate with Murine Double Minute 2 (MDM2) protein in catalyzing ubiquitination and suppression of p53. Unpublished data from our laboratory has suggested that RBBP6 and MDM2 interact with each other through their RING finger domains. RBBP6 has also been shown to have its own E3 ubiquitin ligase activity, catalyzing ubiquitination of Y-Box Binding Protein 1 (YB-1) *in vitro* and *in vivo*. YB-1 is a multifunctional oncogenic protein that is generally associated with poor prognosis in cancer, tumourigenesis, metastasis and chemotherapeutic resistance. Unpublished data from our laboratory shows that RBBP6 catalyzes poly-ubiquitination of YB-1, using Ubiquitin-conjugating enzyme H1 (UbcH1) as E2 ubiquitin conjugating enzyme. We have furthermore shown that the zinc knuckle of RBBP6 interacts specifically with the Ubiquitin-associated domain (UBA) domain of UbcH1.

This thesis reports investigations of two interactions between the RING finger domains of RBBP6 and MDM2 in Chapter 3, and between the zinc finger of RBBP6 and the UBA domain of UbcH1 in Chapter 4. In each case, the previously-reported interaction is first confirmed using GST pull-down assay. Then <sup>15</sup>N-enriched samples of the proteins are prepared and used in Nuclear Magnetic Resonance (NMR) spectroscopy-based chemical shift perturbation assays. The aims of these assays are, firstly, to validate the interaction by determining whether addition of the interacting partner perturbs the <sup>15</sup>N,<sup>1</sup>H-HSQC spectrum of the protein. The second aim is to identify resonances most affected by the interaction, and thereby identify amino acids in the proteins close to the interaction interface, which would serve as useful targets for future mutagenesis studies.

GST pull-down studies showed preliminary evidence of the interaction between the RING finger domains of RBBP6 and MDM2. A <sup>15</sup>N-enriched sample of RBBP6-RING was produced in bacteria

and a chemical shift perturbation assay carried out using the 500 MHz spectrometer at the University of the Western Cape (UWC). Definite changes were observed on addition of unlabeled MDM2-RING. However, interpretation of the changes was hampered by the previously-reported dilution-dependent changes to the spectrum of RBBP6-RING, resulting from changes to the monomer-homodimer equilibrium. Although there is evidence of changes in addition to the dilution dependent effects, definitive conclusions cannot be reached. The assay will have to be repeated, taking steps to minimize the dilution dependent effects.

GST pull-down studies also showed preliminary evidence of the interaction between the zinc finger of RBBP6 and the UBA domain from Ubch1. A number of  $^{15}\text{N}$ -enriched samples of UBA were produced in bacteria and three different chemical shift perturbation assays were carried out, using the 500 MHz spectrometer at UWC and the 700 MHz spectrometer in the United Kingdom (UK) equipped with a cryoprobe. The different  $^{15}\text{N}$ ,  $^1\text{H}$ -HSQC spectra of UBA showed that the domain exists in two different configurations: one showing good spectral dispersion characteristic of a fully folded configuration, the other showing reduced dispersion characteristic of a partially folded configuration. Two separate isoforms for the RBBP6 zinc finger were cloned and expressed; a longer construct which was expected to be partially unstructured, and a shorter construct, centered around the zinc knuckle domain, which was expected to be almost completely structured. However, chemical shift perturbation assays showed that both isoforms stabilized the partially unfolded form of UBA, leading to decay of the spectrum corresponding to the fully folded form, and growth of the spectrum corresponding to the partially unfolded form. This conclusion was supported by the fact that the NMR sample precipitated partially at stoichiometric ratios of 1:1 and higher ([UBA]:[zinc]). The possibility that the UBA unfolded spontaneously, due to the long periods spent in the NMR spectrometer at 25 °C, which was necessitated due to the low sensitivity of the spectrometer at UWC; was addressed by repeating the assay within the course of a single day, using a spectrometer equipped with a cryoprobe at King's College London, thereby negating this possibility.

## List of abbreviations

<b>Abbreviation</b>	<b>Full Name</b>
Amp	Ampicillin
APS	Ammonium persulfate
Bp	Base pairs
BSA	Bovine serum albumin
cDNA	Complementary DNA
CSD	Cold shock domain
C-terminus	Carboxyl terminus
DNA	Deoxyribonucleic acid
DTT	1,4-dithio-D-threitol
E1	E1 ubiquitin activating enzyme
E2	E2 ubiquitin conjugating enzyme
E3	E3 ubiquitin ligase
EDTA	Ethylenediaminetetra acetic acid
GST	Glutathione S-transferase
HA	Hemagglutinin
HECT	Homologous to E6-AP carboxyl terminus
IPTG	Isopropyl-1-thio-D-galactoside
Kb	Kilo base
kDa	Kilo Dalton
LB	Luria Bertani broth
MDM2	Murine double minute 2
MDMX	Murine double minute 4
MDR1	Multidrug resistance gene 1

Mpe1	Mutant PCFII extrogenic suppressor 1
mRNA	Messenger Ribonucleic acid
NMR	Nuclear magnetic resonance
N-terminus	Amino terminus
P2P-R	Proliferation potential protein-related
PACT	p53-associated cellular protein-testes derived
PAGE	Polyacrylamide gel electrophoresis
PBS	Phosphate buffer saline
PCR	Polymerase chain reaction
PDB	Protein Data Bank
PVDF	Polyvinylidifluoride
Rb	Retinoblastoma
RBBP6	Retinoblastoma binding protein 6
RCF	Relative centrifugal force
RBQ-1	Retinoblastoma-binding Q-protein 1
RING	Really interesting new gene
RNA	Ribonucleic acid
SDS	Sodium dodecyl sulphate
TE	Tris EDTA
TEMED	N, N, N', N'-tetramethylethylenediamine
Tfb	Transformation buffer
Tris	2-amino-2-hydroxymethylpropane-1, 3-diol
Ubc	Ubiquitin conjugating enzymes
UV	Ultra violet
YB-1	Y-box binding protein 1

## List of figures

<b>Figure Name</b>	<b>Page Number</b>
<b>Figure 1.1</b> Domain organization of RBBP6 proteins	5
<b>Figure 1.2</b> Cartoon diagram structure of the RBBP6-RING homo-dimer	8
<b>Figure 1.3</b> Domain structure of p53	9
<b>Figure 1.4</b> Tetramerization of p53 shows frequency and effect of mutations on p53	10
<b>Figure 1.5</b> Control of p53 levels by MDM2	12
<b>Figure 1.6</b> Ubiquitination pathway	15
<b>Figure 1.7</b> Cartoon representation of Ubch1	18
<b>Figure 1.8</b> Cartoon representation of UBC/UBA interaction interface	19
<b>Figure 1.9</b> Cartoon representation of Ubch1 UBA domain in complex with ubiquitin	19
<b>Figure 1.10</b> Cartoon representation of the MDM2-RING/MDM2-RING homo-dimeric complex (A) and MDM2-RING/MDMX-RING (B) hetero-dimeric complex	22
<b>Figure 2.1</b> pGEX-6P2 plasmid map	26
<b>Figure 3.1</b> Purification of GST-RBBP6-RING and GST-MDM2-RING	34
<b>Figure 3.2</b> Western Blot showing the pull-down of HA-RBBP6 by GST-MDM2-RING	37
<b>Figure 3.3</b> Chemical shift perturbation investigation of the interaction between RBBP6-RING and MDM2-RING	39
<b>Figure 3.4</b> Comparison of possible chemical shifts with dilution dependent shifts	41
<b>Figure 3.5</b> Intensity of isolated sample peaks of RBBP6 with the addition of MDM2-RING	42
<b>Figure 4.1</b> Purification of GST-UBA	45
<b>Figure 4.2</b> Purification of GST-zinc	47



<b>Figure 4.3</b> GST pull-down of zinc finger by GST UBA	48
<b>Figure 4.4</b> Chemical shift perturbation investigation of the interaction between UBA and zinc finger	50
<b>Figure 4.5</b> Design of the zinc-C finger construct	52
<b>Figure 4.6</b> The cloning of pGEX-6P2 zinc-C finger construct	53
<b>Figure 4.7</b> Purification of GST zinc-C finger	55
<b>Figure 4.8</b> GST pull-down of zinc-C finger by GST UBA	56
<b>Figure 4.9</b> Size exclusion of UBA, zinc-C and UBA/zinc-C superimposed	57
<b>Figure 4.10</b> Standard curve for the size exclusion column	58
<b>Figure 4.11</b> Chemical shift perturbation investigation of the interaction between UBA and zinc-C finger	60
<b>Figure 4.12</b> Comparison of $^{15}\text{N}$ , $^1\text{H}$ -HSQC spectrum of $^{15}\text{N}$ UBA without zinc-C finger	62



## List of tables

Table Name	Page Number
<b>Table 4.1</b> Primers used to amplify the zinc-C finger fragment	52
<b>Table 7.1</b> Materials and supplier used in this project	76
<b>Table 7.2</b> General stock solutions and buffers used in this project	78



## Table of Contents

Literature Review .....	1
1.1 Introduction.....	1
1.2 Retinoblastoma Binding Protein 6.....	2
1.3 Tumour Suppressor Gene p53.....	9
1.4 Y-box binding protein 1 (YB-1).....	12
1.5 Ubiquitin-proteasome pathway .....	14
1.5.1 Ubiquitin activating enzyme (E1).....	16
1.5.2 Ubiquitin-conjugating enzyme (E2) .....	16
1.5.3 Ubiquitin ligase (E3).....	20
1.6 Aims of the study.....	22
Materials and Methods .....	24
2.1 Antibodies used in this study.....	24
2.1.1 Primary antibodies .....	24
2.1.2 Secondary antibodies .....	24
2.2 Competent cells.....	24
2.3 Transformation.....	25
2.4 Cloning.....	25
2.4.1 Vector details .....	25
2.4.2 PCR amplification of gene fragments .....	26
2.4.3 Restriction digestion and ligation.....	27
2.4.4 Colony screening and sequencing .....	27
2.5 Protein expression and purification .....	28
2.5.1 Protein expression in bacteria.....	28
2.5.2 Expression of <sup>15</sup> N-enriched protein .....	28
2.5.3 Protein purification .....	28

2.5.4 GST removal and size exclusion chromatography.....	29
2.6 SDS-PAGE gel electrophoresis .....	29
2.7 Interaction Assay .....	30
2.7.1 GST pull-down assay.....	30
2.7.2 Western Blotting .....	31
2.8 NMR data collection and analysis.....	31
The structural characterization of the interaction between the RING finger domains of RBBP6 and MDM2 using Nuclear Magnetic Resonance Spectroscopy.....	32
3.1 Introduction.....	32
3.2 Recombinant protein expression and purification of RBBP6-RING and MDM2-RING .....	33
3.3 GST pull-down assay.....	35
3.4 Chemical shift perturbation of <sup>15</sup> N-labelled RBBP6-RING finger by unlabelled MDM2-RING .....	36
Characterization of the interaction between the zinc finger domain of RBBP6 and the UBA domain of Ubch1 using Nuclear Magnetic Resonance Spectroscopy .....	44
4.1 Introduction.....	44
4.2 Recombinant protein expression and purification of UBA and zinc finger proteins .....	44
4.3 GST pull-down assay.....	46
4.4 Chemical shift perturbation assay of <sup>15</sup> N-labelled UBA by unlabelled zinc finger .....	48
4.6 Recombinant expression and purification of zinc-C finger.....	54
4.7 The <i>in vitro</i> interaction between UBA and zinc-C finger .....	54
4.8 Protein interaction investigated by size exclusion chromatography.....	56
4.9 Chemical shift perturbation of <sup>15</sup> N-labelled UBA by unlabeled zinc-C finger .....	58
Conclusions and outlook .....	63
5.1 Characterization of the interaction between the RING finger domains of RBBP6 and MDM2 .....	63
5.2 Characterization of the interaction between the zinc finger domain of RBBP6 and the UBA domain of Ubch1.....	65
References.....	67

Appendix .....	76
List of Chemicals, kits and suppliers .....	76
List of general stock solutions and buffers .....	78
Amino Acid Sequences .....	78
Amino acid sequence of HA-RBBP6-RING .....	78
Amino acid sequence of MDM2-RING.....	79
Amino acid sequence of RBBP6-zinc finger .....	79
Amino acid sequence of RBBP6-zinc-C finger.....	79
Amino acid sequence of Ubch1 UBA .....	80



UNIVERSITY *of the*  
WESTERN CAPE

# Chapter 1

## Literature Review

### 1.1 Introduction

Retinoblastoma Binding Protein 6 (RBBP6) is a RING finger-containing protein which was initially identified due to its interaction with both major tumour suppressor proteins p53 and pRb (Sakai *et al.*, 1995). Human RBBP6 has been implicated in mRNA processing, cell cycle arrest and apoptosis, and is differentially regulated in a growing list of cancers (Li *et al.*, 2007, Dlamini *et al.*, 2019, Ntwasa, 2016). Members of the RBBP6 family are found in all eukaryotic genomes, in many cases at single copy number, but not in prokaryotes nor archaea. All eukaryotes express a minimal form of the protein containing the N-terminal, ubiquitin-like DWNN domain, a zinc finger domain and a RING finger domain (Pugh *et al.*, 2006). Through the RING finger, RBBP6 acts as an E3 ubiquitin ligase catalyzing ubiquitination and suppression of cancer-related proteins Y-box Binding Protein-1 (YB-1) and zBTB38 (Chibi *et al.*, 2008, Miotto *et al.*, 2014). RBBP6 is also reported to play a role in repressing p53 in embryogenesis, facilitating ubiquitination of p53 by MDM2, although it has been proposed that it does not directly participate in ubiquitination of p53 (Li *et al.*, 2007).

p53 is a nuclear transcription factor that transactivates many genes involved in the induction of cell cycle arrest and apoptosis. The p53 protein is normally expressed at a low level as it is regulated by proteasomal degradation mediated largely by Murine Double Minute 2 (MDM2), an E3 ubiquitin ligase (Ozaki and Nakagawara, 2011). Various post-translational modifications regulate p53, namely phosphorylation, methylation, acetylation, sumoylation, and ubiquitination (Weinberg, 2014). MDM2 is the main regulator of p53, targeting it for ubiquitination and subsequent degradation in the proteasome 26S proteasome (Stommel and Wahl, 2005). The importance of MDM2 in regulation of p53 is underlined by the fact that up to 10% of all human

cancers show an increased level of MDM2, resulting in down-regulation of p53 and consequent tumour growth (Stommel and Wahl, 2005). Unpublished data from our laboratory suggests that RBBP6 and MDM2 interact with each other through their RING finger domains. If so, it may represent a situation similar to that whereby MDMX regulates the activity of MDM2 through hetero-dimerization of their RING finger domains.

Y-box binding protein-1 is a multifunctional oncogenic protein whose transcriptional activity leads to poor prognosis in cancer, tumorigenesis, metastasis and chemotherapeutic resistance (Basaki *et al.*, 2010). When translocated to the nucleus, YB-1 is able to promote the transcription of the multidrug resistant 1 (MDR1) gene, leading to the development of drug resistance in the cell and aiding the survival of tumour cells, as well as inhibiting p53 induced cell death and transactivating promoters of genes involved in apoptosis signaling (Zhang *et al.*, 2003). Unpublished results from our laboratory show that RBBP6 is able to catalyze ubiquitination of YB-1 *in vitro*, using Ubch1 as E2 enzyme. Ubch1, also known as E2-25K, is one of a small class of E2 enzymes that contain an ubiquitin-associated domain (UBA) in addition to the E2-catalytic domain. Our results furthermore suggest that the zinc finger of RBBP6 interacts specifically with the UBA domain of Ubch1, an interaction which may play a role in the catalytic activity of Ubch1 with respect to RBBP6 and YB-1.

This investigation aims to characterize two interactions firstly between the RING finger domains of RBBP6 and MDM2, and secondly between the UBA domain of Ubch1 and the zinc finger of RBBP6. This will be carried out using a combination of GST pull-down and Nuclear Magnetic Resonance (NMR) spectroscopy. The hope is that by understanding these interactions, we are able to design ways to regulate the interactions which in turn may lay the foundation for the development of anti-cancer drugs.

## **1.2 Retinoblastoma Binding Protein 6**

RBBP6 is a 250 kDa protein found in all eukaryotic organisms but not in prokaryotes, that has been implicated in mRNA 3'-end processing and regulation of p53, among other important functions (Li *et al.*, 2007). The RBBP6 protein is a RING finger containing protein that has been

reported to suppress p53 during embryogenesis by facilitating its ubiquitination by MDM2. It has also been shown to catalyze ubiquitination and suppression of the oncogenic YB-1 protein *in vitro*, without the requirement for MDM2 (Chibi *et al.*, 2008, Sakai *et al.*, 1995).

RBBP6 was initially isolated and cloned in three sets of independent studies; Sakai and co-workers initially identified a 140 kDa human protein that binds to pRb which they named RBQ-1. RBQ-1 is a truncated human form of RBBP6, corresponding to residues 150-1146 of the full length human protein. RBQ-1 was extracted from a NCI-H69 cell (small lung carcinoma cell line) expression library; it was shown to bind to under phosphorylated pRb and not phosphorylated pRb; the RBQ-1 binding to pRb was also seen to be inhibited by adenovirus E1A protein thus suggesting that the binding of RBQ-1 to pRb had some physiological importance (Sakai *et al.*, 1995).

Simons and co-workers showed that when p53 was used as a probe, a 250 kDa mouse form of RBBP6 was extracted from a mouse testes expression library, which they named PACT (p53 Associated Cellular protein Testes derived) (Simons *et al.*, 1997). Bioinformatic analysis showed that RBQ-1 was as truncated version of PACT protein. PACT was shown to be able to bind to both wild type p53 and pRb but not mutant forms of p53; it was also able to interfere with p53-specific DNA binding activity, which could mean that PACT competes with the specific DNA binding for p53 (Simon *et al.*, 1997).

Witte and Scott identified a murine protein which they named Proliferation Potential Related protein (P2P-R), due to its association with heterogeneous nuclear ribonucleoprotein (Witte and Scott, 1997). Witte and Scott showed that, P2P-R expression levels are reduced during terminal differentiation, and the P2P-R cDNA encodes Rb1-Binding Peptide so that P2P-R is able to bind to the pocket domain of pRb (Witte and Scott, 1997). Gao and co-workers showed that the over-expression of RBBP6 promotes pro-metaphase arrest during mitosis and mitotic apoptosis in Saos2 cells. Since human Saos2 cells do not have functional p53 or pRb, their results implied that RBBP6 was able to promote apoptosis independently of these two tumor suppressor proteins (Gao *et al.*, 2002).



Mutant PCFII Extrogenic suppressor 1 (Mpe1) is the yeast *Saccharomyces cerevisiae* orthologue of human RBBP6 and contains only the DWNN domain, the zinc finger and the RING finger domains (Vo *et al.*, 2001). Vo and co-workers showed that when Mpe1 was inactivated using an antibody specific for Mpe1, there was defective 3'-end mRNA in yeast cells; the authors thus concluded that Mpe1 was essential for cleavage and polyadenylation of pre-mRNA, by promoting association of Cleavage Factor 1 (CF1) with the Cleavage and Polyadenylation factor (CPF) (Vo *et al.*, 2001). These claims were backed up by Lee and Moore over a decade later, who showed furthermore that all 3 domains of Mpe1 were required for native mRNA 3'-end processing (Lee and Moore, 2014). Witte and Scott showed that the truncated form of RBBP6 protein called Proliferation Potential-Related protein (P2P-R) was able to associate closely with heterogeneous nuclear ribonucleoprotein (hnRNPs) which is involved in RNA processing. They also showed that the P2P-R was co-precipitated with SmB, one of the core splicing proteins (Witte and Scott, 1997).

More recently, RBBP6 has been shown to also form part of the human 3'-end processing complex (Shi *et al.*, 2009). Di Giammartino and co-workers showed that the DWNN domain of RBBP6 binds directly to human Cleavage Stimulatory Factor-64 (CstF-64), a subunit of the 3'-end processing complex. Knock down of RBBP6 resulted in changes to the sites of cleavage for 3'-end processing, which led to the decrease of transcription levels of around 4000 genes, many of which were implicated in tumourigenesis (Di Giammartino *et al.*, 2014). The implication of this result is that one of the functions of RBBP6 is to up-regulate expression, at the transcriptional level of growth-promoting genes. Furthermore, they found evidence that isoform 3 of RBBP6, the 13 kDa isoform comprised primarily of the N-terminal DWNN domain, competes with the DWNN domain forming part of full length RBBP6 (isoform 1), and may thereby provide a mechanism for regulation expression of growth promoting genes.

The domain structure of the RBBP6 protein family is represented in Figure 1.1. All eukaryotes contain at least one isoform containing a region homologous to the first 3 domains of human RBBP6, namely the DWNN domain, the zinc finger and RING finger. Since it is the primary form of RBBP6 found in lower eukaryotes, this region has been hypothesized to contain the core ubiquitination activity of the protein. RBBP6 are orthologous in higher eukaryotic organisms

contains long, poorly-conserved C-terminal extensions, which in humans contains an SR domain, a Serine/Arginine-rich motif closely associated with mRNA processing and splicing in particular, as well as binding sites for p53 and pRb (Pugh *et al.*, 2006).

Human RBBP6 is expressed in 4 different isoforms, of 1732, 1758, 118 and 952 amino acids respectively (Q7Z6E9-1, Q7Z6E9-2, Q7Z6E9-3, and Q7Z6E9-4). Isoform 1 corresponds to the full length protein; isoform 2 is identical, apart from splicing out of a single exon. Isoform 3 is expressed from an alternative promoter, and contains the first 101 amino acid residues of isoform 1, followed by 17 residues not found in any other isoform. Isoform 4 contains the first 3 domains of the protein and the un-conserved C-terminus, but lacks a number of domains in between.

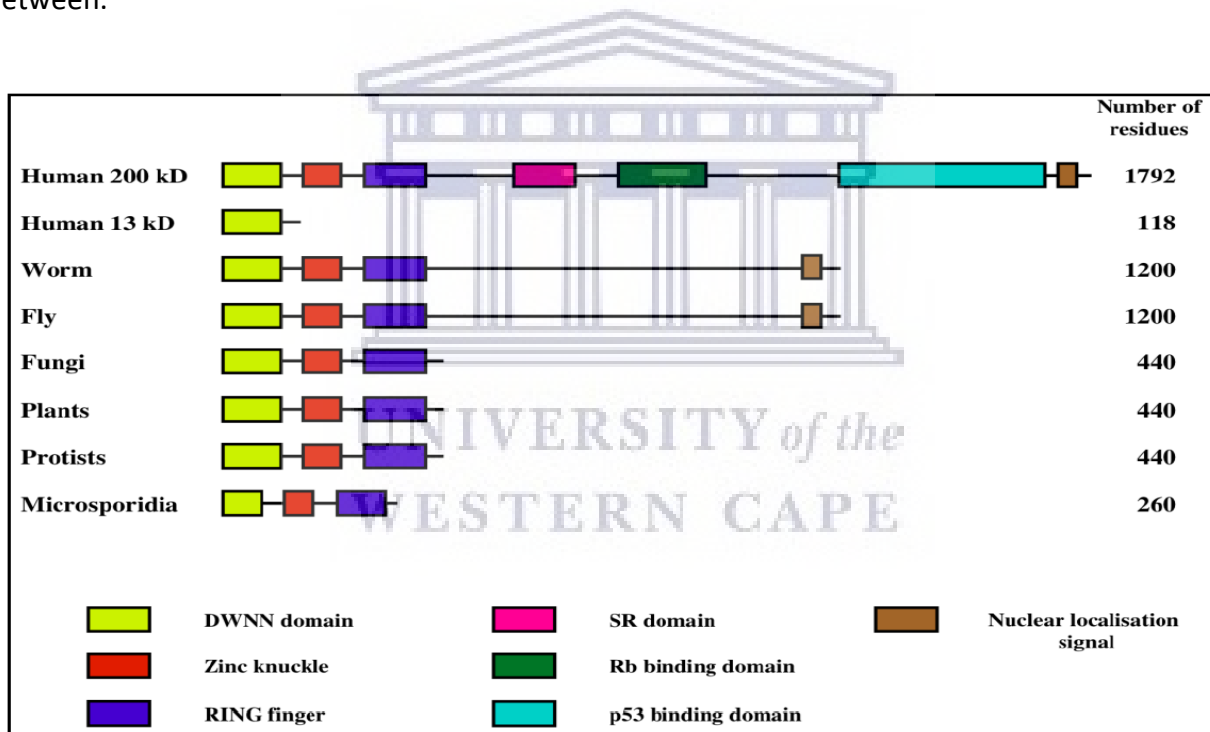


**Figure 1.1 Domain organization of RBBP6 proteins.** All RBBP6 homologues have an N-terminal ubiquitin-like domain, called the DWNN domain, followed by a CCHC zinc finger and a RING finger. Human RBBP6 isoform 1 has additional domains, including a proline rich domain (residues 337–349), SR domain (residues 679–773), as well as the pRb (964–1120) and p53 binding domains (residues 1142–1727). Human RBBP6 is also expressed as a 13 kDa protein containing only the DWNN domain, followed by an un-conserved C-terminal tail. (Figure taken from Pugh *et al.*, 2006)

## DWNN domain

The DWNN domain is found at the N-terminal domain of all RBBP6 isoforms and adopts a structure similar to that of ubiquitin, despite having less than 20 % homology to ubiquitin. Its structure has been determined in humans by NMR spectroscopy (Pugh *et al*, 2006). In addition to its similarity to ubiquitin, vertebrate DWNN domains all contain a di-glycine in the equivalent structural position to the catalytic di-glycine in ubiquitin, suggesting that it may become covalently conjugated to other proteins in a manner similar to ubiquitin and other ubiquitin-like modifiers (Pugh *et al*, 2006).

Isoform 3 of human RBBP6 consists almost entirely of the DWNN domain. Mbita and co-workers showed that the knock downs of isoform 3 of RBBP6 resulted in reduced G2/M cell cycle arrest; whereas over-expression resulted in increased G2/M cell cycle arrest. This demonstrates that isoform 3 may be a cell cycle regulator and play a role in mitotic apoptosis (Mbita *et al.*, 2011). Di Giammartino and co-workers showed that RBBP6 isoform 3, through its DWNN domain, was able to compete with full length RBBP6 (isoform 1) for the binding for the mRNA polyadenylation core machinery thereby inhibiting pre-mRNA 3'-end processing (Di Giammartino *et al.*, 2014).

## Zinc finger domain

The zinc finger are small protein domains in which coordination of a zinc ion contributes to the stability of the zinc domain. The first zinc finger was found in the *Xenopus* transcription factor IIIA (TFIIIA) protein, and more than 15000 zinc finger domains have subsequently been predicted to exist in 1000 different proteins (Gamsjaeger *et al.*, 2007). The zinc finger is diverse in structure and has a broad range of functions across many cellular processes, including transcription, translation, metabolic signaling, cell proliferation and apoptosis (Krishna *et al.*, 2003).

There are 14 different characterized classes of zinc finger proteins. The different classes differ by function as well as the identity and spacing of their zinc binding residues. The different classes have different roles within the cell but they are all able to mediate the interaction of proteins with other molecules such as DNA, RNA, other proteins or lipids (Matthews and Sunde, 2002). The zinc finger domain of RBBP6 is a CCHC type, also known as a zinc knuckle, a feature which is

conserved across all RBBP6 proteins. The structure of the zinc finger is composed of 2 short  $\beta$ -strands connected by a turn followed by a short helix. The RBBP6 zinc finger resembles the classical C2H2 motif, but a part of the helix and  $\beta$ -hairpin are truncated (Krishna *et al.*, 2003).

Some of the CCHC type zinc fingers have shown to be able to bind to ubiquitin. Cordier and co-workers were able to show using NMR chemical shift analysis that in the regulatory C-terminal half of NF- $\kappa$ B essential modulator (NEMO) where the zinc finger motif was located, the zinc-finger was able to form a complex with ubiquitin (Cordier *et al.*, 2008).

### **RING finger domain**

Through its RING domain, RBBP6 acts as an E3 ubiquitin ligase and facilitates the interaction between p53 and Murine Double Minute 2 (MDM2), causing the ubiquitination of p53 and its subsequent degradation in the proteasome (Li *et al.*, 2007). The RING finger domain is a well-known zinc binding cysteine rich motif consisting of a sequence of Cys-X (2)-Cys-X (9-39)-Cys-X (1-3)-His-X (2-3)-Cys-X (2)-Cys-X (4-48)-Cys-X (2)-Cys, (where X can be any amino acid and X(1-3) is equivalent to 1, 2 or 3 amino acids, of any kind), usually abbreviated to C3HC4 (Joazeiro and Weissman, 2000). RING fingers are small domains of about 70 residues in length which fold with the aid of two  $Zn^{2+}$  ions that help stabilize the structure. RING finger domains are classified by the pattern of the zinc coordinating residues; C3HC4 is the most common, with the other classes being C3H2C3, C2H2C4 and C4C4 RING fingers. RBBP6 is a C4C4 RING finger, on account of the 8 conserved cysteine residues (Kappo *et al.*, 2012). All RING finger domains share the same overall fold which consists of two large loops each stabilized by a zinc ion lying parallel to an  $\alpha$ -helix, together packing against a short three-stranded  $\beta$ -sheet (Kappo *et al.*, 2012).

Some RING fingers have been shown to form homo-dimers, and some require dimerization for ubiquitination activity (Nikolay *et al.*, 2004). Dimerization usually takes place along the  $\beta$ -sheets and is stabilized by the interactions between the N and C-termini of both RING monomers (Hashizume *et al.*, 2001). Structural studies carried out by Kappo and co-workers showed that the RBBP6 RING finger domain homo-dimerizes *in vitro*, as shown in Figure 1.2. Progressive dilution of the protein led to chemical shift changes in the  $^{15}N, ^1H$ -HSQC spectrum of the domain

linking the dimeric to the monomeric forms of the protein. From this data an estimate of the dissociation constant of the interaction ( $K_D$ ) of 100  $\mu\text{M}$  was obtained.  $^{15}\text{N}$  relaxation measurements confirmed that at lower concentrations the protein was almost totally monomeric whilst at higher concentrations it was almost all dimeric (Kappo *et al.*, 2012). Based on the structure of the homo-dimer, mutant N312D and K313E were identified that would disrupt the homo-dimer. The  $^{15}\text{N}$ ,  $^1\text{H}$ -HSQC spectra of both mutants were exactly consistent with the low concentration limit of the dilution series, confirming that the mutants were indeed totally monomeric.

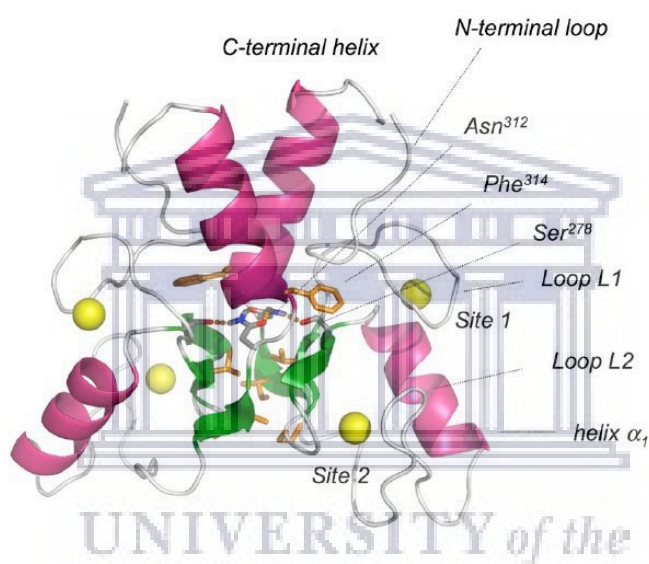


**Figure 1.2** Cartoon diagram structure of the RBBP6-RING homo-dimer. The interface shows the triple stranded  $\beta$ -sheets (green),  $\alpha$ -helices (pink) and zinc ions (yellow). (Figure taken from Kappo *et al*, 2012)

MDM2 is a RING finger containing E3 ubiquitin ligase protein (Weinberg, 2014). In 2007, using a mouse RBBP6-knock out model, Li and co-workers reported that RBBP6 enhances ubiquitination of p53 by HDM2, the human homolog of MDM2. On the other hand over-expression of RBBP6 in HEK293 cells yielded no change to the ubiquitination of p53, whereas co-transfection of HDM2 along with RBBP6 led to an increase in ubiquitination and degradation of p53. Repeating the same experiment using an RBBP6 mutant which lacked the RING domain produced no improvement in the degradation of p53. Li and co-workers concluded from this RBBP6 does not play a direct role

in ubiquitination of p53, but may function as a scaffold to support the assembly of the HMD2-p53 complex (Li *et al.*, 2007).

### 1.3 Tumour Suppressor Gene p53

Due to the dangers of unregulated cell growth on multi-cellular organisms, cells have an effective system to identify sources of dysregulation, taking preventative action and in more extreme cases leading to apoptosis of the cell. This regulatory system is governed by the tumour suppressor protein p53. The p53 protein receives information about irregularities in the cell, activating the p53 protein which in response activates one or more of a number of pathways. These pathways include halting of the cell cycle to prevent further growth, trying to repair the damage or, if the damage within the cell is too severe to be repaired, initiating apoptosis of the damaged cell (Weinberg 2014).

The p53 gene in humans codes for an intermediately-sized protein of 393 residues, which can be divided into a number of functional domains, as shown in Figure 1.3 (Joerger and Fersht, 2008; Wells *et al.*, 2008).



**Figure 1.3 Domain structure of p53.** The human p53 consists of an N-terminal transactivation domain (residues 1-61), a proline rich region (residues 62-93), a central DNA binding domains (residues 94-312), a tetramerization domain (residues 312-360) and the C-terminal regulatory domains (residues 361-393). (Figure adapted from Joerger and Fersht, 2008).

The N-terminal transactivation domain (residues 1 – 61) serves as a binding site for multiple interacting proteins, including components of the transcription machinery, transcriptional coactivators and the negative regulators MDM2 and Murine Double Minute X (MDMX). The N-terminal transactivation domain is unfolded in the absence of an interacting partner. The proline-

rich region (residues 62 – 93) linking the transactivation domain to the DNA binding domain contains 5 PXXP (P representing proline and X represents any amino acid) motifs.

The p53 binds DNA in a sequence-specific manner via the central DNA binding domain (residues 94 – 312). The clustering of most cancer-causing mutations within this region has led to it becoming the focus of many studies aiming to understand the role of mutations in inactivating p53 (Pavletich *et al.*, 1993). The DNA binding domain is natively folded but only marginally stable; many oncogenic mutations are able to destabilize it to the point that it is predominantly unfolded at body temperature. (Natan *et al.*, 2011). The p53 activity depends on its conformation. The protein exists in a latent conformation or active conformation which is either inactive for DNA or active for DNA binding respectively. The conformation can be modified by mutations in the DNA binding domain thus preventing DNA binding (Chene, 2001).

In its active form p53 exists as a tetramer, which is mediated by the tetramerization domain (residues 313-360). Cells carrying a single mutant p53 allele often retain the ability to form tetramers, but these may not function normally. This leads to dominant negative function, in which a single mutant allele can reduce the activity of p53 to less than the 50 % that would be expected if the alleles did not interfere with each other. As illustrated in Figure 1.4, in the most extreme case a single mutant allele may reduce the effective activity to 1/16<sup>th</sup> of its value when both alleles are wild type (Weinberg 2014).

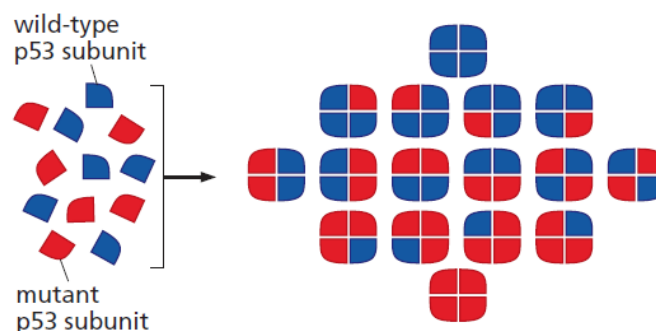


**Figure 1.4 Tetramerization of p53 shows the frequency and effect of mutations on p53.** Cells with a mixture of wild type mutant p53 may form heterozygous p53 tetramers, thus compromising 15 out of the 16 tetramer that may form.

The C-terminal domain (residues 360 – 393) is the site of post-translational modifications, regulating its binding to DNA (Wells *et al.*, 2008). These post-translational modifications include ubiquitination, phosphorylation, acetylation, sumoylation and methylation (Joerger *et al.*, 2004). Ubiquitination of the C-terminus is carried out by MDM2, which targets p53 for proteasomal degradation (Brooks and Gu, 2006), whilst acetylation of the C-terminus enhances the sequence specific binding of p53 to DNA (Gu & Roeder, 1997).

### 1.2.1 Regulation of p53

p53 is regulated by various post-translational modifications including phosphorylation, methylation, acetylation, ubiquitination and sumoylation. p53 levels are generally low as consequence of its short half-life of only around 30 minutes. The main regulator of p53 is the MDM2 protein an E3 ubiquitin ligase which ubiquitinates p53, leading to its degradation in the proteasome (Weinberg, 2014). Between 5 to 10 % of all human cancers show elevated levels of MDM2, resulting in increased p53 down-regulation, thus allowing tumours to thrive (Stommel & Wahl, 2005).

MDM2 binds to p53 through the hydrophobic cleft of MDM2 and the N-terminal transactivation domain of p53; the  $\alpha$ -helix of p53 is buried in the hydrophobic cleft of MDM2 thereby preventing the N-terminal transactivation domain of p53 from transcribing anything. MDM2 is an E3 ligase that catalyzes the ubiquitination of p53, thus resulting in p53 being moved out of the nucleus and into the cytoplasm where the proteasome degrades the ubiquitinated p53. MDM2 contains a nuclear export signal, which allows it to transport p53 out of the nucleus into the cytoplasm (Brooks & Gu, 2005, Lim *et al.*, 2004).

The MDM2 gene promoter contains the DNA-binding motif of p53, which means that elevated levels of p53 leads to elevated levels of MDM2, and vice versa. Hence p53 is the architect of its own destruction, leading to a negative feedback loop which suppresses the levels of both p53 and MDM2 in resting cell (Weinberg, 2014) (see Figure 1.5). While MDM2 is the main regulator of p53, a number of other proteins are also known to regulate p53. These include ARF, MDMX/MDM4, Cop1 and the Pirh2 proteins (Stommel and Wahl, 2005). ARF (alternative reading



frame) binds to MDM2, preventing MDM2 from binding to p53 and ubiquitinating it. MDMX is a p53 binding protein and is very similar to MDM2 protein, and has been shown to work together with MDM2 to enhance the ubiquitination of p53. MDMX binds to p53 but does not ubiquitinate it, but together with MDM2 they form a hetero-dimeric complex through their RING domains (Stommel and Wahl, 2005, Gosh et al., 2003). Pirh2 and Cop1 are E3 ligases that catalyzes the ubiquitination of p53; their expression is induced by p53 transcriptional activity and thus also participate in a negative feedback loop with p53 (Lee and Lozano, 2006).

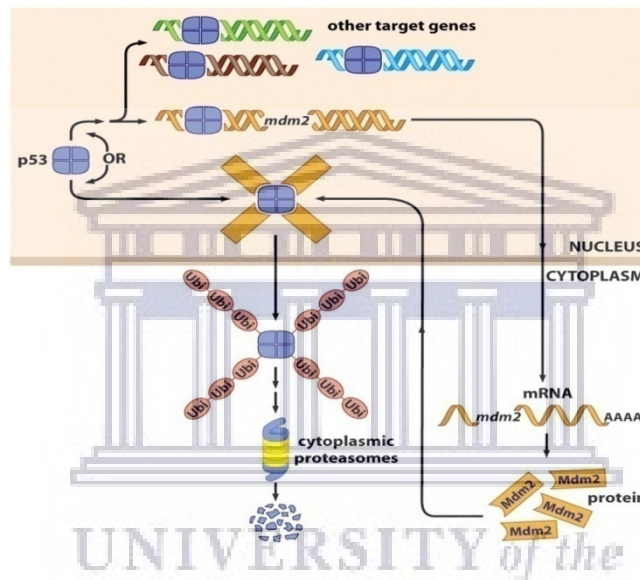


**Figure 1.5 Control of p53 levels by MDM2.** p53 tetramers bind to the promoters of a large constituency of target gene whose transcription the induce, including the gene encoding MDM2; this results in a large increase in MDM2 mRNA and MDM2 protein. The MDM2 molecules then bind to the p53 protein subunits and initiate their ubiquitylation, resulting in export to the cytoplasm resulting in degradation in proteasome. This negative-feedback loop ensures that p53 levels eventually sink back to a low level and, in undisturbed cells, helps to keep p53 levels very low (Figure taken from Weinberg, 2014)

#### 1.4 Y-box binding protein 1 (YB-1)

YB-1 is a multi-functional protein that is involved in a number of growth-promoting processes, including transcriptional regulation of many genes, pre-mRNA splicing in the nucleus, mRNA packaging, mRNA stabilization and translational control. YB-1 is involved in a number of import cellular processes, including differentiation, proliferation and stress response, making YB-1 an

important factor in embryonic development (Dmitry *et al.*, 2014). YB-1 contains 3 domains namely an alanine/proline rich N-terminal domain, a Cold Shock Domain (CSD) and a C-terminal domain containing alternating positively and negatively charged amino acid clusters (Kljashorny *et al.*, 2015). The cold-shock domain is highly similar to those found in prokaryotic cold shock proteins. The CSD functions as a RNA chaperone which destabilizes RNA secondary structures, thereby promoting translation at low temperatures (Matsumoto & Wolffe, 1998). The CSD of YB-1 contains 2 RNA binding motifs, namely ribonucleoprotein 1 (RNP-1) and ribonucleoprotein 2 (RNP-2); the CSD also folds into a 5 stranded anti-parallel  $\beta$ -barrel (Kloks *et al.*, 2002).

YB-1 protein functions in both the cytoplasm and in the cell nucleus. It's also secreted from cells and by binding to receptors on the surface of the cell it can activate intracellular signaling. When it passes from the cytoplasm into the cell nucleus, YB-1 is able to activate the transcription of genes of many protective proteins, including those that will provide the cell with multidrug resistance. During DNA repair in the nucleus, YB-1 enhances the cell resistance to xenobiotics and ionizing radiation. As a result, YB-1 nuclear localization serves as an early marker of multidrug resistance of malignant cells (Eliseeva *et al.*, 2011).

YB-1 was discovered as a DNA binding protein that interacted with an inverted CCAAT box (Y-box) in the promoter of the major histocompatibility complex class II genes (Didier *et al.*, 1988). The Y-box has been shown to be present in the promoter region of multidrug resistance 1 (MDR1) gene. The interaction between YB-1 and the Y-box results in the increased expression of MDR1 gene coding for P-gp in response to DNA-damaging agents (Szczuraszek *et al.*, 2011). The expression of these MDR proteins reduces the chances of finding potentially effective drugs to be used in subsequent cancer treatments. Many clinical studies have shown YB-1 to be involved in tumourigenesis and poor patient outcome (Yan *et al.*, 2014).

Zhang and co-workers showed that p53 was required for the nuclear localization of YB-1; they showed that genotoxic stress induced the nuclear translocation of YB-1 but only in cells with wild type p53 (Zhang *et al.*, 2003). Zhang and co-workers also speculated that there is a direct correlation between nuclear YB-1 with drug resistance and poor tumour prognosis; since p53 translocates YB-1 to the nucleus where the MDR1 gene is then activated. Zhang and co-workers

also showed that YB-1 inhibits p53-induced cell death and its ability to transactivate promoters for genes involved in apoptosis signaling; this shows that some forms of p53 can cause YB-1 to accumulate in the nucleus thus resulting in the inhibition of p53 activity as well as aiding in the development of drug resistance in the cell which in turn aids the survival of tumour cells (Zhang *et al.*, 2003). Basaki and co-workers showed that YB-1 also promotes the progression of the cell cycle through the CDC6-dependent pathway in human cancer cells (Basaki *et al.*, 2010). The depletion of YB-1 resulted in a suppression of cell proliferation and expression of cell cycle related gene CDC6 in cancer cells (Basaki *et al.*, 2010).

Much research has shown nuclear-localized YB-1 to be closely associated with poor prognosis of several types of human cancers such as breast, prostate, lung and colon cancer (Mastumoto & Bay, 2005). YB-1 could serve as a possible target for therapeutic intervention as Lee and co-workers showed that YB-1 in breast cancer cells over expresses human epidermal growth factor receptor (her-2). Using siRNA to inhibit YB-1 in both *in vitro* and *in vivo*, 6 out of the 7 cancer cell lines showed suppression in growth (Lee *et al.*, 2008).

There are a number of strategies through which YB-1 could be regulated. One is by regulating YB-1 at a cellular level via the ubiquitin proteasomal pathway. Chibi and co-workers showed, using a yeast two hybrid screen that RBBP6 was an interacting partner of YB-1 and the overexpression of full length RBBP6 promoted the ubiquitination of YB-1 leading to the eventual degradation via the proteasome (Chibi *et al.*, 2008).

## 1.5 Ubiquitin-proteasome pathway

The ubiquitin-proteasome pathway is a rapid and efficient system in which specific proteins are removed from the cell. The process involves tagging specific proteins with ubiquitin molecules, which are then recognized by the 26S proteasome complex. This results in the proteasome digesting the protein into smaller peptides and recycling them for use by the cell (Pant and Lozano, 2014). Ubiquitination is a post-translational modification in which the C-terminal backbone carboxyl group of ubiquitin is bonded to the sidechain amino group of a lysine molecule of the substrate. The bond formed is identical to a peptide bond, but since the groups involved

in the bond are not both on the backbone, it is referred to as an iso-peptide (essentially a pseudo-peptide) bond instead. Ubiquitination signals a number of different outcomes including protein sorting, localization, activation, repression and degradation (Capili & Lima 2007). Ubiquitin is attached as either monomers or as a poly-ubiquitin chain, in which the seven lysine residues on the ubiquitin serve as acceptors for the attachment of more ubiquitin molecules (Woelk *et al.* 2007). A poly-ubiquitin chain of four or more ubiquitin molecules linked by their Lysine 48 residue, a so-called Lysine 48 linked chain, targets the protein to the 26S proteasome, where it is degraded. Poly-ubiquitin chains linked via Lysine 63 act as a non-proteolytic signal for intracellular trafficking, DNA repair and signal transduction (Deshaies and Jaozeiro. 2009).

The tagging of target proteins involves multiple steps. Step 1 requires an ATP-dependent formation of a thioester bond between the C-terminal Glycine 76 residue of ubiquitin and the E1 ubiquitin-activating enzyme (Haas *et al.*, 1982). In step 2 the ubiquitin-thioester bond is transferred to a conserved cysteine residue on the E2 ubiquitin-conjugating enzyme. Finally in step 3, the E2 catalyzes the formation of an iso-peptide bond between ubiquitin C-terminal carboxylate group and the  $\epsilon$ -amino group of the substrate lysine residue, via an E3 ubiquitin ligase (Ciechanover, 1998). Additional ubiquitin molecules are added to the Lys48 residue of the conjugated ubiquitin, building a poly-ubiquitin chain recognized by the 19S proteasome subunit (Hershko *et al.*, 1998).

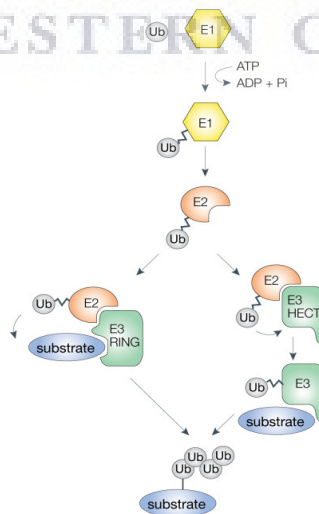


**Figure 1.6 Ubiquitination pathway.** Three types of enzyme are required for the ubiquitination of substrates: ubiquitin-activating (E1), ubiquitin-conjugating (E2) and ubiquitin-protein ligase (E3) enzymes (Figure taken from Woelk *et al.* 2007).

### 1.5.1 Ubiquitin activating enzyme (E1)

The E1 enzyme activates ubiquitin for an array of downstream conjugating enzymes and catalyzes the first step in ubiquitin-protein bond formation (Haas & Rose, 1982). The reaction starts with the binding of ATP by the E1, followed by ubiquitin which leads to the formation of an ubiquitin adenylate intermediate which acts as the donor of ubiquitin to a cysteine in the E1 active site. The E1 carries two molecules of activated ubiquitin, one as a thiol ester bonded ubiquitin and the other as an adenylate. The thiol ester linked ubiquitin is then transferred to the E2 enzyme (Pickart, 2001). The E1 enzyme has very little affinity for ubiquitin prior to the binding of ATP, thus suggesting that this is an ATP dependent reaction. The E1 enzyme is also efficient in the ATP-AMP exchange, this high efficiency of the E1 allows the sufficient supply of activated ubiquitin for the entire downstream conjugation reaction to be produced, despite the concentrations of E1 being less than the concentration of E2 in the reaction (Pickart, 2001).

### 1.5.2 Ubiquitin-conjugating enzyme (E2)

The E2 enzyme is the central component in the transfer of ubiquitin to targets in diverse conjugation pathways. Ubiquitin is transferred from E1 to a conserved cysteine residue on the E2 enzyme. The E2 will then catalyze the formation of an iso-peptide bond between the ubiquitin C-terminal carboxylate group and the  $\epsilon$ -amino group of the substrate lysine residue, via an E3 ubiquitin ligase (Ciechanover, 1998). The E2's differentiate the effects on downstream substrates either with single ubiquitin/ubiquitin like protein molecules or as a chain of it. The E3's may be involved in substrate selection but the E2 are the main determinants for selection of the lysine to construct ubiquitin chains thus is in control of the cellular fate of the substrate (Van Wijk & Timmers, 2010). E2 enzymes have a 150-200 amino acid conserved region called the ubiquitin conjugating domain (UBC) which contains the catalytic cysteine residue that forms a thiol ester bond with ubiquitin and interacts with the E1 (Burroughs *et al.*, 2008). The E2's are divided into 4 different classes based on the extensions to their catalytic core; class I only have the catalytic core and has no extensions; classes II and III have an additional N and C terminal domains respectively, whilst class IV have both N and C terminal domain extensions. These extensions

have functional differences and are involved in subcellular localization, stabilization of the interaction with E1 or modulation of the activity of the interacting E3 (Van Wijk & Timmers, 2010).

### 1.3.2.1 Ubiquitin-conjugating enzyme H1

E2-25K, also known as Ubiquitin-conjugating enzyme H1 (UbcH1) and Huntington Interacting Protein 2 (HIP2) was identified as 25 kDa mammalian E2 conjugating enzyme with the ability to form lysine-48 linked poly-ubiquitin chains in the absence of E3 Ligase (Wilson *et al.*, 2011). The ubiquitin-proteasomal protein degradation system is implicated in a few protein misfolding related diseases, in particular the presence of ubiquitin is seen in intranuclear inclusions in Huntington's disease (Kalchman *et al.*, 1996), and also in neurofibrillary tangles in Alzheimer's disease (Song & Jung, 2004). This may be an indication of a malfunction within the ubiquitin-proteasome pathway contributing to the accumulation of misfolded protein aggregates. UbcH1 is upregulated in Alzheimer's diseases and its presence is required for the toxicity generated by A $\beta$  fragments (Song *et al.*, 2003). UbcH1 is also a binding partner of huntingtin, the main protein mutated in Huntington's disease (Kalchman *et al.*, 1996).

UbcH1 consists of a conserved 150 amino acid N-terminal ubiquitin-conjugating domain (UBC) followed by a 50 amino acid C-terminal ubiquitin-associated domain (UBA) as shown in Figure 1.7 (Wilson *et al.*, 2009). UbcH1 and its homolog represent the only known E2 enzymes that contain an UBA domain as well as the conserved catalytic ubiquitin conjugating (UBC domain) domain. The UBC consists of an N-terminal  $\alpha$ -helix followed by four anti-parallel  $\beta$ -strands along with another three  $\alpha$ -helices (Wilson *et al.*, 2009). The UBA domain contains a highly conserved triple alpha helix arranged in a way that allows the loop between the first two helices (MGF motif) to connect to the end of helix 3. The first alpha helix begins at the start of the conserved UBA domain followed by a loop that binds the residues in the hydrophobic core (Madura, 2002). NMR analysis of the UBA domain has shown multiple hydrophobic patches that could participate in protein-protein interactions; since these hydrophobic patches are present on opposite sides of the UBA domain it is possible for more than one ligand to be bound simultaneously (Madura, 2002). The positioning of the helices of UBA is determined by ring stacking between the side chains of residues Tyr162 in helix 6 and Trp188 in the loop between helices 7 and 8 as seen in Figure 1.8.

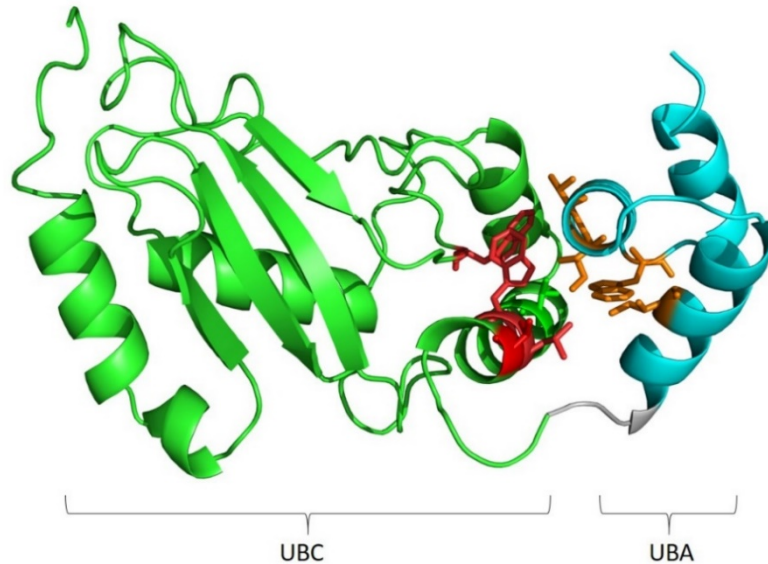


**Figure 1.7 Cartoon representation of UbchH1.** The UBC domain is shown in green and the UBA in turquoise. The sidechains contributing to the hydrophobic interface between the domains are shown in red and orange, respectively (Figure generated using PyMOL).

Figure 1.8 shows the UBC-UBA interaction interface which consists of hydrophobic interactions between residues Met140, Leu147 and Val151 (helix 5) of the UBC domain and residues Ile166 (helix 6) and Ile180 (helix 7) of the UBA domain. In addition there is also 3 hydrogen bonds that exist between the side chains of the UBC and UBA domain, namely between Thr144-Trp188, Trp148-Ser184 and Tyr152-Asn177.

Several initial studies have suggested that the UBA domain was needed for the formation of Lys48-linked poly-ubiquitin chain but not necessarily for normal UBC ligase activity (Haldeman *et al.*, 1997). However the location of the truncation of UBA from UbchH1 was important as slightly longer UBC constructs (still lacking the UBA domain) were still able to catalyze poly-ubiquitin formation although not as well as full length UbchH1 (Pitchler *et al.*, 2005). In the absence of an E3 ligase, deletion of the UBA domain resulted in inefficient formation of poly-ubiquitin chain linkages, indicating that the UBA domain helps direct Lys48-linked chain synthesis in the absence of an E3 partner (Wilson *et al.*, 2011).

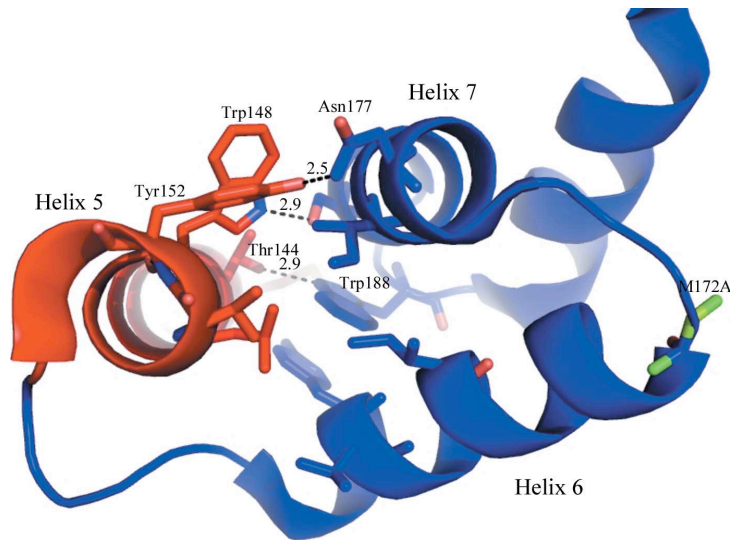


**Figure 1.8 Cartoon representation of UBC/UBA interaction interface.** Helix 5 (red) of UBC domain and helix 6 and 7 (blue) of the UBA domain are involved in the interaction. The three hydrogen bonds between the UBC/UBA domains are shown as dashed lines with length of the hydrogen bonds in Å (Figure taken from Wilson *et al.*, 2009).

Wilson and co-workers identified side chain residues involved in the interaction between UBA and ubiquitin as seen in Figure 1.9. They determined that the interaction interface between the UBA domain of Ubch1 and ubiquitin was made up of residues Met172, Gly173, Phe174 and Leu198 of the UBA domain and Arg42, Ile44, Lys48, Gln49, Leu71 and Arg72 for ubiquitin (Wilson *et al.*, 2011).

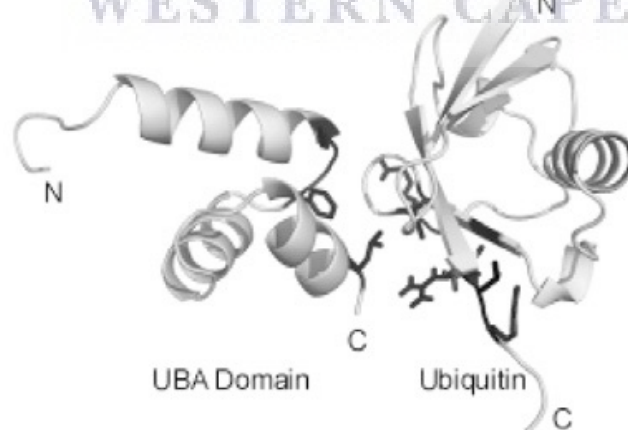


**Figure 1.9 Cartoon representation of Ubch1 UBA domain in complex with ubiquitin.** The UBA domain is represented on the left and ubiquitin is shown on the right. The side chain residues involved in the interaction are shown as sticks (Figure taken from Wilson *et al.*, 2011.)



### 1.5.3 Ubiquitin ligase (E3)

The role of the E3 enzymes is to bring together the substrate, through its substrate-specific binding domain, and the ubiquitin-conjugated E2 enzyme, through its E2-binding domain. There are two main classes of E2-binding domains, RING fingers and HECT domains. (Metzger *et al.*, 2014). The HECT-type E3s catalyze the transfer of ubiquitin in three steps: the HECT domain binds to the E2, the ubiquitin is covalently attached to the catalytic cysteine on the HECT domain and from there to the substrate. RING-type E3s on the other hand, do not become covalently attached to the ubiquitin but act merely as an adaptor protein, bringing the ubiquitin charged E2 and substrate together (Metzger *et al.*, 2014).

#### 1.5.3.1 Murine Double Minute 2

Murine Double Minute 2 is a RING finger containing E3 ubiquitin ligase protein which ubiquitinates p53, leading to the subsequent proteasomal degradation of p53 (Weinberg, 2014). MDM2, along with its close homologue MDMX, inhibits p53 by binding to the N-terminal transactivation domain of p53 thus inhibiting the transcription ability of p53 (Lai *et al.*, 2002). MDM2 is tightly regulated such that p53 activation is still allowed under certain conditions. Under stressful conditions, MDM2 is post-translationally modified and temporarily stops its inhibition of p53 so p53 can respond to the damage or stress (Shadfan *et al.*, 2012).

MDM2 and MDMX are structurally highly similar with lengths of 491 and 490 amino acid residues respectively. MDM2 and MDMX share three conserved regions, namely a RING finger domain, a zinc finger domain and a p53 binding site (Tanimura *et al.*, 1999). Despite the similarities between the two proteins, MDMX does not show any E3 ubiquitin ligase activity, and appears to serve only to enhance the E3 activity of MDM2 by forming a hetero-dimer with MDM2 (Wang & Jiang, 2012) (Badciong & Haas, 2002). MDMX also does not contain nuclear localization and nuclear export signal sequences; therefore unlike MDM2, MDMX is unable to move between the nucleus and cytoplasm. MDMX needs to interact with MDM2 to allow its translocation into the nucleus (Tanimura *et al.*, 1999).

Previous experiments conducted by Tollini and Zhang, knocking out MDM2 and/or MDMX genes in mice have shown that MDMX is required for regulation of p53 in most but not all tissues, whereas MDM2 is required in all tissues that were examined (Tollini & Zhang, 2012). Further biochemical studies suggested that MDM2 and MDMX are able to act in conjunction to regulate p53 but are also able to act independently from each other (Linares *et al.*, 2003). The effectiveness of MDM2 as an E3 ubiquitin ligase is relatively low when levels of MDMX are low. The absence of MDMX results in the formation of MDM2 homo-dimers, which catalyze auto-ubiquitination of MDM2 and its subsequent degradation. As the levels of MDMX increase the effectiveness of MDM2 as an E3 ubiquitin ligase increases as well. Increasing levels of MDMX results in the formation of MDM2/MDMX hetero-dimeric complexes; decreasing auto-ubiquitination of MDM2 and promoting p53 ubiquitination (Linke *et al.*, 2008).

Structural studies conducted by Kostic and co-workers have shown that the MDM2-RING domain forms a homo-dimer *in vitro*. The intermolecular NOEs of the homo-dimer structure were determined by comparing 4 sets of 3D  $^1\text{H}$   $^{15}\text{N}$  NOESY-HSQC spectra. The four 3D spectra acquired were  $^{15}\text{N}$  HDM2,  $^{15}\text{N}$  HDMX, and two complex,  $^{15}\text{N}$  HDM2 with unlabeled HDMX and  $^{15}\text{N}$  HDMX with unlabeled HDM2. Comparison of the 4 spectra identified 24 intermolecular NOEs between the subunits. Spatial constraints derived from these NOEs were added to the intramolecular constraints and used to generate a structure of the complete complex (Kostic *et al.*, 2006). The structure of the heterodimer was subsequently reported by Linke and co-workers using X-ray crystallography (Linke *et al.*, 2008). A schematic representation of the complex is shown in Figure 1.10 (B).

The main interaction involves the  $\beta 3$  and C-terminal residues from the one subunit with  $\beta 2$  from the other subunit; hence, the core of the dimer is formed by a six stranded  $\beta$ -barrel, which is filled by hydrophobic side chains. When comparing the MDM2/MDMX hetero-dimer (Figure 1.8 (B)) with the MDM2 homo-dimer (Figure 1.10 (A)), the structural arrangements of the 2 dimers are very similar (Linke *et al.*, 2008).

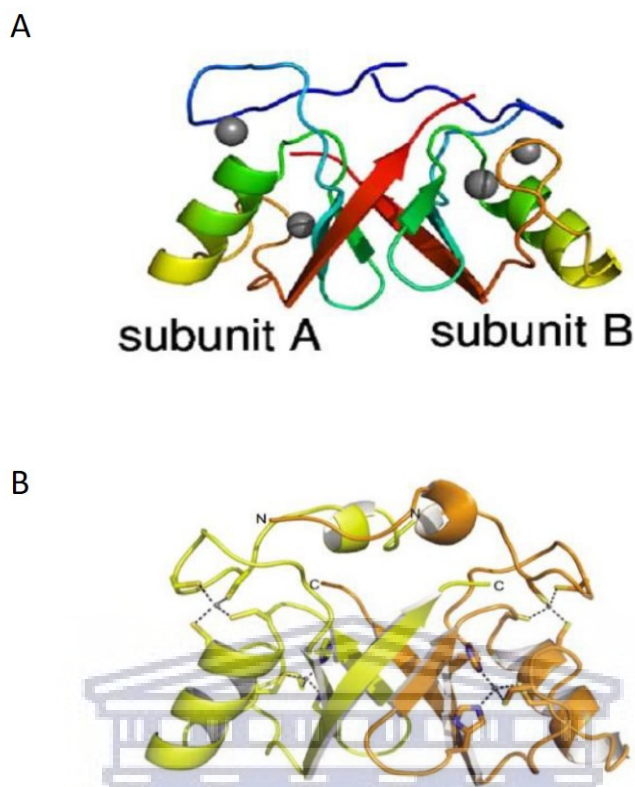


**Figure 1.10** Cartoon representations of the MDM2-RING/MDM2-RING homo-dimeric complex (A) and MDM2-RING/MDMX-RING (B) hetero-dimeric complex. (A) The two subunits of MDM2/MDM2-RING homo-dimer is shown. Zinc ions and coordinating residues are represented as spheres and sticks respectively (Figure taken from Kostic *et al*, 2006). (B) MDM2-RING and MDMX-RING are shown in orange and yellow respectively. The coordinating residues and zinc ions are represented as sticks and spheres respectively (Figure taken from Linke *et al*, 2008).

## 1.6 Aims of the study

RBBP6 is hypothesized to activate the p53 ubiquitination activity of MDM2 by interacting directly with it in a manner that required the RING finger of RBBP6. This is similar to the manner in which MDMX activates MDM2; in that case MDM2 and MDMX form a heterodimer through their respective RING finger domains. The RING finger domain of RBBP6 has been shown to form homo-dimers with very similar structure to the MDM2/MDMX hetero-dimer. Previous results from our laboratory have shown that RBBP6 and MDM2 form a hetero-dimeric complex, possibly through their RING finger domains.

The aim of the first part of the project was to use perform GST pull-down assays to confirm the interaction *in vitro*. This would be followed by performing  $^{15}\text{N},^1\text{H}$ -HSQC-based chemical shift perturbation assays to assess the affinity of the interaction and to identify residues on each domain involved in the interaction. This information will be used to build a model of the interaction complex and to determine the position of the interaction interface.

UbcH1, also known as E2-25K or Huntingtin Interacting Protein 2 (HIP2), interacts with the Huntingtin protein and has been identified as a major determinant of amyloid- $\beta$  neurotoxicity, leading to Huntingtin's disease. UbcH1 is one of a small group of E2 enzymes containing a C-terminal Ubiquitin-associated domain (UBA), in addition to the catalytic domain conserved in all E2 enzymes. Previous results from our laboratory have shown that the UBA domain binds to the zinc finger domain of RBBP6. Confirmation of the interaction would not only support our unpublished data that RBBP6 cooperates with UbcH1 in ubiquitinating YB-1, but would help us to design mutants that may disrupt the interaction, which would be very useful for ongoing functional studies.

The aim of the second part of the project was to confirm the interaction *in vitro* using GST pull-down assays. Confirmation of the interaction would be followed by Nuclear Magnetic Resonance Spectroscopy to investigate the interaction interface between the zinc knuckle domain of RBBP6 and the UBA of UbcH1.  $^{15}\text{N},^1\text{H}$ -HSQC-based chemical shift perturbation assays would be used to assess the affinity of the interaction and to identify residues on each domain closely involved in the interaction. This information would be used to build a model of the interaction complex and to determine the position of the interaction interface.

## Chapter 2

### Materials and Methods

#### 2.1 Antibodies used in this study

##### 2.1.1 Primary antibodies

###### Anti-HA:

Commercial mouse monoclonal raised against the HA-antigen (YPYDVPDYA), Cat. No: A01244-100 (GenScript Inc., Piscataway, NJ 08854, USA).

###### Anti-zinc finger:

Rabbit polyclonal raised against recombinantly-produced RBBP6-zinc finger by the laboratory of Prof Dirk Bellstedt, Biochemistry Department, Stellenbosch University

##### 2.1.2 Secondary antibodies

###### Donkey Anti-rabbit:

Anti-rabbit secondary (HRP-conjugated) sc-2313 (Santa Cruz Biotechnology, Inc., CA, USA)

###### Goat Anti-mouse:

Anti-mouse secondary (HRP-conjugated) sc-2005 (Santa Cruz Biotechnology, Inc., CA, USA)

#### 2.2 Competent cells

Bacterial strains were streaked out on a nutrient agar (0.5 % Peptone, 0.3 % yeast extract, 1.5 % agar, 0.5 % NaCl) plates containing 10 mM MgSO<sub>4</sub> and incubated at 37 °C for 16 hours. A single colony was picked and grown in 20 ml of TYM broth (20 % Tryptone, 0.5 % yeast extract, 0.1 M NaCl, 0.2 % glucose and 10 mM MgCl<sub>2</sub>), at 37 °C shaking, until the OD at 600 nm reached 0.2. The culture was up-scaled with 100 ml of TYM broth and grown at 37 °C shaking until the OD at 600

nm reached 0.2. 400 ml of TYM broth was then added to the sample and at 37 °C shaking until the OD reached between 0.4 and 0.6. The cells were rapidly cooled in ice water and the cells were pelleted by centrifugation at 4300 rcf for 20 minutes. The supernatant was removed and the cells were re-suspended in 250 ml of ice cold Tfb1 (30 mM KCH<sub>3</sub>COO, 50 mM MnCl<sub>2</sub>, 0.1 M KCl, 10 mM CaCl<sub>2</sub> and 15 % glycerol), and incubated at 4 °C for 30 minutes. The cooled cells were centrifuged at 4300 rcf for 8 minutes and supernatant was removed. The cell pellet was finally re-suspended in 30 ml of ice cold Tfb2 (9 mM MOPS, 10 mM KCl, 50 mM CaCl<sub>2</sub> and 15 % glycerol) and 100 µl aliquots were made and stored at -80 °C.

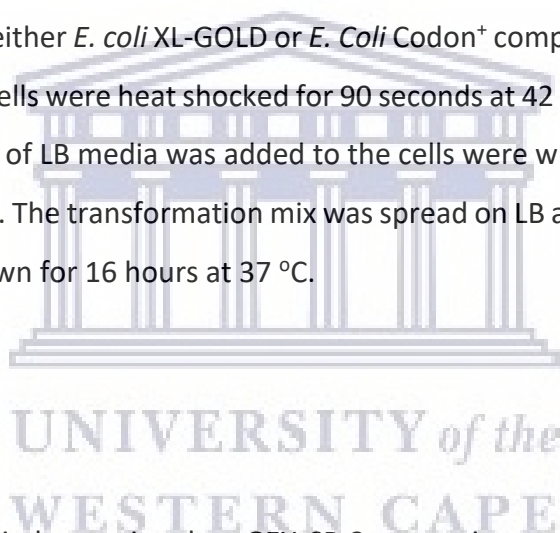
## 2.3 Transformation

DNA was added to 50 µl of either *E. coli* XL-GOLD or *E. Coli* Codon<sup>+</sup> competent cells and incubated on ice for 15 minutes. The cells were heat shocked for 90 seconds at 42 °C followed by incubation on ice for 5 minutes. 500 µl of LB media was added to the cells which were then incubated for 1 hour on a 37 °C shaker. The transformation mix was spread on LB agar plates containing 100 µg/ml of ampicillin and grown for 16 hours at 37 °C.

## 2.4 Cloning

### 2.4.1 Vector details

Protein expression was carried out using the pGEX-6P-2 expression vector. pGEX-6P-2 expresses the target protein fused to the C-terminus of GST. The vector encodes the recognition site for 3C protease between the GST and the MCC, allowing for removal of the GST-tag if necessary. The target gene is under the control of the *tac* promoter, which is inducible with IPTG. An ampicillin resistance gene allows for selection on plates containing ampicillin. The vector map is shown in Figure 2.1.



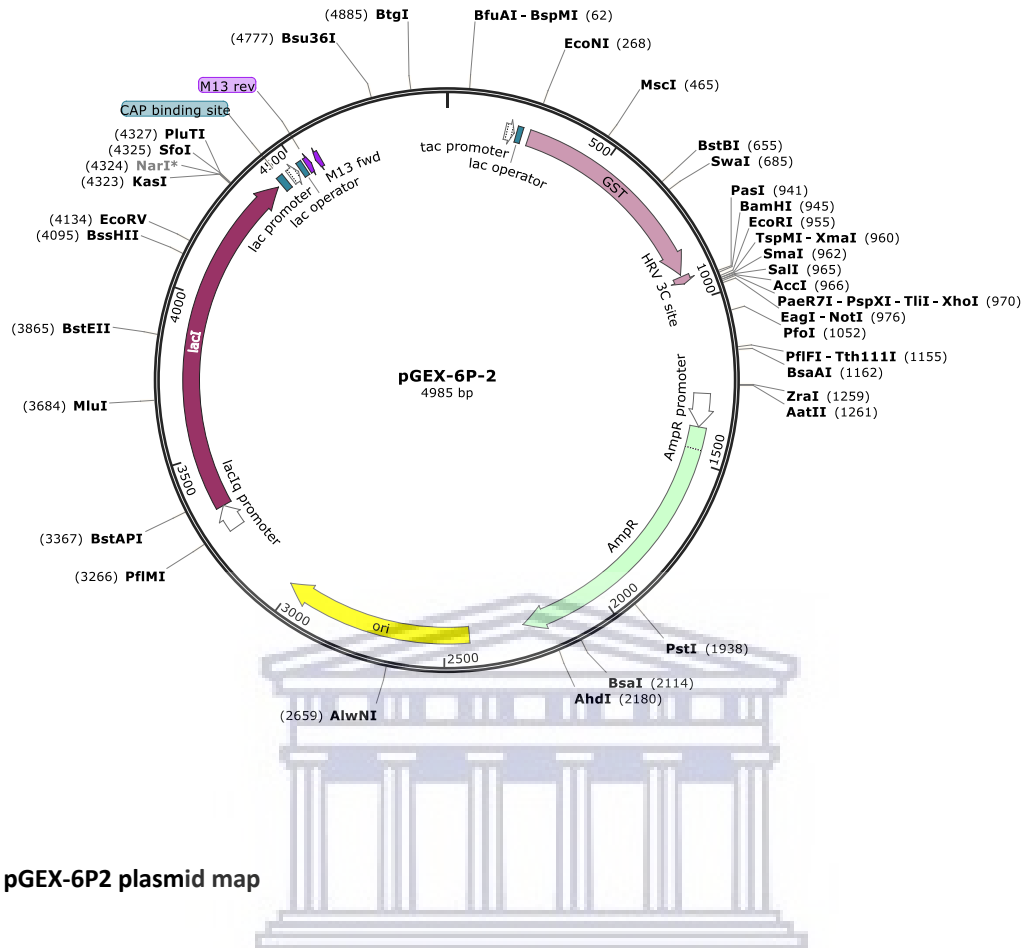


Figure 2.1 pGEX-6P2 plasmid map

#### 2.4.2 PCR amplification of gene fragments

For PCR amplification of the desired coding region reactions consisted of 50 ng of template DNA, 1 x PCR buffer, 1 U Taq DNA polymerase (OneTaq<sup>®</sup> DNA polymerase), and 50 ng of forward and reverse gene specific primers in a final volume of 50ul. The melting temperatures (T<sub>m</sub>) of the primers were calculated using *SnapGene*<sup>®</sup> software (from GSL Biotech; available at [snapgene.com](http://snapgene.com)) and the thermal cycling were carried out using following:

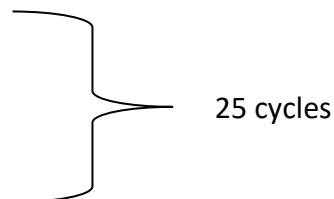
95°C for 5 minutes (Initial denaturation)

95°C for 30 sec (Denaturation)

T<sub>m</sub> -5°C for 1 min (Annealing)

72°C for 1 min/kb (Extension)

72°C for 5 min (Final Extension)



### 2.4.3 Restriction digestion and ligation

During the restriction digestion, 2 µg of DNA was digested in a 50 µl reaction at 37 °C for 1 hour using 2 units of BamHI and XhoI restriction enzymes each, 1 x digestion buffer and filled to the final volume with nuclease free dH<sub>2</sub>O. The digested samples were separated on a 1 % agarose gel in 1 x TAE buffer at 90 volts for 45 minutes. The desired fragment was excised from the gel and purified using a GeneJet Gel extraction kit (ThermoScientific, Massachusetts, USA). The concentrations of the DNA samples were determined using a Nano Drop ND 1000 Spectrometer (ThermoScientific, Massachusetts, USA).

The ligation of the two digested samples was done at a 1:19 and 1:24 ratio (vector: insert) using 20 ng of vector DNA, 1 U T4 ligase and 1x T4 ligase buffer. The ligation reaction was incubated at 4 °C for 16 hours where after it was transformed into *E. coli* XL Gold competent cells and plated on LB agar plates containing 100 µg/ml of ampicillin. Transformed cells were incubated at 37 °C for 16 hours.

### 2.4.4 Colony screening and sequencing

A number of putative positive colonies from the LB agar plates were picked and inoculated into 30 ml of LB medium and grown at 37 °C with shaking for 16 hours. Plasmid DNA was extracted and purified using a Gene Jet Mini Prep kit and the DNA concentration was determined using a Nano Drop spectrometer at 260 nm. To test for the release of insert, 1 µg of plasmid DNA was digested in a 50 µl reaction with 1 U each of BamHI and XhoI restriction enzymes, 1x restriction buffer and filled to the final volume with nuclease free dH<sub>2</sub>O. The digested samples were separated on a 1 % agarose gel at 90 volts to identify positive transformants. The sequence identities of positive transformants were confirmed by direct sequencing, performed at Inqaba Biotechnical Industries, Hatfield, South Africa. Sequences were analyzed and displayed using *SnapGene*<sup>®</sup> software (from GSL Biotech; available at [snapgene.com](http://snapgene.com))



## 2.5 Protein expression and purification

### 2.5.1 Protein expression in bacteria

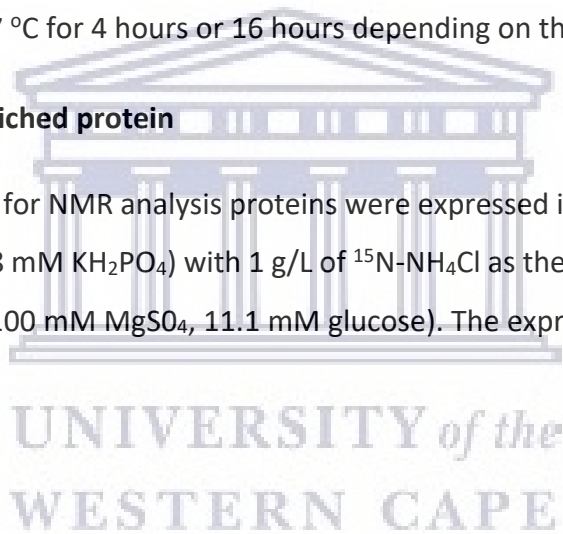
*E. coli* Codon<sup>+</sup> was used to transform the expression constructs. The transformation mixture was grown on LB agar plates containing 100 µg/ml of ampicillin and incubated at 37 °C for 16 hours. Single colonies were picked and grown in 30 ml of LB media containing 100µg/ml of ampicillin; the cultures were incubated at 37 °C on a shaker for 16 hours. The cultures were scaled up into a 1 L volume of LB media containing 100 µg/ml of ampicillin and incubated at 37 °C on a shaker. The OD reading was taken regularly using a UV Spectrophotometer at 600 nm; once the OD reached 0.2, 200 µM of ZnSO<sub>4</sub> was added and at 0.4, 0.1 mM IPTG was added to the culture. The culture was incubated at 37 °C for 4 hours or 16 hours depending on the expression construct.

### 2.5.2 Expression of <sup>15</sup>N-enriched protein

For <sup>15</sup>N-labeling of proteins for NMR analysis proteins were expressed in minimal media (50 mM NaCl, 2.7 mM, Na<sub>2</sub>HPO<sub>4</sub>, 1.8 mM KH<sub>2</sub>PO<sub>4</sub>) with 1 g/L of <sup>15</sup>N-NH<sub>4</sub>Cl as the sole nitrogen source in a nutrient mix (5 mM CaCl<sub>2</sub>, 100 mM MgSO<sub>4</sub>, 11.1 mM glucose). The expression was carried out as described in Section 2.5.1.

### 2.5.3 Protein purification

The culture was centrifuged at 4300 rcf for 20 minutes using a Avanti Centrifuge J-26 XPI and each pellet was re-suspended in 15 ml extraction buffer (5 mM β-mercaptoethanol, 0.5 % Triton X, 100 µM ZnSO<sub>4</sub>, 0.1 mg/ml of lysozyme and half a pellet of protease inhibitor cocktail in 1x PBS). The resuspended samples were sonicated at 30 second intervals for 5 minutes and centrifuged at 4300 rcf for 30 minutes. A glutathione agarose column was equilibrated with wash buffer (5 mM β-mercaptoethanol in 50ml of 1 x PBS). The clarified lysate was run down the column, followed by 3 washes using wash buffer; and then elution buffer (5 mM β-mercaptoethanol, 20 mM reduced glutathione in 1 x PBS) was added until no more protein was being eluted, this was observed by taking 2 µl of protein being eluted straight from the column and added to 48 µl of Bradford reagent for every few ml of protein being eluted. All column fractions were collected



after each step and separated on a 16 % SDS-PAGE gel which was stained and de-stained using Coomassie Brilliant Blue R dye and water respectively.

#### 2.5.4 GST removal and size exclusion chromatography

The sample protein was placed inside SnakeSkin® Pleated Dialysis Tubing (MWCO 3500Da) (Thermo Scientific, Massachusetts, USA) along with 1mg/ml protease from human 3C rhinovirus, produced in-house as a GST-fusion protein. The dialysis tube was placed into 3C protease cleavage buffer (50 mM Tris-HCl pH 7, 150 mM NaCl, 1 mM EDTA and 1 mM DTT) and cleaved overnight at 4 °C, with the buffer being changed every 2 hours, for a total of 4 times. In the morning, the sample was separated on a 16 % SDS-PAGE gel to determine if the fusion protein had been cleaved. The target was then concentrated down to 5 ml using Amicon Ultra-15 Centrifugal Filter Units. Then 1 ml of the concentrated protein was loaded onto a Superdex™ 75 HR 10/30 column (Amersham Biosciences) equilibrated with 1 x degassed PBS operated on an ÄKTA FPLC Purification System (GE Healthcare, Little Chalfont, UK). Elution fractions were analyzed on a 16 % SDS-PAGE gel.

#### 2.6 SDS-PAGE gel electrophoresis

Proteins were separated on a 16 % denaturing polyacrylamide gels (SDS-PAGE) prepared using Laemmli's method (Laemmli, 1970), as follows:

<b>Resolving gel 16 %</b>	<b>Stacking gel 4 %</b>
1.6 ml dH <sub>2</sub> O	1.5 ml dH <sub>2</sub> O
1.3 ml Separating buffer	0.625 ml Stacking buffer
2 ml acrylamide (40% acrylamide:bis-acrylamide)	0.375 ml acrylamide (40 % acrylamide:bis-acrylamide)
52.5 µl 10 % SDS	25 µl 10 % SDS

25 $\mu$ l 10 % APS	12.5 $\mu$ l APS
5 $\mu$ l TEMED	2.5 $\mu$ l TEMED

Protein samples were prepared by adding equal volumes of sample protein and 2x sample buffer and heated at 95 °C for 10 minutes. The samples were loaded onto the gel and separated using a Mini-PROTEAN Tetra Cell (BioRad, Hercules, CA, USA). The gel was stained with Coomassie staining solution upon completion for 15-20 minutes and de-stained in dH<sub>2</sub>O until the background was clear.

## 2.7 Interaction Assay

### 2.7.1 GST pull-down assay

For the GST pull-down assay, 100  $\mu$ l of glutathione agarose slurry was washed with 500  $\mu$ l of dH<sub>2</sub>O and then equilibrated with 500  $\mu$ l of Binding Buffer (1 mM DTT, 5 % BSA, 5 % glycerol, 1 x PBS). The beads were centrifuged in-between each wash at 17000 rcf for 5 minutes. The beads were aliquoted equally into 1.5 ml Eppendorf tubes and washed with 500  $\mu$ l of binding buffer. The 5 tubes were labeled "Beads and prey", "Beads and bait", "Beads only", "GST" and "Experimental". 10  $\mu$ g of pure GST was added to the GST tube, GST tagged protein ("bait") was added to the experimental tube and nothing else was added to the beads only tube. The tubes were incubated at 4 °C on a roller for 1 hour. After the incubation period the protein to be detected by the antibody ("prey") was added to the 3 tubes "Beads and prey", "GST" and "Experimental" and incubated at 4 °C on a roller for another hour. The tubes were then centrifuged at 17000 rcf for 5 minutes. The beads were washed 3 times with 500  $\mu$ l binding buffer, 2 times with PBS-DTT (1 x PBS and 1 mM DTT). The samples were centrifuged in-between each wash at 17000 rcf for 5 minutes with the supernatant being discarded. The samples were then boiled at 95 °C for 5 minutes in 30  $\mu$ l of sample buffer and stored at -20 °C.

### 2.7.2 Western Blotting

The samples from the GST pull-down assay were separated on a 16 % SDS-PAGE gel along with loading and blotting controls. Separated proteins were transferred onto a activated PVDF membrane for 10 minutes using a Trans Blot Transfer System (Bio-Rad, Johannesburg, South Africa), and blocked with 1 % casein (0.5 g casein, 300  $\mu$ l 3 M NaOH, 1 x PBS-T to a final volume of 50 ml) for 1 hour. The membrane was briefly rinsed with 1x PBST followed by the addition of primary monoclonal antibody, at a 1:2000 dilution with 1 x PBST, to the membrane. The membrane was incubated overnight with the antibody. After the overnight incubation the membrane was washed 3 times for 5 minutes each with 1 x PBS-T followed by the addition of secondary antibody at a 1:1000 ratio diluted with 1 x PBS-T and incubated for 1 hour on the shaker. The membrane was then washed 3 times for 5 minutes each with 1 x PBS-T. The membrane was developed using Clarity Western ECL 15 Substrate (BioRad, Johannesburg, South Africa) and viewed using a UVP BioSpectrum Imaging System (UVP, Upland, California).

### 2.8 NMR data collection and analysis

NMR samples were mixed with 10 % deuterium oxide ( $D_2O$ ) and loaded into 5 mm NMR tubes. The sample height was adjusted to a height of 4 cm to assist with shimming of the  $B_0$  field. For the RBBP6-RING/MDM2-RING interaction, 50 mM sodium phosphate buffer containing, 150 mM NaCl, 1 mM DTT and pH 6.0 was used; for the UBA/zinc finger interaction, 50 mM sodium phosphate buffer containing, 100 mM NaCl and pH 7.0 was used. 1-D proton and  $^{15}N$ -HSQC spectra were recorded on Bruker 500 MHz AVANCE III and Bruker 700 MHz AVANCE III spectrometers, equipped with a room temperature triple resonance (HCN) probe and a QCI cryoprobe respectively (Bruker, Billerica, Massachusetts). The NMR spectra were processed using NMRPipe (Delaglio *et al.*, 1995) and visualization and analysis were carried out using NMRView (Johnson & Blevins 1994).

## Chapter 3

### The structural characterization of the interaction between the RING finger domains of RBBP6 and MDM2 using Nuclear Magnetic Resonance Spectroscopy

#### 3.1 Introduction

RBBP6 is reported to activate the p53 ubiquitination activity of MDM2 by interacting directly with it in a manner requiring the RING finger of RBBP6. In trying to account for this behaviour, we hypothesized that RBBP6 and MDM2 may interact directly through their RING finger domains, in a manner similar to that in which MDMX interacts with MDM2 (as described in Chapter 1). The RING finger domains of MDM2 and MDMX each form homo-dimers across the equivalent interface, and they hetero-dimerize across the same interface (Linke *et al.*, 2008). The RING finger domain of RBBP6 also homo-dimerizes across the equivalent interface, suggesting that it may be able to form homodimers with MDM2 across the same interface. Reports suggest that an equilibrium may exist between MDM2 homo-dimers and hetero-dimers with MDMX, which may play a role in regulating the activity of MDM2 (Linke *et al.*, 2008). The possibility that RBBP6 may use a similar mechanism to regulate the ubiquitination activity of MDM2 is an interesting one which we considered worth investigating.

To test this hypothesis, we expressed the RING finger domains from RBBP6 and MDM2 in *E.coli* and investigated their interaction *in vitro* using GST pull-down assays. This was followed by Nuclear Magnetic Resonance-based chemical shift perturbation assays, with the aim, firstly, of confirming the interaction and, secondly, of identifying residues in each domain directly involved in the interaction interface. These residues would then form the targets for future attempts to create knock out mutants.

### 3.2 Recombinant protein expression and purification of RBBP6-RING and MDM2-RING

Plasmids pGEX-6P2-HA-RBBP6-RING and pGEX-6P2-MDM2-RING, expressing GST-HA-RBBP6-RING and GST-MDM2-RING respectively, had previously been generated in our laboratory. The GST domain enabled affinity purification out of *E. coli* lysate, as well as precipitation using glutathione-conjugated agarose, and a 3C-protease site allowed cleavage and removal of the GST domain if necessary. A hemagglutinin (HA) tag had been inserted between the 3C-protease site and the beginning of RBBP6-RING, allowing for immunodetection with anti-HA antibodies.

GST-HA-RBBP6-RING protein was expressed at large scale and purified using glutathione affinity chromatography, as described in Section 2.5. Eluted fractions were analyzed on a 16 % SDS-PAGE gel, as shown in Figure 3.1 (A). A thick band at the expected size (35 kDa) can be seen in the eluted fractions, lanes 6 – 8. Cleavage with 3C protease resulted in two bands (lane 1 of panel (B)); isolated RBBP6-RING can be seen at 15 kDa, which is slightly higher than the expected molecular weight of 10 kDa, but is consistent with previous reports (Kappo *et al*, 2012). GST is visible at 25 kDa and a small amount of un-cleaved fusion protein at 35 kDa. The sample in lane 1 was loaded onto a size exclusion column and excellent separation was achieved between the HA-RBBP6-RING (lanes 6-9) and GST (lanes 2-5), resulting in a highly purified sample of HA-RBBP6-RING.

GST-MDM2-RING protein was expressed and purified in a similar manner. The results of the glutathione affinity purification are shown in panel (C). A faint band of the expected size (35 kDa) can be seen in the eluted fraction (lane 6). Since the GST tag was required for precipitation of GST-MDM2-RING, the protein was left uncleaved.

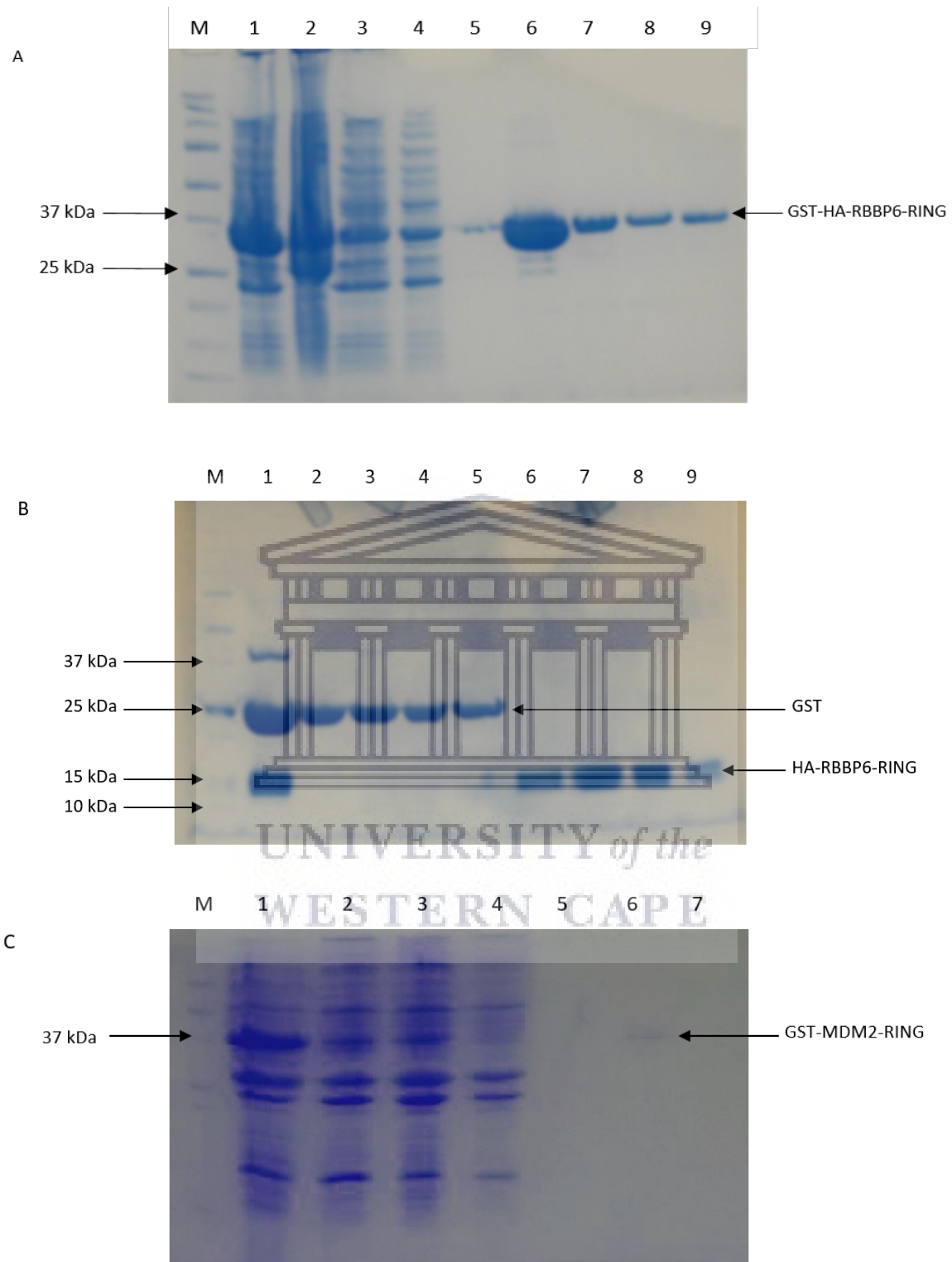


**Figure 3.1 Purification of GST-RBBP6-RING and GST-MDM2-RING** (A) Affinity purification of GST-HA- RBBP6-RING using a Glutathione-conjugated agarose column. GST-HA-RBBP6-RING (35 kDa) was eluted with reduced glutathione (lanes 6 – 9) at 35 kDa. Lane 1 shows the soluble lysate and lane 2 the insoluble fraction. The lack of a substantial band in the insoluble fraction shows that the protein is predominantly soluble. Lane M contained the Precision Plus

protein standard. (B) Cleavage of GST-HA-RBBP6-RING and separation of HA-RBBP6-RING (lanes 6 – 9) from GST (lanes 2 – 5). (C) GST-MDM2-RING fusion protein was purified using a Glutathione agarose column, lane 6 shows the purified GST-MDM2-RING eluted at 35 kDa. The eluted protein is faint, and it is possible that it did not bind effectively to the affinity column, since there appears to be a lot more in the soluble lysate (lane 1).

### 3.3 GST pull-down assay

In a GST pull-down assay, glutathione-conjugated agarose is used to precipitate a GST-tagged protein (the "bait"), out of a mixture containing both the bait and a potential interaction partner (the "prey"). After extensive washing to remove non-interacting proteins, proteins retained by the beads are separated on SDS-PAGE and co-precipitated proteins detected by western blotting with antibodies targeting the prey protein. An identical reaction, but with the GST-tagged bait replaced by GST alone, controls for interactions between the prey and GST, or between the prey and the glutathione agarose, as well as for non-specific interactions due to insufficient washing.

The results of a GST pull-down assay using GST-MDM2-RING as bait and HA-RBBP6-RING as prey are shown in Figure 3.2. They suggest that HA-RBBP6-RING is pulled down by GST-MDM2-RING (lane 6), but not by GST alone (lane 4), nor by the glutathione agarose alone (lane 5). Immuno-detection was carried out using anti-HA antibodies targeting the HA tag incorporated into RBBP6-RING; anti-HA is highly specific for HA and is not expected to cross-react with any other proteins, and therefore the low molecular weight band in lane 6 is overwhelmingly likely to correspond to HA-RBBP6-RING. This is supported by the presence of a band of the same size in lane 2, which contains HA-RBBP6-RING alone, loaded directly onto the gel and not subjected to precipitation or washing. The higher molecular weight bands in lane 6, and to a lesser extent in lanes 4 and 5, are most likely to correspond to some form of aggregation on the agarose beads, possibly due to the multiple washes. It is possible that they correspond to BSA, which is present in the buffer and migrates at the corresponding size, although BSA is unlikely to cross-react with the anti-HA antibody. Alternatively, the bands may correspond to RING finger domains that have unfolded and precipitated as a result of loss of coordinating zinc ions, resulting from the multiple washes. If this is the case then future assays should possibly include a low concentration of zinc ions in the wash buffers. Of more importance is the band at the bottom of lane 6. Although the



molecular weight marker is on little help in determining the size of the band, it is consistent with the size of the band in lane 2, which unequivocally corresponds to HA-RBBP6-RING, since that was all that was loaded into lane 2. In effect lane 2 plays the role of a custom molecular weight marker, more than making up for the failed molecular weight marker on the extreme left.

Lanes 1 and 3 confirm that the band observed in lane 6 is not GST-MDM2-RING, since it is not detected by the anti-HA antibody. In any case, there is no serious danger of confusion since, even if GST-MDM2-RING were detected by the anti-HA, it could easily be distinguished from HA-RBBP6-RING due to its higher molecular weight.

Although HA-RBBP6-RING is present in small amounts when GST alone is used as bait, overwhelmingly more is present when GST-MDM2-RING is used as bait. From this we conclude that an interaction does exist between RBBP6-RING and MDM2-RING.

A total of 0.6  $\mu\text{g}$  of HA-RBBP6-RING was loaded directly into lane 2 of the SDS-PAGE gel. For the experimental sample (lane 6), 20  $\mu\text{g}$  of HA-RBBP6-RING was originally added to the GST pull-down assay; following several rounds of washes, the final pellet was re-suspended in 30  $\mu\text{l}$  of sample buffer, of which 10  $\mu\text{l}$  was loaded onto the SDS-PAGE. If all 20  $\mu\text{g}$  of HA-RBBP6-RING was pulled down by the 20  $\mu\text{g}$  of GST-MDM2-RING, lane 6 should contain  $20 \mu\text{g}/3 = 6.7 \mu\text{g}$  of HA-RBBP6-RING and the signal in lane 6 should be  $6.7 \mu\text{g}/0.6 \mu\text{g} \sim 11$  - times more intense than the signal in lane 2. Taking into account that the signal in lane 6 is spread across a number of different bands, it is possible that the total signal is approaching 11 times the signal in lane 2. Hence the interaction between the two RINGs appears to be strong.

### **3.4 Chemical shift perturbation of $^{15}\text{N}$ -labelled RBBP6-RING finger by unlabelled MDM2-RING**

The interaction between the RING finger domains of RBBP6 and MDM2 was investigated further by NMR chemical shift perturbation assay. The  $^{15}\text{N},^1\text{H}$ -Heteronuclear Single Quantum Coherence ( $^{15}\text{N},^1\text{H}$ -HSQC) spectrum forms the basis for most heteronuclear protein NMR investigations (Bodenhausen & Ruben, 1980). The  $^{15}\text{N},^1\text{H}$ -HSQC spectrum of a protein is a 2-dimensional

spectrum in which each 2-dimensional peak arises from an NH or NH<sub>2</sub> group in the protein. There is therefore one resonance for each residue in the protein, except Proline, corresponding to the backbone NH group, as well as resonances for sidechain NH groups, such as the tryptophan indole NH and the arginine ε NH, and the sidechain NH<sub>2</sub> group of asparagine and glutamine. Since the <sup>15</sup>N,<sup>1</sup>H-HSQC spectrum of each protein is distinctive, it can be used to confirm the identity of a protein sample. The degree of dispersion of the peaks is a good indicator as to whether a protein is folded or unfolded (Wishart *et al.*, 1991). Since the positions of the peaks are sensitive to the hydrogen bonding status of the corresponding NH group the <sup>15</sup>N,<sup>1</sup>H-HSQC spectrum is a sensitive probe of the ligand binding state of a protein. The most abundant isotope of nitrogen, <sup>14</sup>N, is NMR silent; therefore detection of the <sup>15</sup>N,<sup>1</sup>H-HSQC spectrum of a protein requires that <sup>14</sup>N atoms be replaced by <sup>15</sup>N atoms. This is most conveniently done by producing them in *E. coli* grown on minimal media, with <sup>15</sup>N-ammonium chloride as the sole nitrogen source.

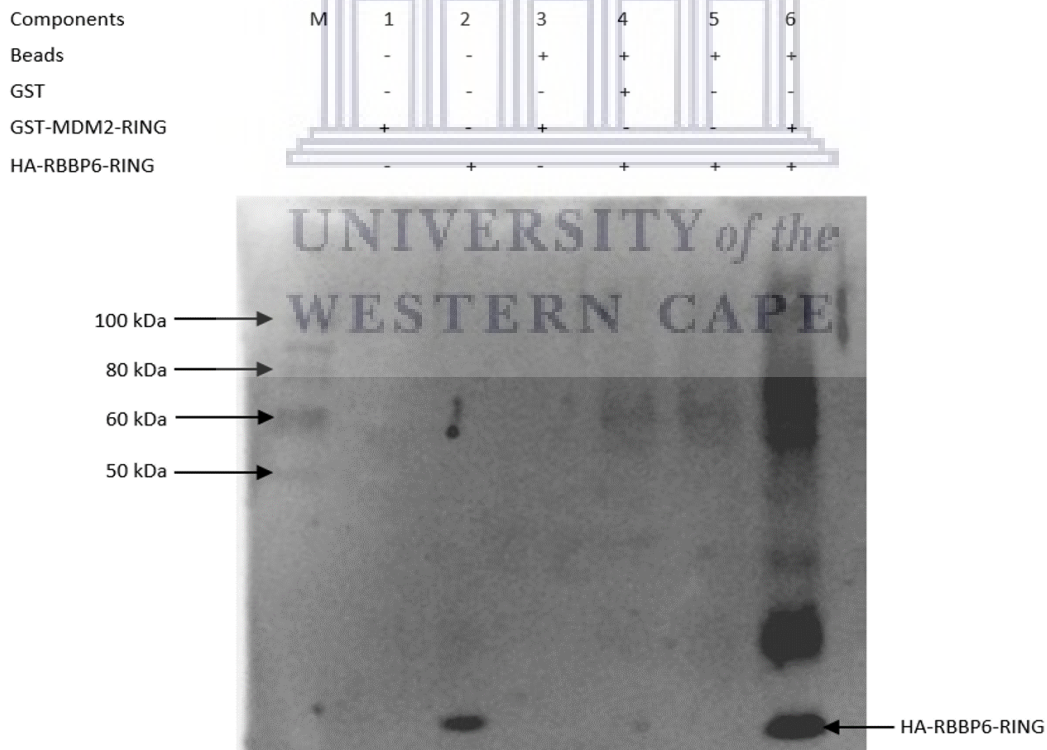


**Figure 3.2 Western Blot showing the pull-down of HA-RBBP6 RING by GST-MDM2-RING.** HA-RBBP6-RING is pulled down by GST-MDM2-RING (lane 6) but not by GST alone (lane 4) and nor by the beads alone (lane 5); the signal spread throughout the lane is 11 times stronger than that of the loading control HA-RBBP6-RING (lane 2). No signal was detected from the GST-MDM2-RING negative control in lane 1. Lane M contains the Western Marker.

The Chemical Shift Perturbation (CSP) assay investigates the changes produced in the  $^{15}\text{N},^1\text{H}$ -HSQC spectrum of a  $^{15}\text{N}$ -enriched protein when a second, non-enriched, protein is added. The  $^{15}\text{N},^1\text{H}$ -HSQC spectrum of the non-enriched protein is not detected, only its effects on the spectrum of the  $^{15}\text{N}$ -enriched protein. Peaks whose positions shift as a function of ligand concentration correspond to residues situated close to the interaction interface. Using the techniques of triple resonance spectroscopy, it is possible to identify the residue giving rise to each peak, a procedure known as “assignment” of the spectrum; if the  $^{15}\text{N}$ -labelled protein has been assigned, then the CSP assay can be used to map the binding site onto the surface of the protein, if the structure is known, or to identify targets for site-directed mutagenesis. If the spectrum has not been assigned, CSP can still be used to confirm the interaction with a high degree of certainty and to determine a dissociation constant.

$^{15}\text{N}$ -labelled RBBP6-RING was expressed and purified as described in Sections 2.5 and 3.2 respectively. The sample was concentrated down to a volume of 800  $\mu\text{l}$ , yielding a final concentration of 85  $\mu\text{M}$ , and used to record a  $^{15}\text{N},^1\text{H}$ -HSQC spectrum at 500 MHz. The total acquisition time was 14 hours, due to the low concentration of the sample, the low field strength of the spectrometer and the use of a room-temperature probe.

The  $^{15}\text{N},^1\text{H}$ -HSQC spectrum of  $^{15}\text{N}$ -RBBP6-RING is shown in Figure 3.3 (in red). Firstly, it is consistent with the published spectrum of this protein (Kappo *et al.*, 2012), confirming that the expected protein had been expressed. Secondly, the spectrum shows good dispersion of resonances between 6.6 ppm and 9.6 ppm, which is a good indication that the protein is folded.

For the chemical shift assays, unlabeled MDM2-RING was expressed and purified as described previously. GST was removed from MDM2-RING in the manner described in Section 2.5.4 and the sample was concentrated down and added to the  $^{15}\text{N}$ -RBBP6-RING sample to a final concentration of 38  $\mu\text{M}$  and 53  $\mu\text{M}$  of MDM2-RING respectively, yielding molecular ratios of 1:0.4 and 1:0.6 (RBBP6-RING:MDM2-RING) respectively. A  $^{15}\text{N},^1\text{H}$ -HSQC spectrum was recorded after each addition of MDM2-RING, each with a total acquisition time of 14 hours. The different spectra were superimposed on each other using the NMR visualization program NMRViewJ (One

Moon Scientific, 2018). The free spectrum, the 1:0.4 and the 1:0.6 titrations are all overlaid in Figure 3.3, coloured red, blue and green respectively.

Clear chemical shift perturbation can be seen in some resonances, indicated by the red arrows in Figure 3.3. The chemical shifts move in the same direction in 2-dimensional space with increasing MDM2-RING concentration; this is expected in the case of fast exchange, which is appropriate when the average time for which a ligand is bound to a protein is shorter than the typical acquisition time of the NMR signal (the Free Induction Decay, or FID), which is of the order of 100 ms. In this case, the position of the resonance corresponds to the population-weighted average of the positions of the fully unbound and fully bound resonances respectively, which shifts as a function of ligand concentration.

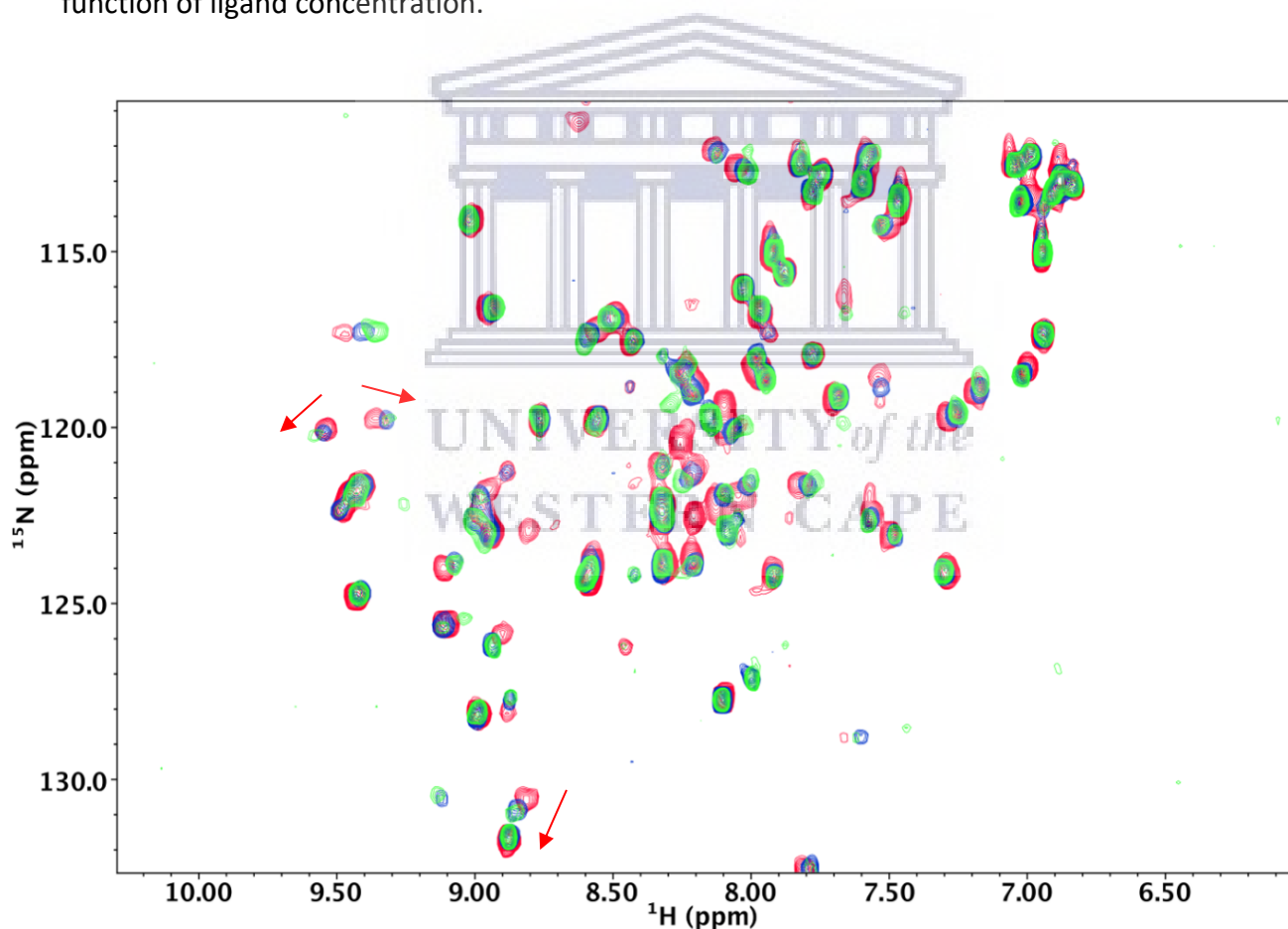


**Figure 3.3** Chemical shift perturbation investigation of the interaction between RBBP6-RING and MDM2-RING. The  $^{15}\text{N},^1\text{H}$ -HSQC spectrum of  $^{15}\text{N}$ -enriched RBBP6-RING (red) is consistent with the published spectrum of this protein. The  $^{15}\text{N}$ -RBBP6-RING spectra is overlaid following addition of 40 % (blue) and 60 % (green) molar ratio of MDM2-RING.

Kappo and co-workers have reported that RBBP6-RING homo-dimerizes at high concentrations whilst at low concentrations it is monomeric (Kappo *et al.*, 2012). They showed that as the concentration of RBBP6-RING decreased from 1000  $\mu\text{M}$  to 25  $\mu\text{M}$ , the peaks corresponding to the amino acids in the dimerization interface shifted, consistent with a change from predominantly homo-dimeric to predominantly monomeric. Figure 3.4 shows our results superimposed on the data of Kappo and co-workers; the red arrows indicate the dilution-dependent shifts, from high concentration (mainly dimeric) to low concentration (mainly monomeric). The shifts indicated A and B indicate that our shifts align very well with the low concentration end of the dilution series, extending it past the end of the sequence recorded by Kappo and co-workers. The data therefore suggests that the changes seen on addition of MDM2-RING can be accounted for by dilution of  $^{15}\text{N}$ -RBBP6-RING, as a result of addition of MDM2-RING. The height of the cross sections through a sample of peaks in Figure 3.5 confirm the progressive dilution of  $^{15}\text{N}$ -RBBP6-RING as MDM2-RING is added.

The question that remains is whether any changes are observed on addition of MDM2-RING that are not attributable to dilution of  $^{15}\text{N}$ -RBBP6-RING. There are a number of places where the initial spectrum of  $^{15}\text{N}$ -RBBP6-RING (without MDM2-RING) differs from that of Kappo and co-workers; although the NMR spectra of different samples of the “same protein” are usually identical, changes to a few resonances can happen most likely due to re-orientation of flexible regions such as the C-terminus, or from small changes in pH. In cases where the changes occur in crowded regions of the spectrum it is not possible to determine which peak in the original spectrum corresponds to which peak in the new spectrum, at least not without totally re-assigning the spectrum, which is not possible without a  $^{13}\text{C}$ ,  $^{15}\text{N}$ -labelled sample.

There are, however a few peaks in the  $^{15}\text{N}$ , $^1\text{H}$ -HSQC spectrum of  $^{15}\text{N}$ -RBBP6-RING that are sufficiently isolated, making it possible to link new peaks to a previous series of shifting peaks. Even though the peak may have shifted relative to the data of Kappo and co-workers, we expect dilutions to affect the resonances in roughly the same direction. With the addition of MDM2-RING the  $^{15}\text{N}$ -RBBP6-RING the spectra appears to broaden a little as opposed to the spectrum becoming narrower, which is expected if the  $^{15}\text{N}$ -RBBP6-RING were to become more diluted.

These may therefore be evidence of perturbation caused by the addition of MDM2-RING and not due to dilution effects.

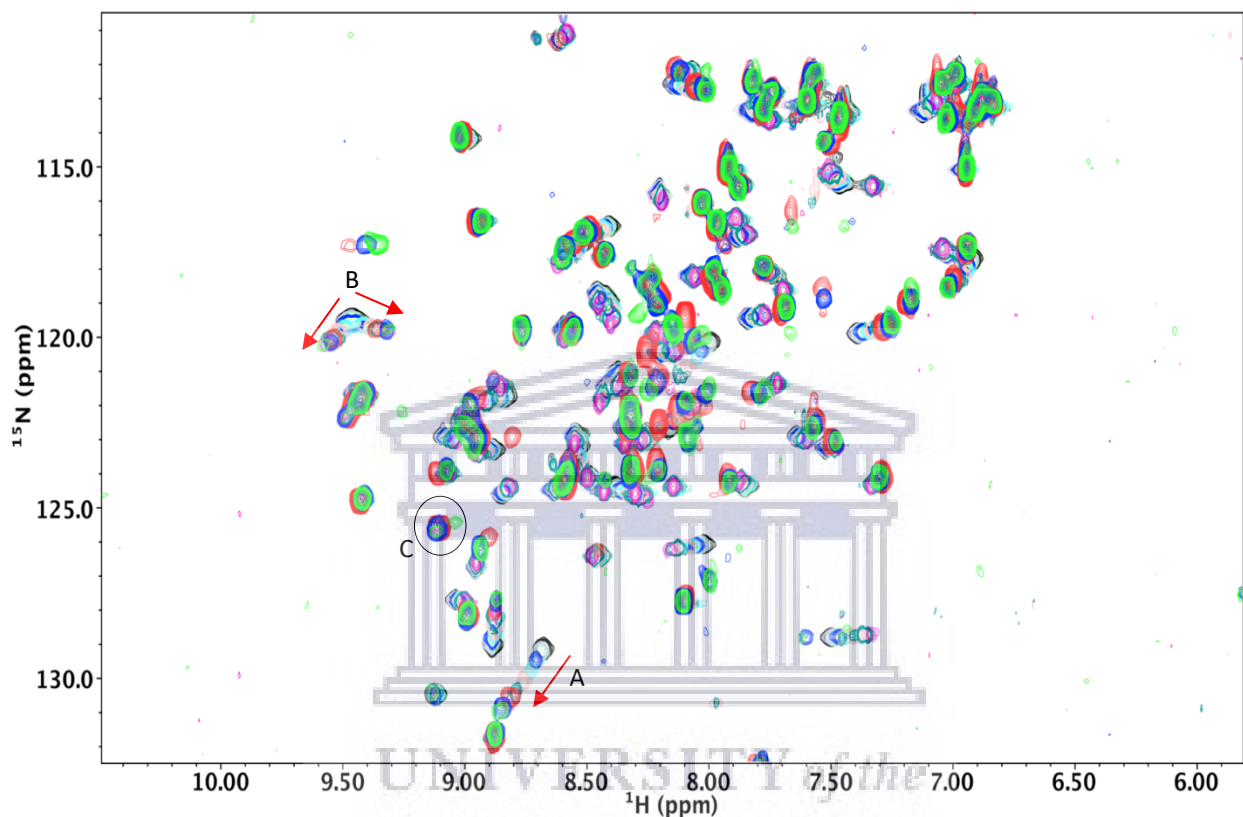


**Figure 3.4 Comparison of possible chemical shifts with dilution dependent shifts.**  $^{15}\text{N}, ^1\text{H}$ -HSQC spectrum of  $^{15}\text{N}$ -RBBP6-RING at different concentrations; 1000  $\mu\text{M}$  (black), 800  $\mu\text{M}$  (grey), 600  $\mu\text{M}$  (light green), 400  $\mu\text{M}$  (blue), 200  $\mu\text{M}$  (turquoise), 100  $\mu\text{M}$  (pink), 50  $\mu\text{M}$  (teal) and 25  $\mu\text{M}$  (purple) from Kappo *et al.*, was overlaid with our data with the colour code  $^{15}\text{N}$ -RBBP6-RING (red),  $^{15}\text{N}$ -RBBP6-RING:MDM2-RING at 1:0.4 (blue) and  $^{15}\text{N}$ -RBBP6-RING:MDM2-RING at 1:0.6 (green).

There is also evidence of some splitting of peaks in the 60 % titration that may correspond to the presence of a new spectrum of the hetero-dimer (indicated with circle at point C in Figure 3.4). However, these peaks are not far above the noise, and greater stoichiometric ratios of MDM2-RING are required in order to determine whether a trend is present in the data. Since the highest concentration of MDM2-RING in the reaction was only 60 % of a 1:1 ratio, that means that the biggest possible effect you could possibly see is a 60 % effect; thus if there were a chemical shift

change we would see a max of 60 % of its total range, and if a new spectrum appears it would be a maximum of 60 % of the original spectrum. It is quite possible in this case that the effect is there but not completely visible under the condition of our experiment. This means that this experiment cannot rule out the possibility of an interaction.

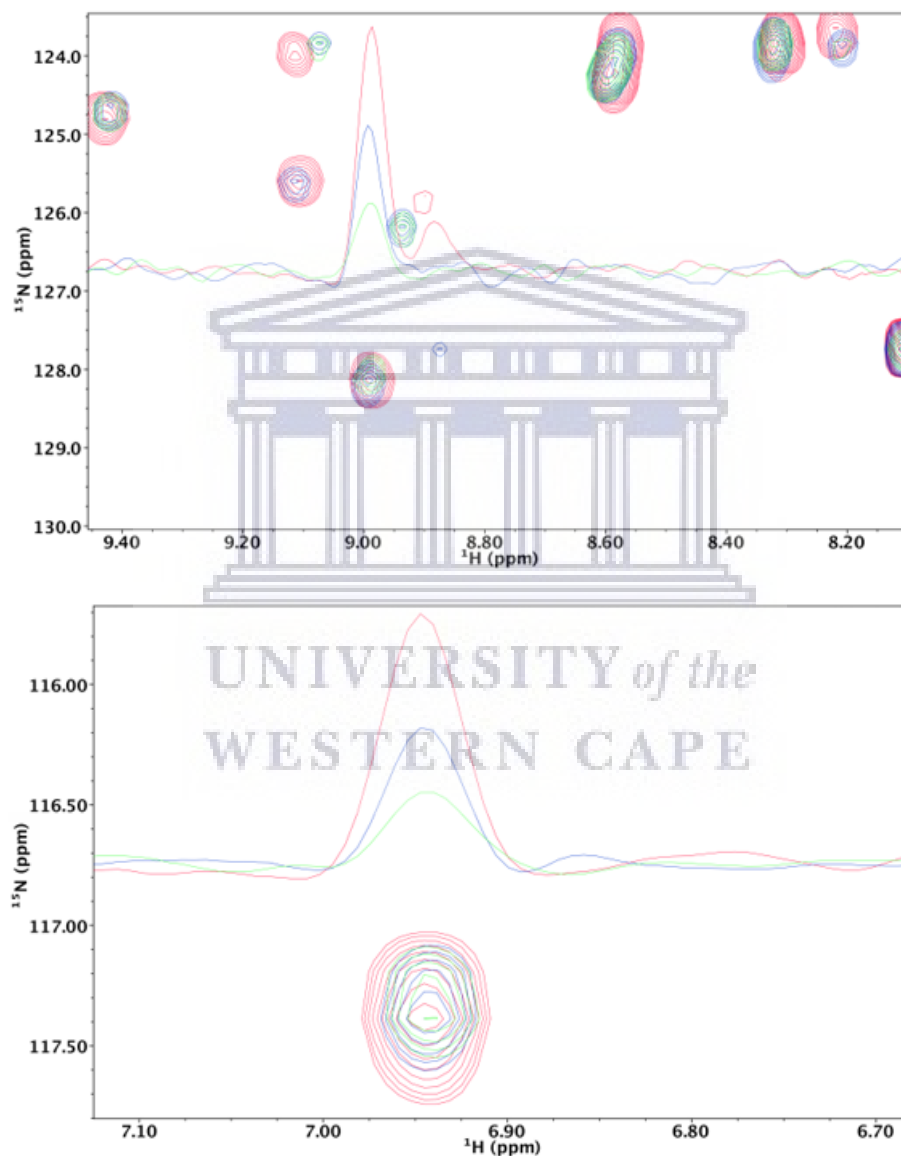


**Figure 3.5 Intensity of isolated sample peaks of RBBP6-RING with the addition of MDM2-RING.** The resonance of  $^{15}\text{N}$ -RBBP6-RING (red) overlay with the addition of MDM2-RING at the ratios of 1:0.4 ( $^{15}\text{N}$ -RBBP6-RING:MDM2-RING) (blue) and 1:0.6 ( $^{15}\text{N}$ -RBBP6-RING:MDM2-RING) (green) respectively. The cross-section through an isolated peak show a consistent progressive dilution of RBBP6-RING with the addition of MDM2-RING.

In summary, the tendency of RBBP6-RING to homo-dimerize makes chemical shift perturbation assays based on  $^{15}\text{N}$ -RBBP6-RING very difficult to interpret. A possible solution to this problem would be to keep the concentration of  $^{15}\text{N}$ -RBBP6-RING as low as 25  $\mu\text{M}$ , since at this concentration, according to Kappo and co-workers,  $^{15}\text{N}$ -RBBP6-RING is predominantly monomeric; however at such low concentrations it would take a very long time to record the spectra and could possibly affect the quality of the spectra. Since MDM2-RING is also known to form homo-dimers, it would also not make sense to base the  $^{15}\text{N},^1\text{H}$ -HSQC on the MDM2-RING either, as it would not alleviate the problems with the dilution-dependent shifts.

An alternative approach would be to use a mutant of RBBP6-RING that does not homo-dimerize. Kappo and co-workers showed that the N312D and K313E mutants of RBBP6-RING are both completely monomeric and would therefore not be sensitive to the changes in concentration that affected the wild type RBBP6-RING (Kappo *et al.*, 2012). Before beginning with NMR studies, however it would be advisable to determine, through GST pull-down assay, if these mutant forms of RBBP6-RING are still able to interact with MDM2-RING.

A third approach would be to begin with a concentrated sample of  $^{15}\text{N}$ -RBBP6-RING and perform a dilution series followed immediately by titration of MDM2-RING. That would enable the effects of dilution and of MDM2-RING to be compared, under the same experimental conditions. If the changes produced by MDM2-RING were qualitatively different from those produced by dilution, we would be able to conclude that interaction was responsible for some of the changes.



## Chapter 4

### Characterization of the interaction between the zinc finger domain of RBBP6 and the UBA domain of UbCH1 using Nuclear Magnetic Resonance Spectroscopy

#### 4.1 Introduction

Unpublished results from our laboratory have suggested that the UBA domain from Ubch1 binds to the zinc finger domain of RBBP6, a result that is important because it supports previous data suggesting that Ubch1 cooperates with RBBP6 in ubiquitinating the oncogenic protein Y-Box Binding Protein 1 (YB-1). In order to confirm this hypothesis, a GST pull-down assay was used to confirm the interaction, using proteins heterologously expressed in bacteria. <sup>15</sup>N-enriched samples of the UBA domain were then expressed in bacteria and used to investigate the same interaction using Nuclear Magnetic Resonance Spectroscopy.

#### 4.2 Recombinant protein expression and purification of UBA and zinc finger proteins

Bacterial expression plasmids pGEX-6P2-UBA and pGEX-6P2-zinc, encoding residues 157 – 199 of Ubch1 and residues 80 - 197 of RBBP6 respectively, had been generated previously by co-workers in the laboratory. Both were expressed as fusions to the C-terminus of GST, with molecular weights of 30.4 and 39.7 kDa, respectively.

GST-UBA was expressed at large scale and purified using glutathione affinity chromatography, using a 15 ml column operated by gravity flow, as described in Section 2.5. The resulting fractions were analyzed on a 16 % SDS-PAGE gel, as shown in Figure 4.1 (A). A thick protein band at the expected size can be seen in lane 5, following elution from the glutathione-conjugated agarose column.

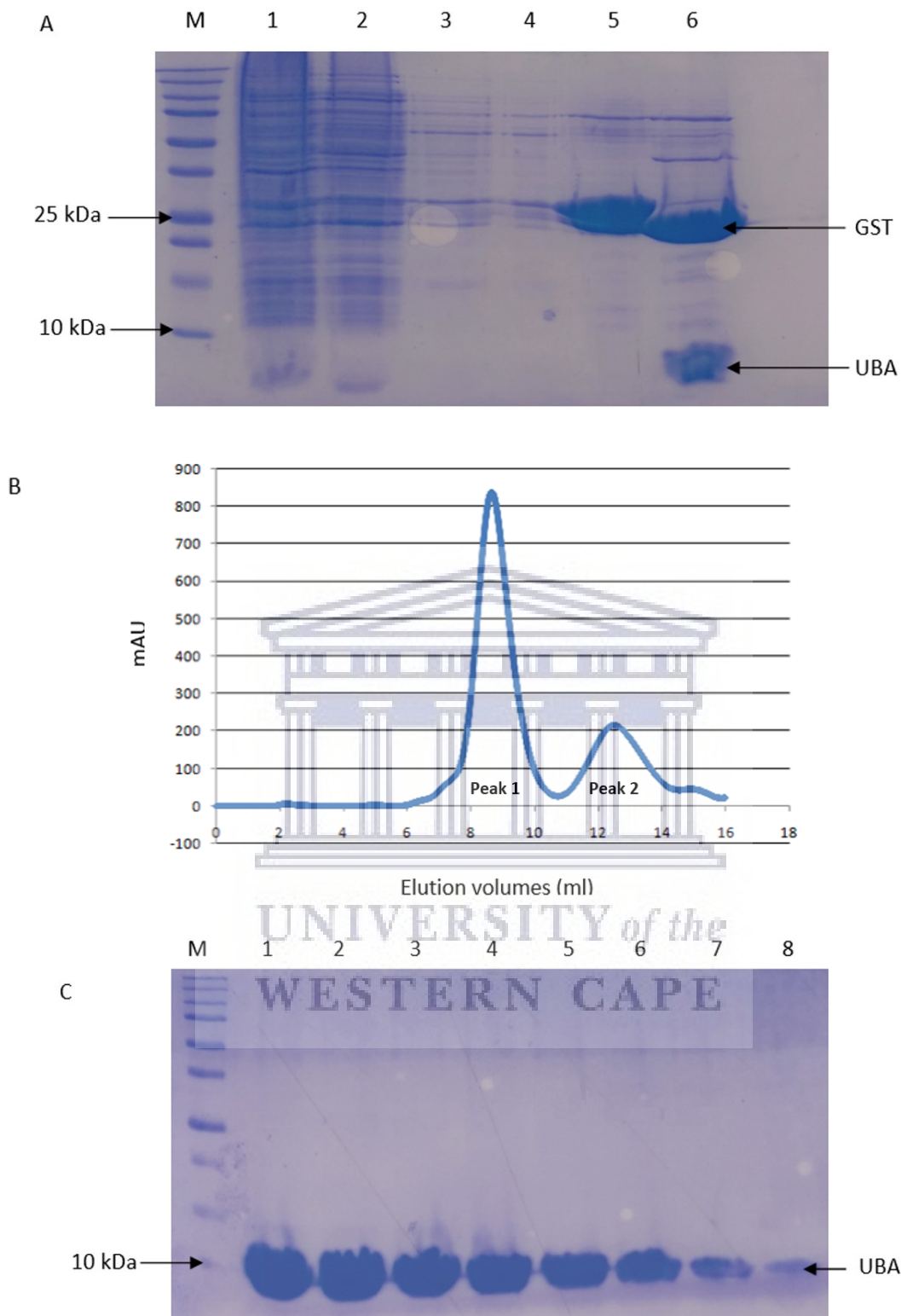


**Figure 4.1 Purification of GST-UBA** (A) Affinity purification of GST-UBA using glutathione affinity chromatography. GST-UBA eluting at 30 kDa in lane 5. Lane 6 shows a complete cleavage of GST (25 kDa) from the UBA (5 kDa). Lane M contained the Precision Plus protein standard. Lanes (B) Good separation of the isolated UBA from GST was achieved using size exclusion chromatography. Peak 1 corresponds to GST and peak 2 to the UBA domain. (C) SDS-PAGE analysis of fractions across peak 2 in panel B. Lanes 1 – 8 shows highly purified UBA at 5 kDa, confirming the UBA was effectively separated from GST.

Removal of the GST tag from GST-UBA was achieved by cleaving the protein with 3C protease, expressed in-house as a GST-fusion protein, as described in Section 2.5.4. The pGEX-6P-2 expression vectors include a recognition site for 3C protease between the GST and the multiple cloning site. The result of the cleavage is shown in lane 6 of Figure 4.1 (A); cleaved UBA can be seen at 5 kDa and the GST is visible at 25 kDa. The cleaved UBA was separated from the GST using a size exclusion column (see Section 2.5.4), as shown in Figure 4.1 (B); excellent separation was achieved between GST (peak 1) and UBA (peak 2). Fractions across peak 2 were analyzed on a 16% SDS-PAGE gel and confirmed to contain highly purified protein with a molecular weight consistent with that of UBA domain (see Figure 4.1 (C)).

GST-zinc was expressed and purified in the same manner as described above (Figure 4.2(A)). A thick band at the expected size (38.7 kDa) can be seen in the eluted fraction (lane 5). Removal of the GST tag was achieved, as before, using 3C protease resulting in bands of 25 kDa, representing GST, and 14 kDa, representing the zinc finger (lane 6). As before, zinc finger was separated from GST using a size exclusion column (see Section 2.5.4), as shown in Figure 4.2 (B), and excellent separation was achieved between the GST (peak 1) and zinc finger (peak 2). Fractions across peak 2 contained highly purified zinc finger protein, as shown in panel C.

### **4.3 GST pull-down assay**

The putative interaction between the UBA from Ubch1 and the zinc finger from RBBP6 was investigated using a GST pull-down assay. For this assay, uncleaved GST-UBA was used as the “bait” and zinc finger (GST removed) as the “prey”; GST-UBA was precipitated from a mixture of GST-UBA and zinc finger by multiple rounds of centrifugation in the presence of glutathione-conjugated agarose beads, separated by thorough washing with buffer. The presence of co-precipitated zinc finger was probed using antibodies raised in rabbit against recombinant zinc finger.

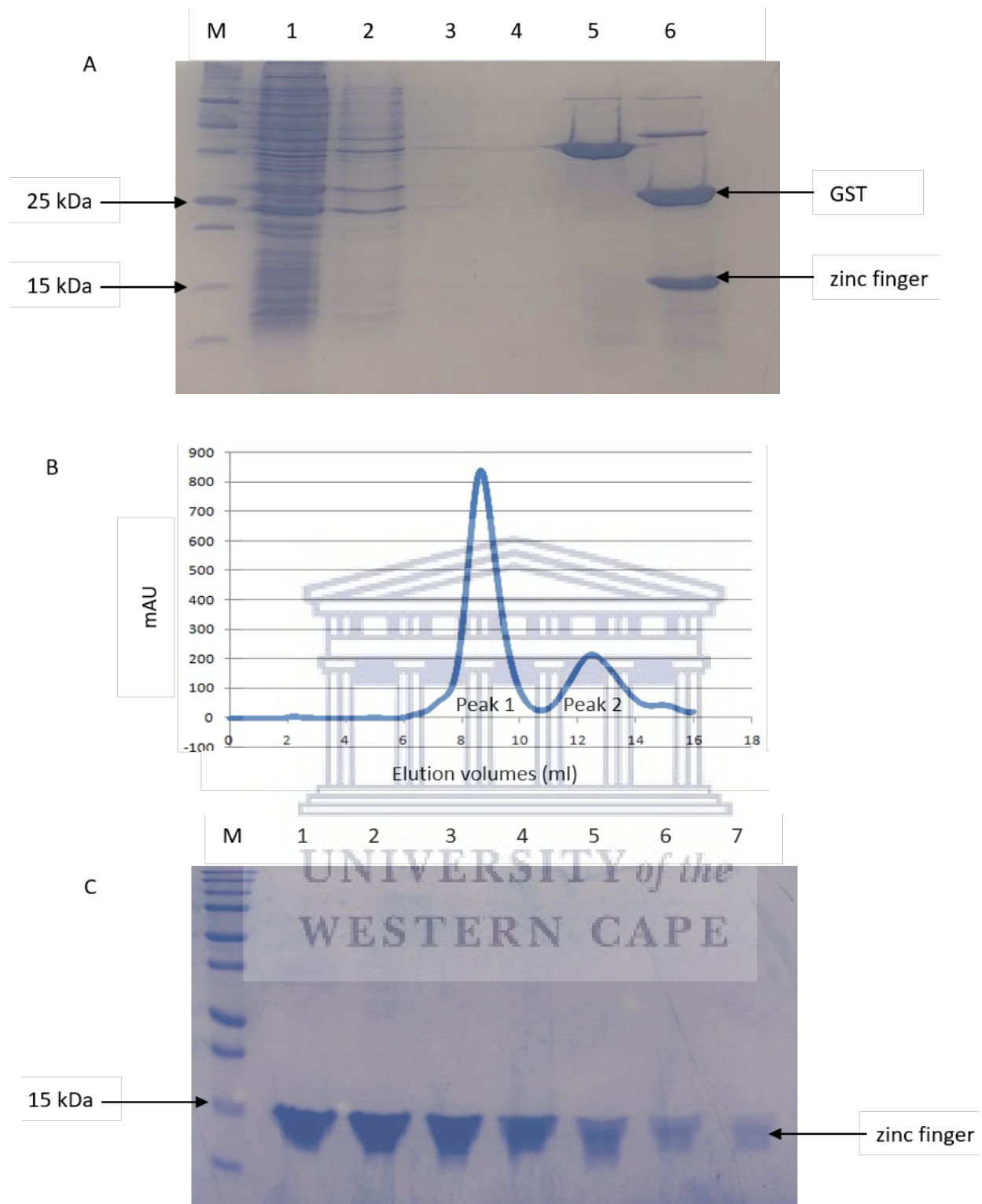


**Figure 4.2 Purification of GST-zinc** (A) Affinity purification of GST-zinc using Glutathione affinity chromatography. GST-zinc eluting at 38 kDa in lane 5. Lane 6 shows a complete cleavage of GST (25 kDa) from zinc (13.7 kDa). Lane M contained the Precision Plus protein standard. (B) Good separation of the isolated zinc finger from GST was achieved using size exclusion chromatography. Peak 1 corresponds to GST and peak 2 to the zinc finger. (C) SDS-PAGE analysis of fractions across peak 2 in panel B. Lanes 1 – 7 shows highly purified zinc finger at 14 kDa, confirming the zinc finger was effectively separated from GST

The results of the pull-down are shown in Figure 4.3. Zinc finger was precipitated by GST-UBA (lane 7), but not by GST alone (lane 5), nor by the glutathione agarose beads alone either (lane 4). Lane 2, which contains only zinc finger loaded directly onto the gel, without washing, shows that the anti-zinc finger antibody does in fact detect the zinc finger. The presence of a band at the same level as that in lane 7 confirms that the band seen in lane 7 corresponds to the zinc finger.

Lane 1, which contains only GST-UBA loaded directly onto the gel, without washing, shows that the antibody does not detect GST-UBA at the size corresponding to the zinc finger. The absence of a band confirms that the band seen in lane 7 does not correspond to GST-UBA. Hence Figure 4.3 confirms the presence of a clear and unambiguous interaction between the zinc finger from the RBBP6 and the UBA domain from Ubch1.

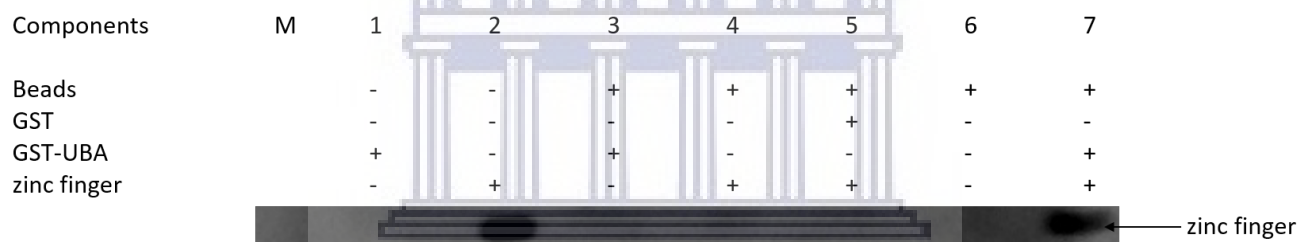


**Figure 4.3 GST pull-down of zinc finger by GST UBA.** Zinc finger is successfully pulled down by GST-UBA (lane 7) but not by GST alone (lane 5) nor by the beads alone (lane 4). Zinc finger was loaded directly into lane 2, without being subjected to washes. GST-UBA was loaded directly into lane 1, without being subjected to washes.

#### 4.4 Chemical shift perturbation assay of $^{15}\text{N}$ -labelled UBA by unlabelled zinc finger

The interaction between UBA and the zinc finger domain was investigated further by NMR chemical shift perturbation assays. As described in Chapter 3, this assay investigates the chemical shift perturbations produced in the  $^{15}\text{N}$ - $^1\text{H}$ -HSQC spectrum of a  $^{15}\text{N}$ -enriched protein when a second un-labelled protein is added. The un-labelled protein is not detected in the  $^{15}\text{N}$ - $^1\text{H}$ -HSQC spectrum; only its effects on the spectrum of the labelled protein are detected.

A  $^{15}\text{N}$ -enriched sample of UBA was expressed as described in Sections 2.5 and purified in the same manner as for unlabelled UBA.  $^{15}\text{N}$ -UBA was separated from GST using 3C protease and size

exclusion chromatography, concentrated to 670  $\mu\text{M}$  and used to record a  $^{15}\text{N},^1\text{H}$ -HSQC spectrum at 500 MHz for 14 hours. As seen in Figure 4.4 (A), the spectrum showed a good dispersion of resonances, which is indicative of a folded protein. The spectrum is consistent with the previously published spectrum (Wilson *et al.*, 2011); particularly characteristic is the isolated resonance around 10 ppm that corresponds to the side chain (indole) resonance of the single tryptophan residue in the UBA domain, W188. In our spectrum, although not in that of Wilson *et al.*, the resonance is split into a larger and a smaller resonance, suggesting that the tryptophan may be occupying two slightly different conformations in slow exchange with each other. Slow exchange means that, on average, the protein stays in each of the two states for longer than the time taken to record the basic unit of NMR data, the Free Induction Decay (FID), which is of the order of 100 ms.

For the chemical shift assays, unlabelled zinc finger domain was added to  $^{15}\text{N}$ -UBA, producing molar ratios 1:0.5, 1:1 and 1:2 (UBA:zinc) respectively. A  $^{15}\text{N},^1\text{H}$ -HSQC spectrum was recorded after each addition of zinc finger domain, with total acquisition time in each case being 14 hours. A large number of differences were observed as the zinc finger domain was added; an overlay of the 1:2 spectrum (green) on the 1:0 spectrum is shown in Figure 4.4. Broadly characterized, addition of the zinc finger domain leads to loss of dispersion of the spectrum. This is particularly apparent in the resonances between 8.5 and 9.0 ppm. The  $\text{NH}_2$  group with  $^{15}\text{N}$  shift around 110 ppm also decays. Loss of these peaks is generally associated with loss of secondary structure, resulting in the resonances approaching the “random-coil” chemical shifts associated with free amino acids. The effects on the indole, in the extreme left hand corner, are specifically interesting; the resonance shifts entirely to the weaker of the two peaks seen in the absence of zinc finger domain.

These changes suggest that the addition of the zinc finger domain stabilizes the less folded configuration discussed above. This conclusion is supported by our observation that, following recording of the 1:1 ( $^{15}\text{N}$ -UBA:zinc) spectrum, some cloudiness was observed in the sample tube, which we removed by centrifugation. After recording the 1:2 ( $^{15}\text{N}$ -UBA:zinc) spectrum, significant precipitation was observed at the bottom of the NMR tube.

Hence our data suggests that the zinc finger domain binds to one configuration of the UBA and causes it to precipitate. An alternative explanation is that  $^{15}\text{N}$ -UBA unfolded spontaneously, without the assistance of the zinc finger domain, perhaps due to the long hours spent in the NMR spectrometer at 25 °C. A useful control for this would have been to prepare an identical sample of  $^{15}\text{N}$ -UBA and leave it at 25 °C for the same length of time as the one to which zinc finger domain was added, in order to determine whether it also unfolded. However this was not done. Alternatively, using a higher sensitivity spectrometer would allow the entire titration to be carried out in a shorter time, which should eliminate the possibility of unfolding due to time spent at 25 °C.

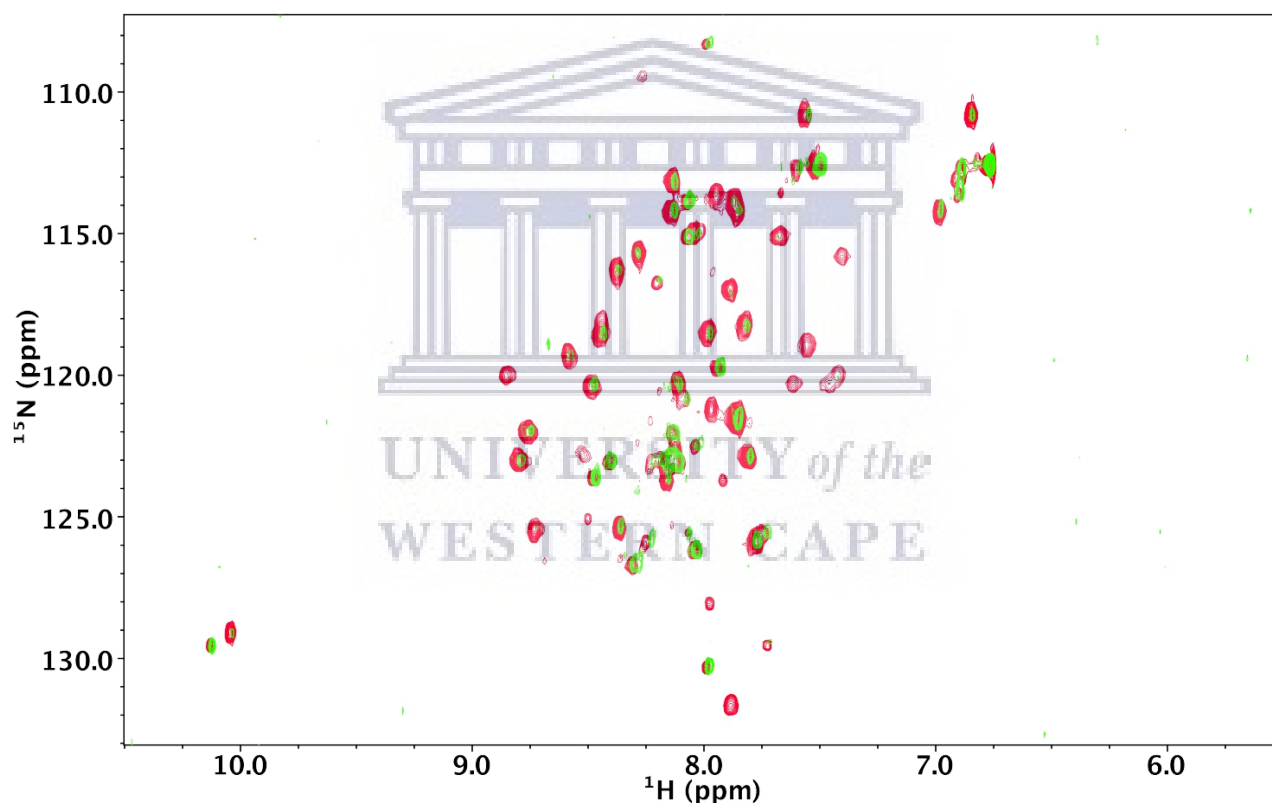


**Figure 4.4** Chemical shift perturbation investigation of the interaction between UBA and zinc finger domain. The  $^{15}\text{N}$ ,  $^1\text{H}$ -HSQC spectrum of  $^{15}\text{N}$ -enriched UBA (red) is overlaid following the addition of zinc finger (green) at a molar ratio of 1:2.

Yet another explanation is that a significant fraction of the zinc finger may be unfolded, which may lead to non-specific hydrophobic interactions between the unfolded portion of the zinc finger domain and the unfolded conformation of the UBA. A structure of the RBBP6 zinc finger

domain in the Protein Data Bank suggests that only the region immediately around the CCHC motif is structured; in the case of our particular construct, this would suggest that the N-terminal half of the construct was unfolded. In an attempt to eliminate this possibility, we decided to make a shorter fragment, corresponding to the C-terminal half of the previous zinc finger construct.

#### **4.5 Design and cloning of zinc-C finger**

The zinc finger domain used in the previous section spanned residues 80-197 of RBBP6. As can be seen from Figure 4.6 (A), the zinc finger domain motif, Cys-Cys-His-Cys, is located near the C-terminus of this fragment. We therefore decided to sub-clone residues 156-197, comprising the C-terminus of the previous fragment, which was named zinc-C. Primers pGEX-zinc-C-F and pGEX-zinc-C-R were designed as shown in Table 4.1

BamHI (green) and XhoI (yellow) restriction sites were incorporated into the forward and reverse primers respectively, for cloning into the same sites of pGEX-6P-2. The reverse primer also included two stop codons (red).

A cDNA of the expected size (150 bp) was successfully amplified, as shown in lane 2 of Figure 4.6, using the previous zinc finger domain construct as a template. The pGEX-6P-2-RBBP6-RING expression plasmid, containing the RING finger from RBBP6 inserted into the BamHI and XhoI sites of pGEX-6P-2, was digested with BamHI and XhoI, as shown in Figure 4.6 (B), releasing an insert of 250 bp corresponding to the RING finger in lane 4. The larger band in lane 4, corresponding to the pGEX-6P-2 vector, was excised from the gel and ligated with the amplicon following digestion with BamHI and XhoI as described in Section 2.4.3. Plasmid DNA was extracted from the positive transformants and digested with BamHI and XhoI, releasing a fragment of the expected size of 120 bp as seen in lanes 3 and 5 of Figure 4.6 (D). Plasmid DNA was subjected to sequencing (Inqaba Biotechnological Industries, Hatfield, South Africa) and found to be identical with the expected sequence.



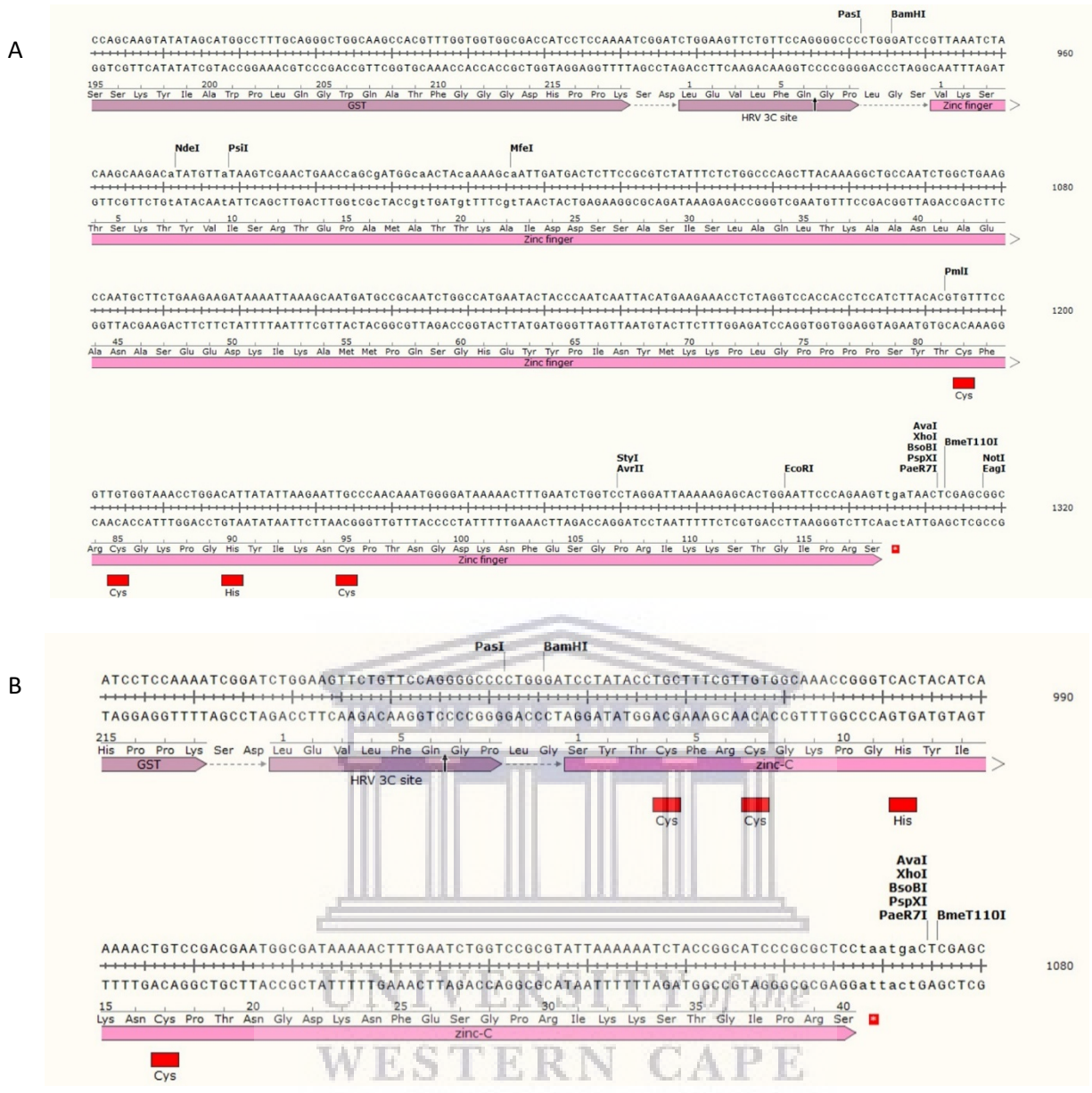


**Figure 4.5 Design of the zinc-C finger construct.** (A) Zinc finger domain of RBBP6 construct at 354 bp. (B) Newly designed zinc-C finger leaving the zinc finger motifs (CCHC) intact, the newly constructed construct has been shortened to 120 bp.

**Table 4.1: Primers used to amplify the zinc-C finger fragment.** The restriction enzyme sites in green (BamH1) and yellow (Xho1); the two stop codons are shown in red.

Primer	Primer Sequence	Melting Temperature
pGEX-zinc-C-F	5' – GAGGCG <b>GGA TCC</b> TCT TAC ACG TGT TTC CGT TGT – 3'	60 °C
pGEX-zinc-C-R	5' – GAGGCG <b>CTC GAG TCA TTA</b> ACT TCT GGG AAT TCC AGT GC – 3'	60 °C

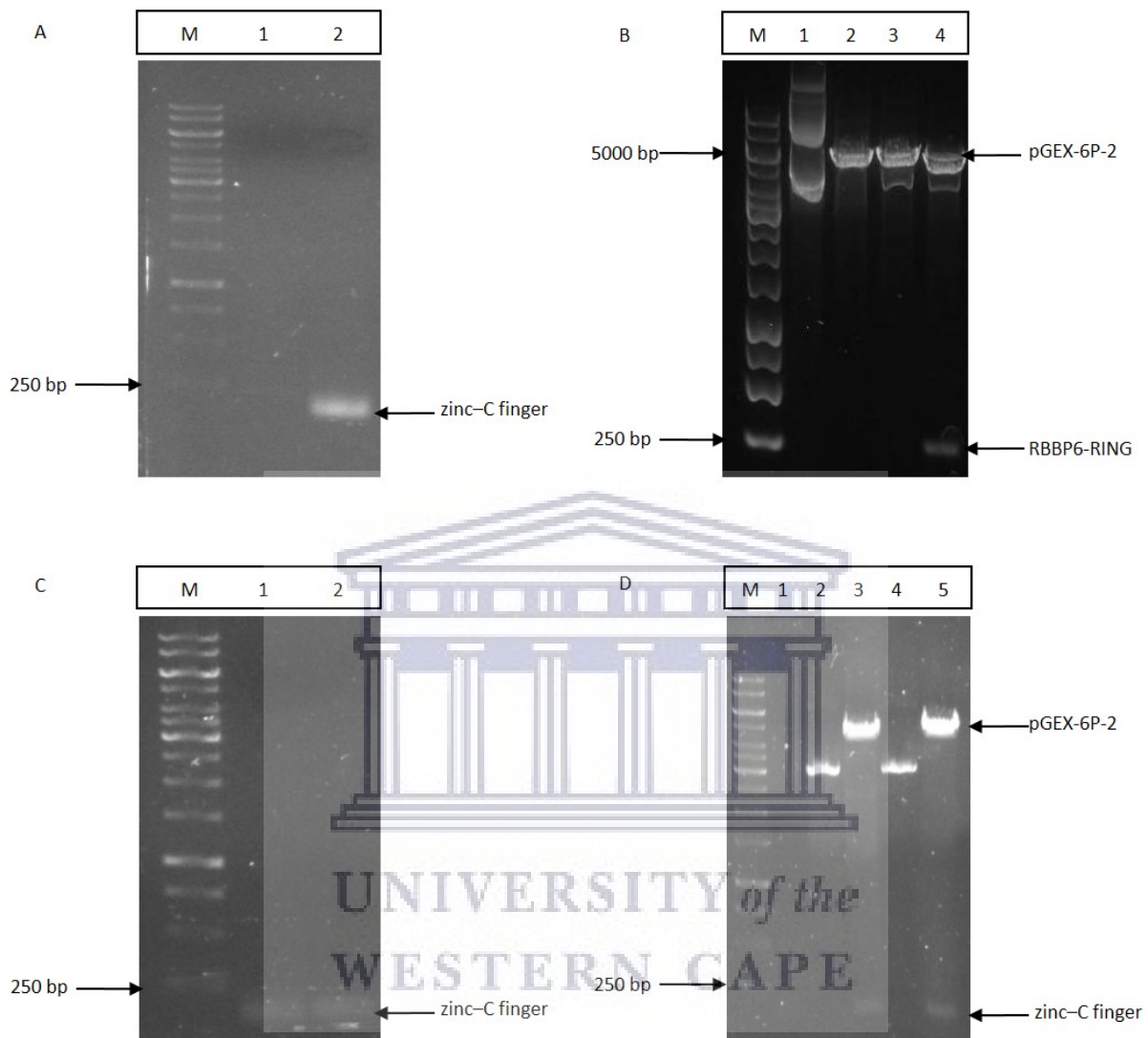


**Figure 4.6 The cloning of pGEX-6P2-zinc-C finger construct.** (A) Positive amplification of the zinc-C finger from zinc finger construct, lane M contains the O'GeneRuler 1Kb DNA ladder, lane 1 show the negative PCR control and lane 2 shows the positive amplification of zinc-C finger. (B) Double digest of the pGEX-6P2-RBBP6-RING construct, lane 1 shows the undigested construct; lanes 2 and 3 show the construct cut with BamH1 and Xho1 respectively, lane 4 shows the double digestion of the vector releasing the RBBP6-RING insert at 250 bp. (C) Double digestion of the amplified zinc-C construct, lane 1 shows undigested zinc-C fragment and lane 2 shows the zinc-C fragment double digested with BamH1 and Xho1. (D) pGEX-6P2-zinc-C finger was double digest confirming correct construct was ligated; lane 2 the undigested construct and lane 3 shows roughly a 120 bp insert being released after digestion with BamH1 and Xho1. Lanes 4 and 5 shows the same construct digested as in lanes 2 and 3 but generated using a different ligation ratio, thus confirming pGEX-6P2-zinc-C finger construct was generated at ligation ratios of 1:19 and 1:24 respectively.

#### 4.6 Recombinant expression and purification of zinc-C finger

The newly constructed pGEX-6P2-zinc-C was expressed at a large scale and purified in the same manner as described in Section 4.2. The zinc-C finger was successfully expressed and purified from the GST-tag, as shown in Figure 4.7.

#### 4.7 The *in vitro* interaction between UBA and zinc-C finger

GST pull-down assays involving zinc-C as the “prey” and GST-UBA as the “bait” were carried out as described above. The results are shown in Figure 4.8. The strong band in lane 7 shows that zinc-C is strongly pulled down by GST-UBA, but not by GST alone (lane 5) and nor by the glutathione beads (lane 3). Lane 1 contains zinc-C loaded directly onto the gel (no washes), and serves as a positive control for detection of zinc-C by the polyclonal antibody raised against the full zinc finger (residues 80-197 of RBBP6). It also confirms that the band in lane 7 is indeed zinc-C. Lane 2 contains GST-UBA, again loaded directly onto the gel (no washes), and serves as a negative control, showing that the antibody targeting the zinc-C antibody confirms that the band in lane 7 is not UBA.



UNIVERSITY of the  
WESTERN CAPE

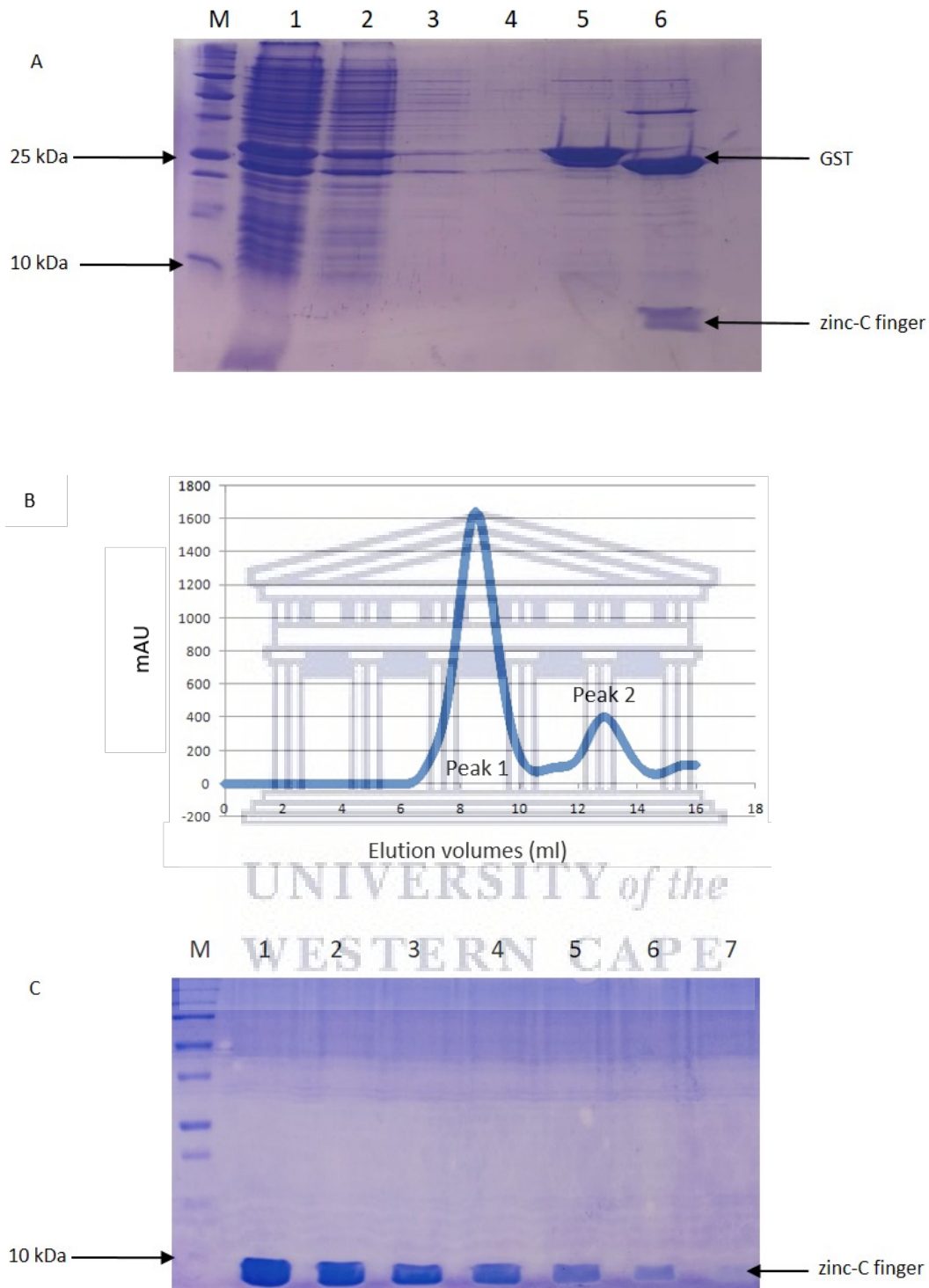


**Figure 4.7 Purification of GST zinc-C finger.** (A) Affinity purification of GST-zinc-C using glutathione affinity chromatography. GST-zinc-C eluting at 30 kDa in lane 5. Lane 6 shows a complete cleavage of GST (25 kDa) from zinc-C (4.5 kDa). (B) Good separation of the isolated zinc-C finger from GST was achieved using size exclusion chromatography. Peak 1 corresponds to GST and peak 2 to the zinc-C finger. (C) SDS-PAGE analysis of fractions across peak 2 in panel B. Lanes 1 – 7 shows highly purified zinc-C finger at 4.5 kDa.



**Figure 4.8 GST pull-down of zinc-C finger by GST UBA.** Zinc-C finger is successfully pulled down by GST-UBA (lane 7) but not by GST alone (lane 5) nor by the beads alone (lane 5). Zinc-C finger was loaded directly into lane 1, without being subjected to washes. GST UBA was loaded directly into lane 2, without being subjected to washes. Lane M contained the western marker.

#### 4.8 Protein interaction investigated by size exclusion chromatography

Analytical size exclusion chromatography (SEC) was performed to confirm the interaction between the UBA and zinc-C finger domains. Equal amounts of UBA and zinc-C proteins were separately subjected to size exclusion chromatography and the respective chromatograms were recorded. They are overlaid in blue and red respectively in Figure 4.9. Following this, equimolar quantities of UBA and zinc-C finger were incubated for an hour to allow for complex formation, after which, the protein mixture was subjected to SEC and the chromatogram was recorded. It is overlaid on the other two in green. Also shown is the sum of the two separate chromatograms, (in yellow), which corresponds to what we would expect to see if there were no interaction between the two proteins. The trace of the mixture (in green) is significantly different from the yellow line; it has lower intensity and has a shoulder eluting earlier than the main peak. We hypothesized that this shoulder may correspond to the bound complex between the UBA and zinc-C finger.

In order to test this hypothesis, we made a model by assuming that a fraction  $\alpha$  ( $\alpha$  is between 0 and 1) of each protein forms part of a hetero-dimeric complex. A fraction  $(1-\alpha)$  therefore remains monomeric. We constructed two traces: Trace A corresponds to the non-interacting monomers, and is the same as the yellow line in Figure 4.9. Trace B, corresponding to the hetero-dimers, was generated by shifting Trace A, using Excel, by a volume  $\delta$  ml. Trace B was scaled by a factor  $\alpha$ , and Trace A by a factor of  $(1-\alpha)$ , and the two were added to give the trace shown in purple.

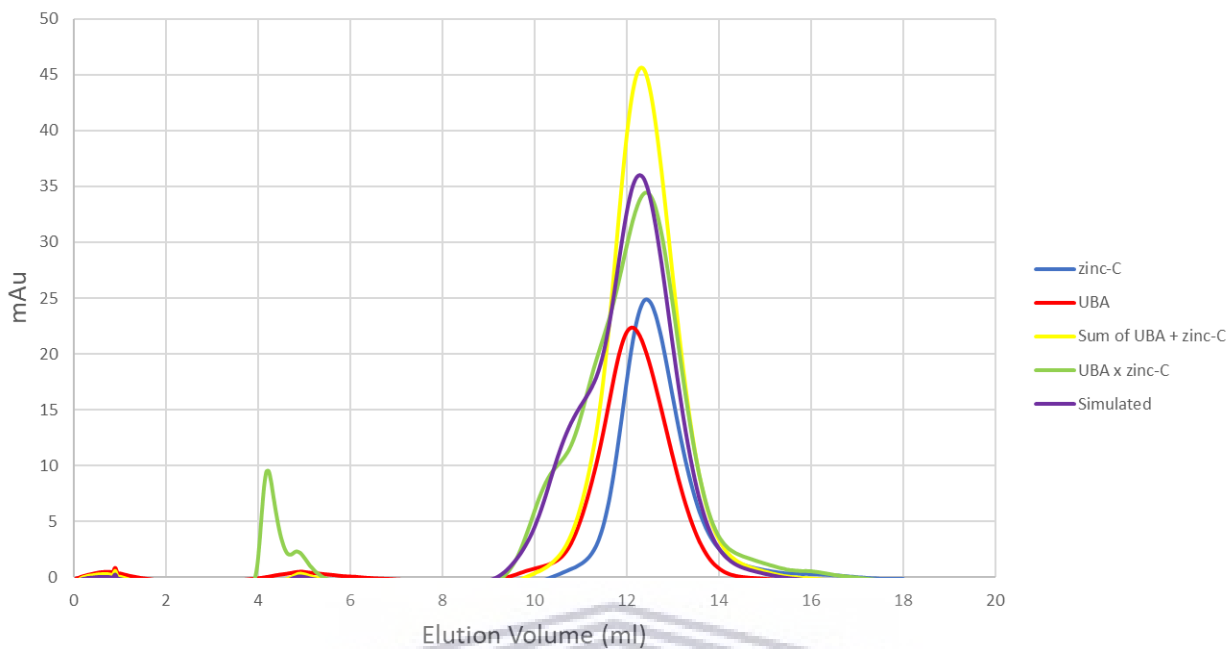


**Figure 4.9 Size exclusion of UBA, zinc-C and UBA/zinc-C superimposed.** The UBA and zinc-C were run on the size exclusion separately shown in red and blue respectively. The simulated sum of the monomeric UBA and monomeric zinc-C is shown in yellow; whilst the UBA and zinc-C sample run down the size exclusion column together shown in green. The simulated trace by manually tuning the  $\alpha$  and  $\delta$  parameters to fit the UBA x zinc-C trace is shown in purple.

The values of  $\alpha$  and  $\delta$  were then varied by trial and error to optimize the fit of the purple line to the yellow line. The best fit was obtained with  $\alpha = 0.24$  and  $\delta = 1.5$  ml, from which we concluded that 24 % of each protein was involved in the hetero-dimeric complex, and that the complex eluted 1.5 ml earlier than the average of the monomers, which is around 12.15 ml.

If the earlier peaks correspond to the hetero-dimer, then we would expect it to have a mass approximately twice that of the individual monomers. In order to estimate the approximate size of the complex, a standard curve was constructed, using the known masses and elution volumes of the two monomers, as well as two standard proteins of known MW whose elution volumes has previously been measured on the same column. The MWs and elution volumes are shown in the table in Figure 4.10. Fitting a straight line through the points yielded a slope of -5.0. From this we conclude that a shift of 1.5 ml corresponds to a fold increase in MW of  $10^{1.5/5.0} = 2.0$ . This is consistent with the shoulder corresponding to the hetero-dimer.

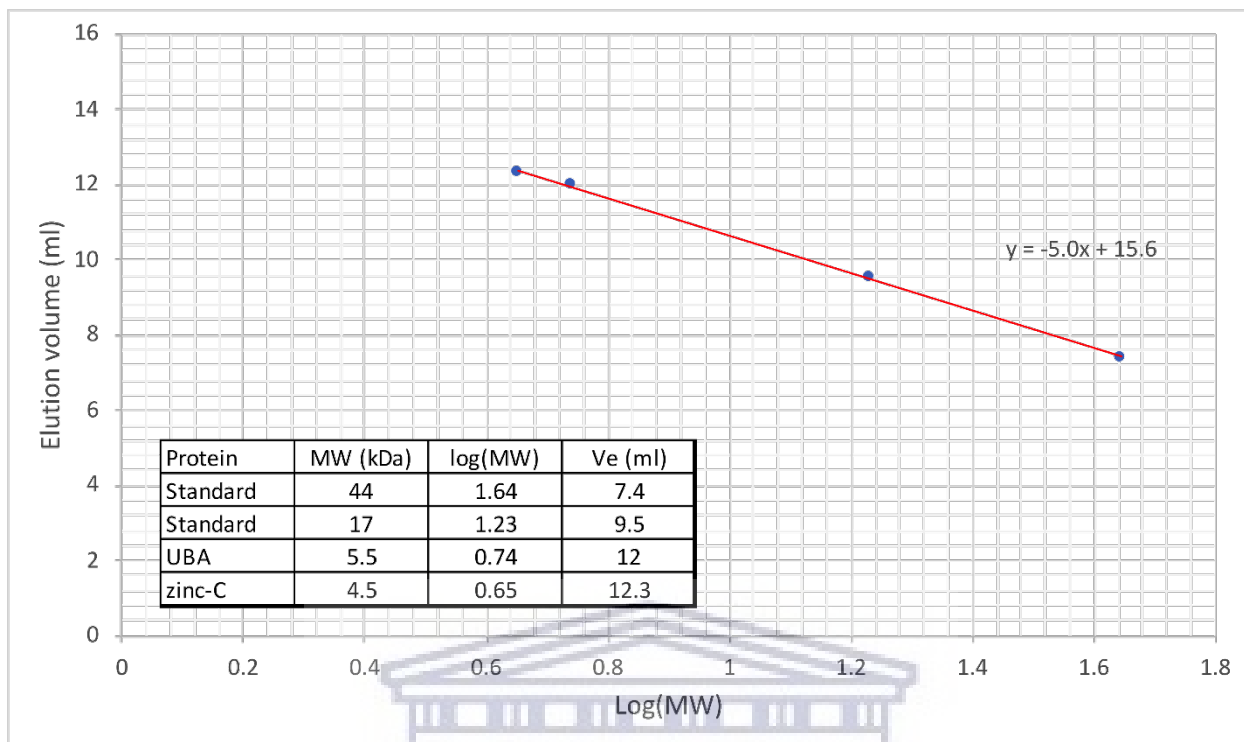


**Figure 4.10 Standard curve for the size exclusion column.** The masses and elution volumes of UBA and zinc-C, as well as the masses of two protein whose elution volumes on the same column had previously been determined, were used to construct a standard curve.

#### 4.9 Chemical shift perturbation of $^{15}\text{N}$ -labelled UBA by unlabeled zinc-C finger

GST pull-down assays and SEC analysis showed that the UBA interacted with the zinc-C finger protein, localizing the interaction to a small region of RBBP6 centered on the zinc finger (CCHC) motif. In order to identify amino acids directly involved in the interaction, the interaction was investigated further by NMR chemical shift perturbation assay.

$^{15}\text{N}$ -UBA was expressed and purified as described in Sections 2.5 and 4.2 respectively.  $^{15}\text{N}$ -UBA was concentrated to 786.4  $\mu\text{M}$  and used to record a  $^{15}\text{N}$ - $^1\text{H}$ -HSQC spectrum at 500 MHz for 14 hours. As can be seen in Figure 4.12 (A), the spectrum is consistent with that recorded previously (Figure 4.4). Unlabeled zinc-C finger was added to  $^{15}\text{N}$ -UBA, giving molar ratios of 50 % and 100 % ( $[\text{zinc-C}] / [\text{UBA}] * 100$ ) respectively.

The results showed a spectrum extremely similar to that of Figure 4.4, panel B, following addition of the longer zinc finger construct; addition of zinc-C leads to reduction of the more dispersed peaks between 8.5 and 9.0 ppm, and increase of some of the smaller peaks, including increase of the smaller indole peak. Again, this is consistent with zinc-C stabilizing the secondary configuration, which is also the less well-folded of the two, due to the lower dispersion.

Poorly structured proteins are more likely to aggregate in solution, and this was what was observed. After acquisition of the 50 % zinc-C addition there was some evidence of cloudiness in the NMR tube, indicating a small amount of aggregation; after the 100 % addition there was significant precipitate at the bottom of the NMR tube.

Hence our data suggest that the UBA fragment exists in more than one conformation in solution, a stable one and a less stable one, and that zinc-C binds strongly to the less stable conformation. But, as before, it is also possible that the stable conformation of UBA converts spontaneously to the less stable one, without the involvement of zinc-C. Since samples did not precipitate spontaneously when stored at 4 °C, this could be due to the long periods (14 hours per spectrum) spent in the NMR tube at 25 °C.

In order to rule out this possibility, new samples were expressed and purified and the experiment repeated using a 700 MHz spectrometer fitted with a cryoprobe. This was carried out at King's College London by our collaborator, Dr Andrew Atkinson. The greater sensitivity afforded by the cryoprobe allowed the entire titration series to be carried out over the course of a single day, ruling out the possibility of the protein precipitating spontaneously. The <sup>15</sup>N-UBA was concentrated to 760 μM and used to record a <sup>15</sup>N,<sup>1</sup>H-HSQC spectrum. Zinc-C was then added to final relative concentrations of 20 %, 50 %, 100 % and 300 % ( $[\text{zinc-C}] / [\text{UBA}] * 100$ ), and <sup>15</sup>N,<sup>1</sup>H-HSQC spectrum recorded after each addition.

The results, shown in Figure 4.11, confirm the previous results generated at UWC on lower field strength spectrometers. In the absence of added zinc-C (red), the indole resonance (bottom left) shows that, here too, the protein is present in two configurations; however, compared to previous spectra, the two configurations are present in almost equal amounts (50 % : 50 %). This can be seen more clearly in Figure 4.12, which shows a comparison of the <sup>15</sup>N-UBA spectrum



generated at UWC (A) and the spectrum from the spectrometer fitted with the cryoprobe (B), both in the absence of zinc finger. The peaks indicated by the blue oval are strong in panel B, but almost unseen in panel A. The sample was lyophilized prior to shipping to the U.K., and re-suspended on arrival, which may account for the different relative populations of the two conformations.

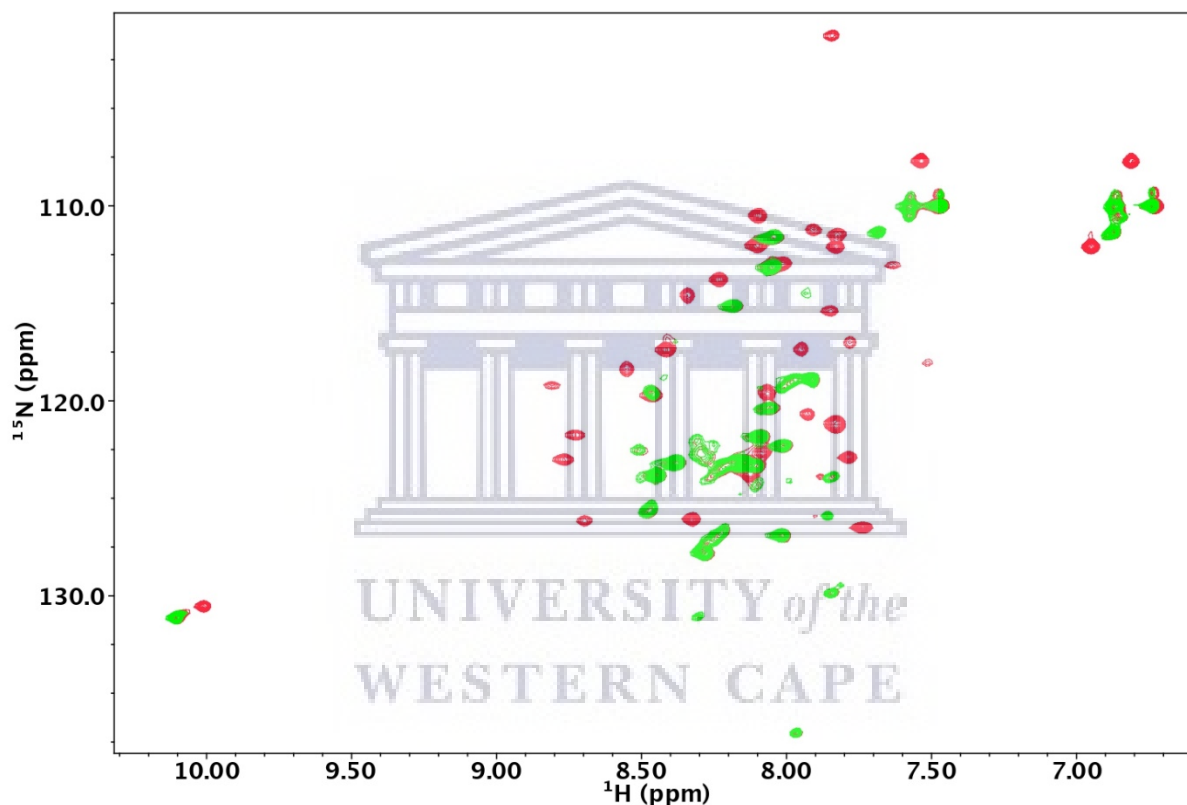


**Figure 4.11** Chemical shift perturbation investigation of the interaction between UBA and zinc-C finger. The  $^{15}\text{N}$ -UBA spectra (red) is overlaid following addition of zinc-C finger at a molar ratio of 300 % (green) ( $[\text{zinc-C}] / [\text{UBA}] * 100$ ).

As before, addition of zinc-C led to enhancement of the less folded conformation. By 300 % there is complete loss of the rightmost indole resonance, the resonances between 9.0 and 8.5 ppm and the  $\text{NH}_2$  group at 108 ppm ( $^{15}\text{N}$ ). As before, the sample showed sign of precipitation after recording of the 300 % addition, but not at the 100 % addition. However, since the whole

titrations was carried out within one day, the precipitation is very unlikely to be the result of time spent at 25 °C. Hence it is most likely to be the result of the addition of zinc-C.

Analyzing the structure of Ubch1 on PyMol (Figures 1.7 and 1.8), it can be seen that Trp188 circled in red in Figure 4.12 forms just one of a number of hydrophobic residues forming part of the interacting interface that connects the E2 domain to the UBA domain. Since we are only working with the UBA domain, removal of the E2 domain will have left a hydrophobic patch which will be energetically unfavorable and will destabilize the remaining protein. This may account for the presence of two conformations.

This raises the question of whether the interaction is biologically meaningful, or whether it is merely an artefact of using small fragments of proteins which do not adopt the same conformations as the full proteins. The reality is that the isolated UBA does not occur in nature, and all conclusions reached using it must therefore be treated with caution. The more structured configuration does not necessarily represent the biologically relevant configuration; the less structured configuration may be the more stable configuration when the rest of Ubch1 is there to stabilize it. Or a configuration shift may be required for the UBA to bind to zinc finger, and that configuration may be stable in the context of the whole protein. It would therefore be useful to know whether the zinc finger of RBBP6 interacts with the whole of Ubch1; however this investigation was not done.

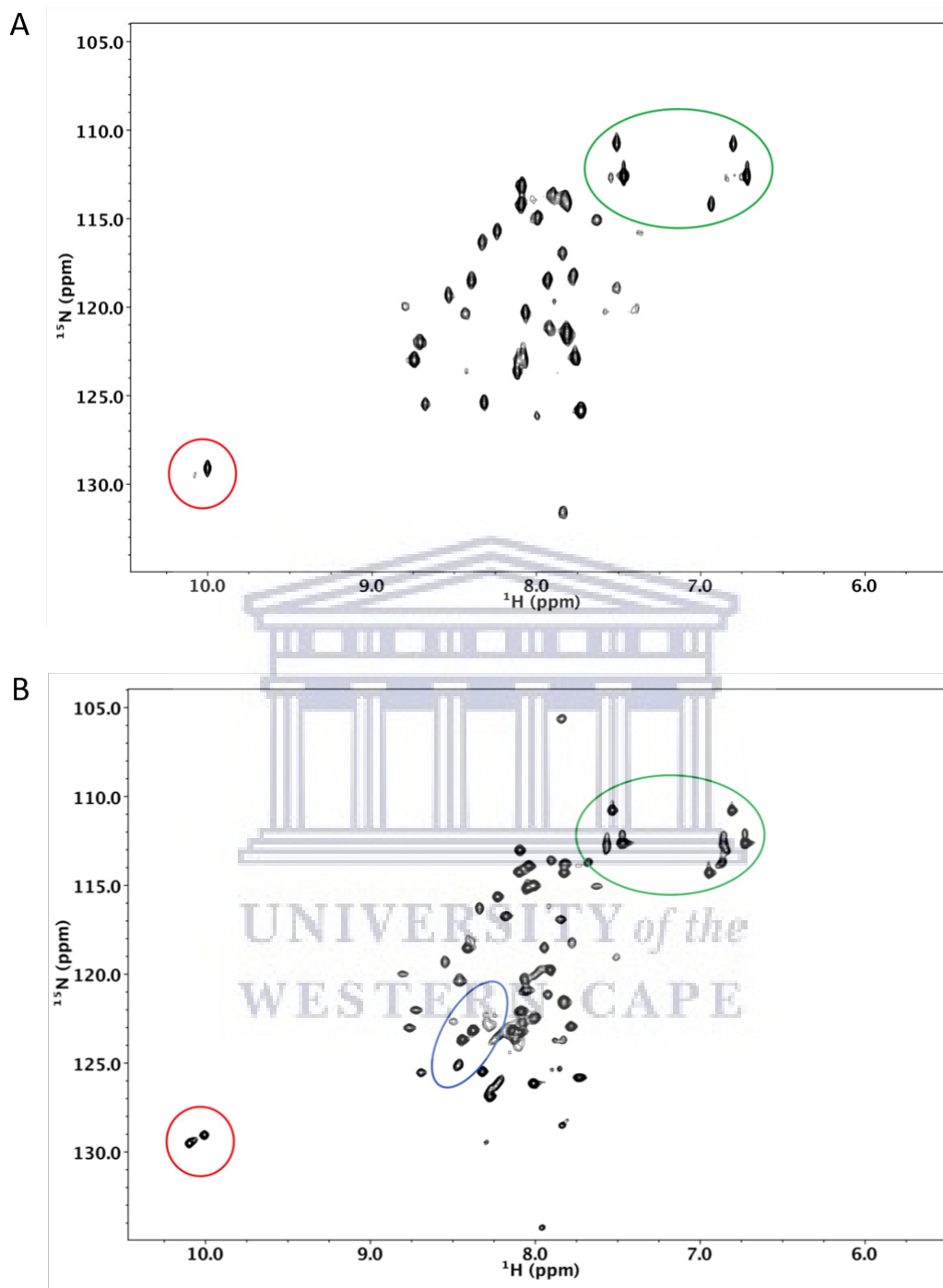


**Figure 4.12 Comparison of  $^{15}\text{N}$ ,  $^1\text{H}$ -HSQC spectrum of  $^{15}\text{N}$  UBA without zinc-C finger.** The different conformation of the UBA is seen in the two different spectra's, panel A contains the spectra obtained from UWC shows one conformation of the UBA whilst the spectra in panel B obtained from the spectrometer fitted with the cryoprobe shows the both conformations of UBA in almost equal amounts (50%:50%).

## Chapter 5

### Conclusions and outlook

In this study, GST pull-down assays and NMR spectroscopy were used to characterize protein-protein interacting partners of RBBP6. More specifically, the aim was to use GST pull-down assays to confirm the interactions between the RING domains of RBBP6 and MDM2 *in vitro*, as well as between the zinc finger domain of RBBP6 and the UBA domain of Ubch1. This would be followed by NMR-based chemical shift perturbation assays to assess the affinity of the interactions and to identify residues on each domain involved in the interaction. The information would be used to build a model of the interaction complex to determine the position of the interaction interface, and to identify targets for mutagenesis aimed at modulating the interaction.

#### 5.1 Characterization of the interaction between the RING finger domains of RBBP6 and MDM2

The RING finger domains from RBBP6 and MDM2 were expressed as fusions with GST using existing expression constructs, and purified using glutathione affinity chromatography. The ability of GST-MDM2-RING (the “bait”) to co-precipitate HA-RBBP6-RING (the “prey”) was investigated by GST pull-down assay, and detected using Western blotting with antibodies targeting the HA-tag. The results confirm that MDM2-RING was able to pull down RBBP6-RING and the analysis of the signal suggests that the interaction is relatively strong.

Next, NMR-based chemical shift perturbation assays were used to confirm the interaction. The RBBP6-RING was isotopically labelled with  $^{15}\text{N}$  by being expressed in minimal media supplemented with  $^{15}\text{N}$  enriched ammonium chloride. The  $^{15}\text{N},^1\text{H}$ -HSQC spectra of the  $^{15}\text{N}$ -RBBP6-RING was recorded before and after addition of un-labelled MDM2-RING. A number of significant changes were observed, which is suggestive of an interaction between the two RINGs. Unfortunately, the observed shifts in the peaks of the overlaid spectrum were also consistent

with the dilution-dependent shifts reported by Kappo and co-workers; which result from homo-dimerization of RBBP6-RING.

However, some aspects of the changes do appear to be different from the dilution-dependent changes, which means that the data do not rule out the possibility of an interaction between RBBP6-RING and MDM2-RING. Firstly with the addition of MDM2-RING to  $^{15}\text{N}$ -RBBP6-RING the spectra seem to become a little broader, as opposed to becoming narrower as would be expected if the changes were entirely caused by the protein becoming more monomeric. The broadening would indicate that the effective MW of the protein was increasing, which is what would happen if it were forming a hetero-dimeric complex with MDM2-RING. Secondly, one or two new unassigned peaks appear and some peaks disappear, and a number of the chemical shift changes appear to be in a direction different from that caused by dilution. The new peaks are not very far above the noise, and therefore we cannot be sure that they are significant. Greater sensitivity measurement will be required to follow up on these. Furthermore, due to the poor stability of MDM2-RING, we were unable to achieve more than 60 % relative stoichiometry; this has the consequence that we would not be able to observe more than 60 % of any change in the spectra of the RBBP6-RING protein. The investigation should therefore be repeated with greater stoichiometry. One way of achieving this would be to optimize the expression of MDM2-RING; however its poor solubility may not allow its concentration to be increased much further. A more reliable method may be to decrease the concentration of RBBP6-RING; while this would greatly increase the NMR acquisition time, this could be countered by using a machine with a higher sensitivity fitted with a cryoprobe. Another method may be to use one of the monomeric mutants of the RBBP6-RING finger, since they will not be affected by dilutions and therefore any changes can be entirely attributed to interactions. Naturally, it would be advisable to confirm using GST pull-down that the mutant RBBP6-RING does interact with MDM2-RING before moving onto NMR based studies.

Although significant steps were taken to minimize the background signal caused by the homo-dimerization of RBBP6-RING such as using as low a concentration of RBBP6-RING as was feasible within the constraints of available spectrometer time, and as high a concentration of MDM2-

RING as could be achieved with ultracentrifugation devices, the dilution-dependent background signal of RBBP6-RING was still too high to get a clear signal of the hetero-dimeric complex. Hence the RBBP6-RING/MDM2-RING complex was not investigated further at the time.

In conclusion, although our NMR data is inconclusive, it also does not rule out the possibility that RBBP6 and MDM2 do interact through their RING finger domains. The unambiguous evidence provided by our GST pull-down assay allows us to conclude that this important interaction does exist.

## **5.2 Characterization of the interaction between the zinc finger domain of RBBP6 and the UBA domain of Ubch1**

The UBA domain from Ubch1 and the zinc finger from RBBP6 were expressed as fusions with GST and purified from existing expression constructs. The ability of GST-UBA (the “bait”) to pull down RBBP6-zinc finger (the “prey”) was investigated using GST pull-down assay, probing for co-precipitated zinc finger by western blotting with antibodies targeting the zinc finger. The results confirm that the UBA was able to pull down the zinc finger.

Analytical size exclusion chromatography showed that when the two proteins were loaded simultaneously onto the column, the resulting chromatogram featured a pronounced shoulder eluting earlier than would have been expected, based on the chromatograms of the individual domains. The peak was also significantly smaller than would have been expected, consistent with some of the protein forming part of a hetero-dimeric complex. Estimation of the effective size of a putative complex giving rise to this shoulder showed that it is consistent with a hetero-dimeric complex between the UBA and the zinc finger.

NMR-based chemical shift perturbation assays were used to confirm the interaction, using the same methodology as for the RING-RING interaction. The good solubility of the <sup>15</sup>N-UBA meant that it was possible to get up to 3-times stoichiometric ratio of prey to bait (in the case of the RING-RING interaction it was only 0.6-times). The entire assay was performed three times, some months apart, but yielded the same result each time, namely that addition of the zinc-finger

caused UBA to unfold and eventually precipitate. This was evident physically, from cloudiness in the NMR tube, as well as in the  $^{15}\text{N},^1\text{H}$ -HSQC spectrum, where well-dispersed resonances corresponding to well-structured regions decayed, and new, less well-dispersed resonances, grew. This happened first with a longer form of the zinc finger, of which the first half was suspected to be poorly structured; this raised the possibility that the unfolded nature of the zinc finger was responsible for unfolding of the UBA. Hence, a second construct was cloned and expressed, corresponding to a narrow region immediately surrounding the zinc finger motif. But the same effect was observed.

Analysis of the  $^{15}\text{N},^1\text{H}$ -HSQC spectrum of the UBA showed that two configurations were present even in the absence of zinc finger; one corresponding to the published structure, and another, partially unfolded, configuration. This was most clearly evident in the sidechain indole resonance of the only tryptophan in UBA, which gave rise to 2 resonances where one would have been expected. The three samples produced showed differing relative amounts of the two configurations. Addition of the zinc finger caused the structure to switch to the partially unfolded configuration.

In conclusion, the NMR data confirms that an interaction exists between the zinc finger of RBBP6 and the UBA domain of Ubch1. Binding to a partially unfolded configuration is nevertheless binding. But the important question is whether binding to a partially unfolded configuration is less biologically significant than binding to a fully folded configuration. We are not yet able to answer this question. However, it is quite possible that the partially unfolded configuration may be more folded in the context of the complete Ubch1. It is also possible that the structure is flexible, and that the configuration changes seen in the data are required for binding to RBBP6. Further investigations will be required to answer these questions.

## References

1. Badciong, J., Haas, A., (2002). MDMX is a RING Finger ubiquitin ligase Capable of Synergistically Enhancing MDM2 Ubiquitination. *Journal of Biological Chemistry*, 277, 49668-49675
2. Baleja, J., (2001). Structure determination of Membrane-Associated Proteins from Nuclear Magnetic Resonance data. *Analytical Biochemistry*, 288, 1-15
3. Basaki, Y., Taguchi, K., Izumi, H., Murakami, Y., Kubo, T., Hosoi, F., Watari, K., Nakano, K., Kawaguchi, H., Ohno, S., Kohno, K., Ono, M., Kuwano, M., (2010). Y-box binding protein-1 (YB-1) promotes cell cycle progression through CDC-dependent pathway in human cancer cells. *European Journal of Cancer*, 46, 954-965
4. Bodenhausen, G., Ruben, D.J., (1980). Natural abundance nitrogen -15 NMR by enhanced heteronuclear spectroscopy. *Chemical Physics Letters*, 69(1), 185 – 189
5. Brooks, C.L., Gu, W., (2006). p53 ubiquitination: Mdm2 and beyond. *Molecular cell*, 21(3) 307-315
6. Burroughs, A.M., Jaffee, M., Iyer, L.M., Aravind, L., (2008). Anatomy of the E2 ligase fold: implications for enzymology and evolution of ubiquitin/Ub-like protein conjugation. *Journal of structural biology*, 162, 205-218
7. Capili, A.D., Lima, C.D., (2007). Taking it step by step: mechanistic insights from structural studies of ubiquitin/ubiquitin-like protein modification pathways. *Current Opinion in Structural Biology*, 17, 726-735
8. Chene, P., (2001). The role of tetramerization in p53 function. *Oncogene*, 20, 2611-2617
9. Chibi, M., Meyer, M., Skepu, A., Rees, D.J.G., Moolman-Smook, J.C., Pugh, D.J.R., (2008). RBBP6 Interacts with Multifunctional Protein YB-1 through Its RING Finger Domain, Leading to Ubiquitination and Proteosomal Degradation of YB-1, *Journal of Molecular Biology*, 384, 908-916.
10. Ciechanover, A., (1998). The ubiquitin-proteasome pathway: on protein death and cell life. *EMBO Journal*, 17, 7151-7160



11. Clore, G.M., Gronenborn, A.M., (1998). NMR structure determination of proteins and protein complexes larger than 20 kDa. *Current Opinion in Chemical Biology*, 2(5), 564-570
12. Cordier, F., Grubisha, O., Traincard, F., Veron, M., Delepierre, M., Agou, F., (2008). The zinc finger of NEMO is a functional ubiquitin-binding domain. *Journal of Biological Chemistry*, 284(5), 2902-2907
13. Cordier, F., Grzesiek, S., (1999). Direct observation of hydrogen bonds in proteins by inter-residue  $^3\text{h J NC}$  'scalar couplings. *Journal of the American Chemical Society*, 121(1), 1601-1602
14. Di Giammartino, D.C., Li, W., Ogami, K., Yashinski, J.J., Hoque, M., Tian, B., Manley, J.L., (2014). RBBP6 isoforms regulate the human polyadenylation machinery and modulate expression of mRNAs with AU-rich 3' UTRs. *Genes and Development*, 28, 2248-2260
15. Didier, D., Schiffenbauer, J., Woulfe, S., Zacheis, M., (1988). Characterization of the cDNA encoding a protein binding to the major histocompatibility complex class II Y box, *Proceedings of the National Academy of Science.*, 85, 7322-7326
16. Dlamini, Z., Ledwaba, T., Hull, R., Naicker, S., and Mbita, Z., (2019). RBBP6 Is Abundantly Expressed in Human Cervical Carcinoma and May Be Implicated in Its Malignant Progression. *Biomarkers in Cancer*, 11, 1179299x19829149
17. Eliseeva, I.A., Kim, E.R., Guryanov, S.G., Ovchinnikov, L.P., Lyabin, D.N., (2011). Y-Box Binding Protein 1 and Its Functions, *Biochemistry.*, 76., 1402-1433
18. Fielding, L., (2003). NMR methods for the determination of protein-ligand dissociation constants. *Current Topics in Medicinal Chemistry*, 3(1), 39-53
19. Gamesjaeger, R., Liew, C.H., Loughlin, F.E., Crosslet, M., Mackay, J.P., (2007). Sticky fingers: zinc-fingers as protein-recognition motifs. *Trends in biochemical sciences*, 32, 63-70
20. Gao, S., Witte, M.M., Scott, R.E., (2002). P2P-R protein localizes to the nucleolus of interphase cells and the periphery of chromosomes in mitotic cells which show maximum P2P-R immunoreactivity. *Journal of Cellular Physiology*, 191, 145-154
21. Gu, W., Roeder, R.G., (1997). Activation of p53 sequence-specific DNA binding by acetylation of the p53 C-terminal domain. *Cell*, 90(4) 595-606

22. Haas, A.L., Rose, I.A., (1982). The mechanism of ubiquitin activating enzyme; A kinetic and equilibrium analysis. *Journal of Biological Chemistry*, 257, 10329-10337
23. Haas, A.L., Warms, J.V., Hershko, A., Rose, I.A., (1982). Ubiquitin-activating enzyme mechanism and role in protein-ubiquitin conjugation. *Journal of Biological Chemistry*, 257, 2543-2548
24. Hashizume, R., Fukuda, M., Maeda, I., Nishikawa, H., Oyake, D., Yabuki, Y., Ogata, H., Ohta, T., (2001). The RING heterodimer BRCA1-BARD1 is a ubiquitin ligase inactivated by a breast cancer-derived mutation, *Journal of Biological Chemistry* 276, 14537-14540
25. Hershko, A., Ciechanover, A., (1998). The ubiquitin system. *Annual Review of Biochemistry*, 67, 425-479
26. Hollstein, M., Sidransky, D., Vogelstein, B., Harris, C.C., (1991). p53 mutations in human cancers. *Science*, 253, 49-54
27. Joazeiro, C.A., Weissman, A.M., (2000). RING finger proteins: mediators of ubiquitin ligase activity. *Cell* 102, 549-552
28. Joerger, A.C., Allen, M.D., Fersht, A.R., (2004). Crystal structure of a super stable mutant of human p53 core domain. Insights into the mechanism of rescuing oncogenic mutations. *The Journal of biological chemistry*, 279(2) 1291-1296
29. Joerger, A.C., Fersht, A.R., (2008). Structural biology of the tumor suppressor p53. *Annual Review Biochemistry*, 77, 557-582
30. Kalchman, M.A., Graham, R.K., Xia, G., Koide, H.B., Hodgson, J.G., Graham, K.C., Goldberg, Y.P., Gietz, R.D., Pickart, C.M., Hayden, M.R., (1996). Huntingtin is ubiquitinated and interacts with a specific ubiquitin-conjugating enzyme. *Journal of Biological Chemistry*, 271, 19385-19394
31. Kappo, M.A., AB, E., Hassem, F., Atkinson, R.A., Faro, A., Muleya, V., Mulaudzi, T., Poole, J.O., McKenzie, J.M., Chibi, M., Moolman-Smook, J.C., Rees, D.J.G., & Pugh, D.J.R., (2012). Solution structure of the RING finger- like domain of Retinoblastoma Binding Protein-6 (RBBP6) suggests it functions as a U-Box. *Journal of Biological Chemistry* 287 (10), 7146-7158.

32. Kellenberger, E., Dominguez, C., Fribourg, S., Wasielewski, E., Moras, D., Poterszman, A., Boelens, R., and Kieffer, B., (2005). Solution structure of the C-terminal domain of TFIIF P44 subunit reveals a novel type of C4C4 ring domain involved in protein-protein interactions. *Journal of Biological Chemistry*, 280, 20785-20792
33. Kerscher, O., Felberbaum, R., Hochstrasser, M., (2006). Modification of proteins by ubiquitin and ubiquitin-like proteins. *Annual review of cell and developmental biology*, 22, 159-180
34. Kljashtorny, V., Nikonov, S., Ovchinnikov, L., Lyabin, D., Vodovar, N., Curmi, P., Manivet, P., (2015). The Cold Shock Domain of YB-1 segregates RNA from DNA by non-bonded interactions, *PLOS ONE*, 10, 1371
35. Kloks, C., Spronk, C., Lasonder, E., Hoffmann, A., Vuister, G., Grzesiek, S., Hilbers, C., (2002). The solution structure and DNA-binding properties of the cold-shock domain of the human Y-box proteins YB-1. *Molecular Biology*, 316, 317-326
36. Ko, S., Kang, G.B., Song, S.M., Lee, J.G., Shin, D.Y., Yun, J.H., Sheng, Y., Cheong, C., Jeon, Y.H., Jung, Y.K., Arrowsmith, C.H., Avvakumov, G., Paganon, S.D., Yoo, Y.J., Eom, S.H., Lee, W., (2010). Structural basis of E2-25K/UBB+1 interaction leading to proteasome inhibition and neurotoxicity. *The Journal of Biological Chemistry*, 46, 36070–36080
37. Krishna, S.S., Majumdar, I., Grishin, N.V., (2003). Structural classification of zinc fingers: survey and summary. *Nucleic Acids Res.*, 31, 532-550
38. Lai, Z., Yang, T., Kim, Y., Sielecki, T., Diamond, M., Strack, P., Rolfe, M., Caligiuri, M., Benfields, P., Auger, K., Copeland, R., (2002). Differentiation of Hdm2-mediated p53 ubiquitination and Hdm2 autoubiquitination activity by small molecular weight inhibitors. *PNAS*, 99, 14734–1473
39. Lee, C., Dillon, J., Wang, M.Y.C., Gao, Y., Hu, K., Park, E., Astanehe, E., Hung, M., Eirew, P., Eaves, C.J., Dunn, S.E., (2008). Targeting YB-1 in HER-2 over-expressing breast cancer cells induces apoptosis via the mTOR/STAT3 pathway and suppresses tumor growth in mice. *Cancer Research*, 68, 8661-8666
40. Lee, M.H., & Lozano, G., (2006). Regulation of the p53-MDM2 pathway by 14-3-3 sigma and other proteins. *Seminars in Cancer Biology*, 16(3), 225-234

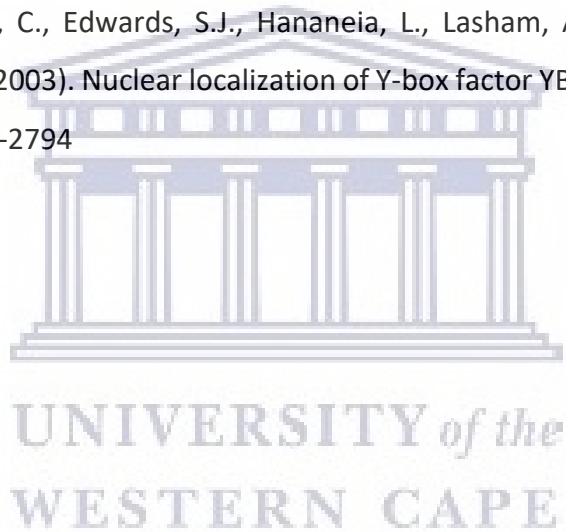
41. Lee, S., Choi, J., Sung, Y., Park, H., Rhim, H., Kang, S., (2001). E3 ligase activity of RING finger proteins that interact with Hip-2 a human ubiquitin-conjugating enzyme. *FEBS*, 503, 61-64
42. Lee, S., Moore, C., (2014). Efficient mRNA polyadenylation requires a ubiquitin-like domain, a zinc knuckle, and a RING finger domain, all contained in the Mpe1 protein. *Molecular and cellular biology*, 34, 3955-3967
43. Li, L., Deng, B., Xing, G., Teng, Y., Tian, C., Cheng, X., Yin, X., Yang, J., Gao, X., Zhu, Y., Sun, Q., Zhang, L., Yang, X., and He, F., (2007) PACT is a negative regulator of p53 and essential for cell growth and embryonic development, *Proceedings of the National Academy of Science USA*, 104, 7951-6.
44. Liew, C.K., Gamsjaeger, R., Mansfield, R., Mackay, J.P., (2008). NMR spectroscopy as a tool for the rapid assessment of the conformation of GST-fusion proteins. *Protein Society*, 17(9), 1630-1635
45. Lim, S.K., Shin, J.M., Kim, Y.S., Baek, K.H., (2004). Identification and characterization of murine mHAUSP encoding a deubiquitinating enzyme that regulates the status of p53 ubiquitination. *International Journal of Oncology*, 24(2), 357-364
46. Linares, L., Hengstermann, A., Ciechanover, A., Muller, S., Scheffner, M., (2003). HDMX stimulates HDM2-mediated ubiquitination and degradation of p53. *PNAS*, 100, 12009-12014
47. Linke, K., Mace, P., Smith, C., Vaux, D., Silke, J., Day, C., (2008). Structure of the MDM2/MDMX RING domain heterodimer reveals dimerization is required for their ubiquitylation *in trans*. *Cell Death and Differentiation*, 15, 841-848
48. Lyabin, D.N., Doronin, A.N., Eliseeva, I.A., Guens, G.P., Kulakovskiy, I.V., Ovchinnikov, L.P., (2014). Alternative forms of Y-Box Binding Protein 1 and YB-1 mRNA. *PLOS ONE*, e104513
49. Madura, K., (2002). The Ubiquitin-Associated (UBA) Domain: On the Path from Prudence to Prurience. *Cell Cycle*, 1:4, 233-242
50. Matsumoto, K., Bay, B.H., (2005). Significance of the Y-box proteins in human cancers. *Journal of Molecular and Genetic Medicine*, 1, 11-17

51. Matsumoto, K., Wolffe, A.P., (1998). Gene regulation by Y-box proteins: coupling control of transcription and translation, *Cell Biology*, 8, 318-323
52. Matthews, J.M., Sunde, M., (2002). Zinc Fingers – Folds for Many Occasions. *IUBMB.*, 54, 351-355
53. Mbita, Z., Meyer, M., Skepu, A., Hosie, M., Rees, J., Dlamini, Z., (2011). De-regulation of RBBP6 isoform 3 DWNN in human cancers. *Molecular and cellular biochemistry*, 362, 249-262
54. Metzger, M.B., Pruneda, J.N., Klevit, R.E., Weissman, A.M., (2014). RING-type E3 ligases: master manipulators of E2 ubiquitin-conjugating enzymes and ubiquitination. *Biochim Biophys Acta*, 1843, 47-60
55. Natan, E., Baloglu, C., Pagel, K., Freund, S.M.V., Morgner, N., Robinson, C.V., Fersht, A.R., Joerger, A.C., (2011). Interaction of the p53 DNA-Binding Domain with its N-Terminal Extension Modulates the Stability of the p53 Tetramer. *Journal of Molecular Biology*, 409(3), 358-368
56. Nikolay, R., Wiederkehr, T., Rist, W., Kramer, G., Mayer, M.P., Bukau, B., (2004). Dimerization of the human E3 ligase CHIP via a coiled-coil domain is essential for its activity, *Journal of Biological Chemistry*, 279, 2673-2678
57. Ntwasa, M., (2016). Retinoblastoma Binding Protein 6, Another p53 Monitor. *Trends in cancer*, 2, 635-637
58. Pant, V., Lozano, G., (2014). Limiting the power of p53 through the ubiquitin proteasome pathway. *Genes and development*, 28, 1739-1751
59. Pavletich, N.P., Chambers, K.A., Pabo, C.O., (1993). The DNA-binding domain of p53 contains four conserved regions and the major mutation hot spots. *Genes & Development*, 7, 7556-2564
60. Pickart, C.M., (2001). Mechanisms underlying ubiquitination. *Annual review of biochemistry*, 70, 503-533
61. Pugh, D.J., Ab, E., Faro, A., Luty, P.T., Hoffmann, E., and Rees, D.J. (2006). DWNN, a novel ubiquitin-like domain, implicates RBBP6 in mRNA processing and ubiquitin-like pathways. *BMC Structural Biology* 6, 1.

62. Rule, G.S., Hitchens, T.K., (2005). Fundamentals of Protein NMR Spectroscopy. Springer
63. Saijo, M., Sakai, Y., Kishino, T., Niikawa, N., Matsuura, Y., Morino, K., Tamai, K and Taya, Y., (1995). Molecular cloning of a human protein that binds to the retinoblastoma protein and chromosomal mapping. *Genomics* 27, 511-519
64. Sakai, Y., Saijo, M., Coelho, K., Kishino, T., Niikawa, N., and Taya, Y., (1995). cDNA sequence and chromosomal localization of a novel human protein, RBQ-1 (RBBP6), that binds to the retinoblastoma gene product. *Genomics* 30, 98-101.
65. Shadfan, M., Lopez-Pajares, V., Yuan, Z.M., (2012). MDM2 and MDMX: Alone and together in regulation of p53. *Translational Cancer Research*, 1(2), 88-89
66. Shi, Y., Di Giammartino, D.C., Taylor, D., Sarkeshik, A., Rice, W., Yates, R., Frank, J., Manley, J.L., (2009). Molecular architecture of the human pre-mRNA 3' processing complex. *Mol Cell*, 33(3), 365-376
67. Simons, A., Melamed-Bessudo, C., Wolkowicz, R., Sperling, J., Sperling, R., Eisenbach, L., and Rotter, V., (1997). PACT: cloning and characterization of a cellular p53 binding protein that interacts with pRb. *Oncogene* 14, 145-155.
68. Song, S., Jung, Y.K., (2004). Alzheimer's disease meets the ubiquitin proteasome system. *Trends in Molecular Medicine*, 10(11), 565-570
69. Song, S., Kim, S.Y., Hong, Y.M., Jo, D.G., Lee, J.Y., Shim, S.M., Chung, C.W., Seo, S.J., Yoo, Y.J., Kob, J.Y., Lee, M.C., Yates, A.J., Ichijo, H., Jung, Y.K., (2003). Essential role of E2-25K/Hip-2 in mediating amyloid-beta neurotoxicity. *Molecular Cell*, 12, 553-563
70. Stommel, J.M., Wahl, G.M., (2005). A new twist in the feedback loop: stress activated MDM2 destabilization is required for p53 activation. *Cell cycle*, 4(3), 411-417
71. Szczuraszek, K., Halon, A., Materna, V., Mazur, G., Wrobel, T., Kuliczowski, K., Donizy, P., Holm, P., Lage, H., Surowiak, P., (2011). Elevated YB-1 expression is a new unfavorable prognostic factor in Non-Hodgkin's Lymphomas. *Anticancer Research*, 31, 2963-2970
72. Tanaka, K., (2009). The proteasome: overview of structure and functions. *Proceedings of the Japan Academy, Series B, Physical and biological sciences*, 85, 12-36
73. Tanimura, S., Ohtsuka, S., Mitsui, K., Shirouzu, K., Yoshimura, A., Ohtsubo, M., (1999). MDM2 interacts with MDMX through their RING finger domains. *FEBS Letters*, 447, 5-9

74. Tollini, A., Zhang, Y., (2012). p53 Regulation Goes Live - MDM2 and MDMX Co-Star: Lessons Learned from Mouse Modeling. *Genes and Cancer*, 3, 219-225
75. Van Wijk, S.J., Timmers, H.T., (2010). The family of ubiquitin-conjugating enzymes (E2s): deciding between life and death of proteins. *The FASEB Journal*, 24, 981-993
76. Vo, L., Minet, M., Schmitter, J., Lacroute, F., Wyers, F., (2001). Mpe1, a zinc knuckle protein, is an essential component of yeast cleavage and polyadenylation factor required for the cleavage and polyadenylation of mRNA. *Molecular and cellular biology*, 21, 8346-8356
77. Weinberg, R., (2014). *The biology of cancer second edition*, Garland Science, USA
78. Wells, M., Tidow, H., Rutherford, T.J., Markwick, P., Jensen, M.R., Mylonas, E., Svergun, D.I., Blackledge, M., Fersht, A.R., (2008). Structure of tumor suppressor p53 and its intrinsically disordered N-terminal transactivation domain. *PNAS*, 105(15), 5762-5767
79. Wells, M., Tidow, H., Rutherford, T.J., Markwick, P., Jensen, M.R., Mylonas, E., Svergun, D.I., Blackledge, M., Fersht, A.R., (2008). Structure of tumor suppressor p53 and its intrinsically disordered N-terminal transactivation domain. *PNAS*, 105(15), 5762-5767
80. Wilson, R.C., Edmondson, S.P., Flatt, J.W., Helms, K., Twigg, P.D., (2011). The E2-25K ubiquitin-associated (UBA) domain aids in polyubiquitin chain and synthesis and linkage specificity. *Biochemical and Biophysical Research Communications*, 405, 662-666
81. Wilson, R.C., Hughes, R.C., Flatt, J.W., Meehan, E.J., Ng, J.D., Twigg, P.D., (2009). Structure of full-length ubiquitin-conjugating enzyme E2-25K (Huntington-interactin protein 2). *Acta Crystallographica Section F: Structural Biology and Crystallization Communications*, 65, 440-444
82. Wishart, D.S., Sykes, B.D., Richards, F.M., (1991). Relationships between nuclear magnetic resonance chemical shift and protein secondary structure. *Journal of Molecular Biology*, 222(2), 311-333
83. Witte, M.M., Scott, R.E., (1997). The proliferation potential protein-related (P2P-R) gene with domains encoding heterogeneous nuclear ribonucleoprotein association and Rb1 binding shows repressed expression during terminal differentiation. *Proceedings of the National Academy of Science of the United States of America*, 94(4), 1212-1217

84. Woelk, T., Sigismund, S., Penengo, L., Polo, S., (2007). The ubiquitination code: a signaling problem. *Cell Division* 2, 12
85. Wuthrich, K., (2003). Nobel lecture: NMR studies of structure and function of biological macromolecules. *Bioscience Reports*, 23(4), 116-168
86. Yan, X., Yan, L., Zhou, J., Liu, S., Shan, Z., Jiang, C., Tian, Y., Zhiming, J., (2014). High expression of Y-box-binding protein 1 is associated with local recurrence and predicts poor outcome in patients with colorectal cancer. *International Journal of Clinical & Experimental Pathology*, 7(12), 8715-8723
87. Yu, H., (1999). Extending the size limit of protein nuclear magnetic resonance. *Proceedings of the National Academy of Sciences*, 99, 332-334
88. Zhang, Y.F., Homer, C., Edwards, S.J., Hananeia, L., Lasham, A., Royds, J., Sheard, P., Braithwaite, A.W., (2003). Nuclear localization of Y-box factor YB1 requires wild type p53. *Oncogene*, 22, 2782-2794





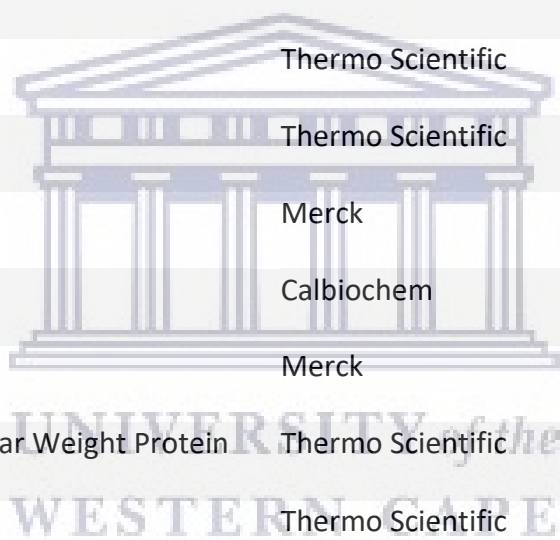
## Appendix

### List of Chemicals, kits and suppliers

Table 7.1 Materials and supplier used in this project

Chemicals	Suppliers
Agarose	Promega
Amicon Ultra-15 Centrifugal Filter Units	Merck
Ammonium Chloride <sup>15</sup> N	Silantes
Ammonium persulfate	Merck
Ampicillin	Melford
Antibodies	Santa Cruz Biotechnology
Brilliant Blue R pure	Sigma-Aldrich
Casein from bovine milk	Sigma-Aldrich
Clarity Western ECL substrate	Bio-Rad
Di-sodium hydrogen phosphate (Na <sub>2</sub> HPO <sub>4</sub> )	Merck
Dithiothreitol (DDT)	Melford
Ethylene diamine tetra acetic acid (EDTA)	Merck
GeneJet Gel extraction kit	Thermo Scientific
GeneJet plasmid mini-prep kit	Thermo Scientific
Glutathione agarose beads	ABT
Glycerol	BDH
Green DNA DYE 10,000X	Inqaba Biotech

Isopropyl $\beta$ -D-1-thiogalactopyranoside (IPTG)	Melford
Luria Broth	Merck
Magnesium Sulfate ( $MgSO_4$ )	Sigma-Aldrich
N, N, N', N'-Tetra methylethylene-diamine (TEMED)	Bio-Rad
Nutrient Agar	Merck
Polyethylene glycol (PEG)	Merck
Potassium chloride (KCl)	Merck
Potassium di-hydrogen phosphate ( $KH_2PO_4$ )	Merck
Restriction Enzymes	Thermo Scientific
Snake Skin Dialysis Tubing	Thermo Scientific
Sodium Chloride (NaCl)	Merck
Sodium Dodecyl Sulfate (SDS)	Calbiochem
Sodium Hydroxide (NaOH)	Merck
Super Signal Enhance Molecular Weight Protein ladder (Western Marker)	Thermo Scientific
T4 DNA ligase	Thermo Scientific
TGX Fast Cast Acrylamide Kit 12%	Bio-Rad
TransBlot Turbo Transfer System	Bio-Rad
Tris Base	Merck
Urea	Merck
Zinc Sulfate ( $ZnSO_4$ )	Merck



## List of general stock solutions and buffers

**Table 7.2** General stock solutions and buffers used in this project

Stock Solution	Recipe
<b>10X PBS Buffer for 2 Litres</b>	160g NaCl, 4g KCl, 28.8 Na <sub>2</sub> HPO <sub>4</sub> , 4.8g KH <sub>2</sub> PO <sub>4</sub> pH 7.4
<b>50X TAE Buffer for 1 Litres</b>	121g Tris, 50ml EDTA (0.5M, pH8.0), 28.6 ml Glacial acetic acid.
<b>10X Running Buffer for 2 Litres</b>	60.4g Tris Base, 288.2g Glycine, 20g SDS
<b>3C Cleavage Buffer</b>	50mM Tris HCl pH 7, 150mM NaCl, 1mM EDTA, 1mM DTT

## Amino Acid Sequences

### Amino acid sequence of HA-RBBP6-RING

10            20            30            40            50            60  
GPLGSMYPYD VPDYAAGSED DPIDPELLCL ICKDIMTDAV VIPCCGNSYC DECIRTALLE  
70            80            90            100  
SDEHTCPTCH QNDVSPDALI ANKFLRQAVN NFKNETGYTK RLRKQ

**Number of amino acids:** 99

**Molecular weight:** 11117.50

**Theoretical pI:** 4.47

### Amino acid sequence of MDM2-RING

10            20            30            40            50            60  
EETQDKESV ESSLPLNAIE PCVICQGRPK NGCIVHGKTG HLMACFTCAK KLKRNKPCP  
  
70  
VCRQPIQMIV LTYFP

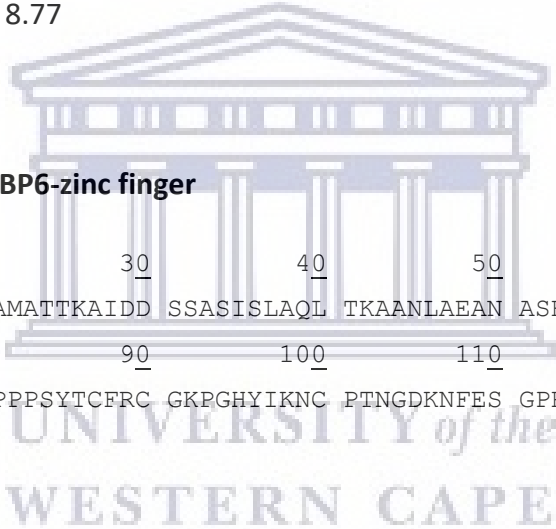
**Number of amino acids:** 75

**Molecular weight:** 8386.93

**Theoretical pI:** 8.77

### Amino acid sequence of RBBP6-zinc finger

10            20            30            40            50            60  
GPLGSVKSTS KTYVISRTEP AMATTKAIDD SSASISLAQL TKAANLAEAN ASEEDKIKAM  
70            80            90            100            110            120  
MPQSGHEYYP INYMKKPLGP PPSYTCFRC GKPGHYIKNC PTNGDKNFES GPRIKKSTGI  
PRS



**Number of amino acids:** 123

**Molecular weight:** 13223.07

**Theoretical pI:** 9.41

### Amino acid sequence of RBBP6-zinc-C finger

10            20            30            40  
GPLGSSYTCF RCGKPGHYIK NCPTNGDKNF ESGPRIKKST GIPRS

**Number of amino acids:** 45

**Molecular weight:** 4857.52

**Theoretical pI:** 9.73

**Amino acid sequence of Ubch1 UBA**

          10                  20                  30                  40  
GPLGSSPEY<sup>T</sup> KKIENLCAM<sup>G</sup> FDRNAVIVAL<sup>L</sup> SSKSWDVETA<sup>A</sup> TELLLSN

**Number of amino acids:** 47

**Molecular weight:** 5056.73

**Theoretical pI:** 4.66



UNIVERSITY *of the*  
WESTERN CAPE